CHARACTERIZING THE MECHANISMS THAT REGULATE CELL POLARITY DURING EUKARYOTIC CHEMOTAXIS

By

Dawit Kamil Jowhar

Dissertation

Submitted to the Faculty of the

Graduate School of Vanderbilt University

in partial fulfillment of the requirements for

the degree of

DOCTOR OF PHILOSOPHY

in

Biological Sciences

August, 2013

Nashville, Tennessee

Approved:

Professor Charles Singleton

Professor Ann Richmond

Professor John Wikswo

Professor Andries Zijlstra

Professor Christopher Janetopoulos

To my family, Kamil, Etsehiwet, Nat, Hebri,

Abraham, Bethelhem, Sol for

your continuous love and support.

To my lovely wife, Dru, for always being supportive

and being my better half.

ACKNOWLEDGMENTS

First and foremost, I would like to thank God for his incessant blessings during my time at Vanderbilt and for opening doors that I thought were not possible.

This research has been supported in part by the Vanderbilt Institute for Integrative Biosystems Research and Education (VIIBRE). Dictybase provided cell lines used for the experiments. A. Muller-Taubenberger provided LimE-RFP construct. Arjan Kornholt from the Van Haastert's lab provided RBD-RFP construct. Thanks to the Richmond Lab particularly Dr. Jiqing Sai for providing input, cells and reagents for HL-60 experiments. Funding for Dawit Jowhar was provided by NIH NRSA Grant 1 F31 GM095282-01A1 and the Gisela Mosig Fund. Funding for Chris Janetopoulos was provided by NIHGM080370.

The following publications and projects have provided significant content for this thesis: (Jowhar, Wright, Samson, Wikswo, & Janetopoulos, 2010), Jowhar and Janetopoulos (2013), (Jowhar, Khodadadi, Wright, Rucker, Housman, Wikswo, Chen, Betzig and Janetopoulos, 2013 in preparation). Work for Chapter V was done in collaboration with the Richmond Lab.

I would like to thank the scores of people who have supported me during my stay at Vanderbilt. First, I would like to thank all members of my committee for their valuable input and time during the past four years. I would like to thank Dr. Singleton, for serving as committee chair, Dr. Richmond, Dr. Wikswo, Dr. Zijlstra and Dr. Janetopoulos, for their diligent efforts in my development as a scientist, always challenging me to ask the right questions, and providing valuable suggestions to improve my research. I have become a better scientist and learner as a result of their dedicated efforts.

I would like to express my deepest gratitude to Dr. John Wikswo, for believing in me, always supporting and challenging ideas, providing exceptional guidance, and providing me with the optimal learning environment to flourish at Vanderbilt. I would like to thank all the members of VIIBRE, particularly, Phil, for taking the time to teach me valuable technical skills, most importantly how to build microfluidic devices. And special thanks to Cheryl, Don, Ron, Allison, Dmitri, Kevin, Schaffer, for everything they do at VIIBRE.

I would like to thank all the members of the Biological Sciences Department and all the administrative support staff particularly Leslie, Carol, Alicia and to The Gisela Mosig Fund and the graduate school for providing travel grants and other support to further my research efforts.

I would like to thank my advisor, Dr. Chris Janetopoulos, for his role as a mentor, all his guidance and support during the past five years, and the learning and working environment he has fostered in the laboratory. His positive attitude and excitement for research and scientific advances provides constant motivation and support to his students. I would like to thank past and present members of the Janetopoulos Lab; Gus for providing advice and training during my research, Yuantai, Kamal, Derrick, Noelle, Ryan, Shanna, Kevin, Sabrina, Arunan, Alayna, Sarah, Ying Jun.

I would like to thank all the friends I made at Vanderbilt, especially Neil, Ernest, Zusi, Teniel, MLD, Jeff, Jon, Leo and all the other classmates and colleagues who have provided insights to my research, comical relief, and efforts to strike “ideal” work-life balance as graduate students. I would like to thank members of OBGAPS, the Black Cultural Center and its advisors, particularly Dr. Don Brunson, for providing support in running this great organization. I am deeply grateful to friends I made at Fisk University before coming to Vanderbilt – Dez, Ryan, Lauren, John, Johnathan, and Kent. I am truly indebted to my first graduate advisor, Dr. Richard Mu, who has been with me every step of the way since my undergraduate days at Fisk University. A special thanks to Dr. Akira Ueda, Dr. Roberto Aga and Dr. Eugene Collins, who both provided valuable guidance when I first started graduate school. I also would like to thank Dr. Lucius Outlaw and Dr. George Hill for providing mentorship and their valuable time.

Lastly, I would like to thank my family in Ethiopia and the US especially Mom, Nat, Sol, Babi, Hebri, Mimi, Aba, and all my aunts, uncles, cousins and nephews who have prayed for me and provided support throughout graduate school and my time in Nashville.

And to my wife and true best friend, Dru. No words could truly describe how much I appreciate your unwavering love and support on this journey. You are my source of joy and happiness. You constantly inspire me and I am a better man because of you.

TABLE OF CONTENTS

Page

DEDICATION ii

ACKNOWLEDGEMENTS iii

LIST OF FIGURES vii

LIST OF ABBREVIATIONS viii

Chapter

I. INTRODUCTION 1

Chemotaxis and its importance 1
Establishment of cell polarity during chemotaxis 2
Dictyostelium as a model system for chemotaxis 4
Dictyostelium development phases 5
Differences and similarities between folic acid and cAMP chemotaxis 6
Receptors 6
Signaling after receptor activation 6
Dictyostelium heterotrimeric g proteins and functions 9
Morphology 10
Current assays for studying chemotaxis and their limitations 12
Thesis focus 14

II. MATERIALS AND METHODS 16

Device design and production 16
Open microfluidic device for chemotaxis studies 16
Device fabrication processes 17
Gradient measurements 20
Gradient characterization 22
Gradient stability over time 24
Experimental setup for polarity reversal experiments 26
Device surface coating for HL-60 cells 26
Imaging 26
Image quantification 27
Bleach correction 27
Cell selection criteria 27
Cell speed 28
Cell length 28
Kymographs 28
Signal peak 28
Cytosol intensity measurement 28
Signal at “old” location vs. “new” location 29
Fold increase 29
Statistical analysis 29
Standard error of the mean 30

Cell reversal 30
Cell line preparation 30
Cell lines and plasmids 30
Transformation protocols 31
Media and buffers 31
cAMP preparation 31
cAMP development 32
Latrunculin-A treatment 32
Uniform cAMP stimulation 32
Vegetative cells 32
HL-60 cell preparation 32
HL-60 cell experimental setup 33

III. POLARIZED VS. UNPOLARIZED CELLS 34

Introduction 34
Results 38
Migration speeds of polarized cells versus unpolarized cells within channels 38
Migration speeds of unpolarized cells within and in the absence of channels 40
Spatial gradient sensing occurs primarily at the leading edge 42
Discussion 42

IV. POLARITY REVERSALS REVEAL THE ROLE OF PI(4,5)P2 IN SIGNALING RESPONSES AND POLARIZED MORPHOLOGY 49

Introduction 49
Results 53
Experimental design 53
Ras activation occurs as the leading edge and only does so where PI(4,5)P2 levels are low 55
PLC null cells reverse polarity faster, and PTEN forms vesicles at the rear of the cell when cells reverse 63
Microtubules interacting with the plasma membrane at the poles is inversely correlated with the presence of F-actin 68
Discussion 74
Advantages of using the open microfluidic system for polarity studies 74
Kymograph analysis reveals distinct features of polarity establishment 74
Relationship between microtubules and the actin cytoskeleton 75
Antagonistic relation between PI(4,5)P2 and Ras activation 76
High levels of PM PI(4,5)P2 put the brakes on actin polymerization And contribute to “backness” 76

V. FUTURE DIRECTIONS 82

REFERENCES 89

LIST OF FIGURES

Figure Page

1. Phosphoinositol distribution after receptor activation 8

2. Morphology differences in polarized versus unpolarized cells 11

3. The open microfluidic device (OMD) for studying gradient sensing and cell migration... 19

4. Gradients and cells in the OMD 21

5. Gradient measurements in different channels 23

6. Gradient stability of open microfluidic device 25

7. Analysis of cell migration in the OMD 39

8. Average cell migration speed is independent of varying mean concentrations and channel widths 41

9. The turning behavior of cells as they exit the narrow channels 45

10. Turning strategy of cells exiting the channel 48

11. Experimental setup for polarity reversal experiments 54

12. Ras activation, PIP3 and PIP2 localization during polarity reversal 57

13. Ras activity occurs in regions that have low PIP2 levels 60

14. PIP3 is not sufficient to direct actin polymerization 61

15. Ras activation increases significantly and quickly at the leading edge of a cell 62

16. *plc*-/PTEN-GFP cells can reverse their polarity after a gradient switch 65

17. Plc null cells take longer to accumulate PTEN at the new rear of the cell compared to wild type cells 67

18. Areas of actin and microtubule polymerization are mutually exclusive 69

19. High PIP2 levels reduce response after uniform stimulation by chemoattractant 72

20. Model for polarity establishment 78

21. HL-60 cells during polarity reversal 85

22. Polarity reversal of HL-60 cells treated with Wortmannin 86

LIST OF ABBREVIATIONS

cAMP – cyclic adenosine mono phosphate

cAR – cAMP receptor

DAG – Diacyl glycerol

DB – developmental buffer

GC – gradient change

GDP - guanosine diphosphate

GTP - guanosine triphosphate

FA – folic Acid

FE – front extension

FRAP - Fluorescence recovery after photobleaching

FRET - Förster resonance energy transfer

FITC - Fluorescein isothiocyanate

hPA – Hecto Pascal

IP3 – Inositol tri-phosphate

OMD – Open microfluidic device

PDMS – poly dimethyl siloxane

PH-CRAC – Pleckstrin homology – cytosolic regulator of adenylyl cyclase

PI3K – Phosphatidylinositol 3-kinase

PI(4,5)P2 - Phosphatidylinositol 4,5-bisphosphate

PI(3,4,5)P3 - Phosphatidylinositol 3,4,5-trisphosphate

PKBA – Protein kinase b

PKBR1 –Protein kinase b related kinase

PLC – Phospholipase C

PM – plasma membrane

PTEN - Phosphatase and tensin homolog

Ras* - Ras activity

ROI - Region of interest

SM – Selective media

TORC – Transducer of regulated camp response

UV – Ultra violet

WASP - Wiskott-aldrich syndrome protein

CHAPTER I

INTRODUCTION

Chemotaxis and its importance

Chemotaxis is the directed migration of cells up or down a chemical gradient. The term was coined by Engelmann and Pfeffer during their observations of directed movement of bacterial cells toward certain stimuli (Engelmann, 1883; Lux and Shi, 2004; Pfeffer, 1884) . It is critical during many eukaryotic processes including development and wound healing (Frost et al., 2009; Schneider et al., 2010; Wood et al., 2006) , numerous disease states including cancer (Condeelis and Segall, 2003; Di Gennaro and Haeggstrom, 2012; Muller et al., 2001; Roussos et al., 2011; Varani, 1982) and the immune response(Franciszkiewicz et al., 2012; Liu et al., 2012).

In fertilization, sperm are attracted toward the egg by the release of chemical factors (Kaupp et al., 2008). In wound healing, chemotaxis plays a very important role as well. One of the first steps in wound healing is the chemotaxis of different cells such as inflammatory and epithelial cells to the wound site (Bennett and Schultz, 1993). Work on monocytes has shown that under the influence of chemoattractants, they occupy the wound site and become activated macrophages.(Kolaczkowska and Kubes, 2013; Singer and Clark, 1999). Chemotaxis toward transforming growth factor beta (TGF-beta) has also been shown in monocytes (Smythies et al., 2006; Wahl et al., 1987). During inflammation, chemokines also provide directional cues for the migration of leukocytes (Luster, 1998). The chemotactic response of phagoctyic leukocytes is one of the first lines of host defense against invasion by microorganisms (Le et al., 2004; Richmond et al., 2009; Schmidt et al., 2013).

During metastasis, chemotaxis is thought to be involved in invasion, and intra/extravasation and growth at a distant site (Roussos et al., 2011). Human melanoma cells have been shown to chemotax toward thrombospondin and have also been shown to express chemokine receptors (Mueller et al., 1994; O'Boyle et al., 2013; Taraboletti et al., 1987). Chemokines have been shown to influence prostate carcinoma cells (Maxwell et al., 2012; Reiland et al., 1999) and are involved in breast cancer metastasis (Hawkins and Richmond, 2012; Muller et al., 2001; Tang, 2013). Carcinoma cells have also been shown to migrate toward epidermal growth factor *in vivo* using a chemotaxis based in vivo invasion assay (Condeelis et al., 2005; Wyckoff et al., 2004).

Establishment of cell polarity during chemotaxis

Cells that perform chemotaxis undergo several steps. The first step is sensing of the chemoattractant gradient and the transmission of the external signal to the interior of the cells via receptors. The second step involves processing and interpretation of the signal. The third is to respond to the chemical gradient by activating both signaling and cytoskeletal components and to move either toward or away from the gradient (King and Insall, 2009; Weiner, 2002).

Cell polarity is defined as the presence of a distinct front and back of a cell. It is one of the properties displayed by the cell during chemotaxis that enables it to respond to the chemical gradient. Cell polarity is important for directional cell movement, and arises due to the asymmetric distribution of signaling and cytoskeletal components during chemotaxis (Chung et al., 2001a; Devreotes and Janetopoulos, 2003). A cell with a polarized morphology can respond robustly to gradients of chemoattractant and also focus its motility machinery in the correct direction (Srinivasan et al., 2013b; Swaney et al., 2010). Some of the asymmetrically distributed cytoskeletal molecules at the leading edge are actin and actin-binding proteins Scar, WASP, filopodin, cofilin, and coronin while myosin II and cortexillin I are found at the trailing edge (Devreotes and Janetopoulos, 2003).

Signaling molecules are also asymmetrically distributed during polarity and migration. At the leading edge, there is localized Ras signaling (Sasaki et al., 2004). There are also localizations of PH domain containing proteins such as CRAC (cytosolic regulator of adenylyl cyclase), PhdA (PH-domain-containing protein A), and Akt (Parent, 2004). The enzyme PI3-kinase phosphorylates PI(4,5)P2 to PI(3,4,5)P3 (Whitman et al., 1988) and is found at the leading edge of the cells while the tumor suppressor and phophatase PTEN creates PI(4,5)P2 from PI(3,4,5)P3 and is found at the rear of the cells respectively (Comer and Parent, 2002; Funamoto et al., 2002; Iijima and Devreotes, 2002). In terms of sensitivity to a chemical gradient, the front of the cell is more sensitive than the rear, which could lead to the focusing of the actin cytoskeleton at the leading edge (Devreotes and Janetopoulos, 2003).

Before examining how polarity is established it is crucial to understand how a cell senses a chemical gradient and internally amplifies this response. Work from Devreotes and Janetopoulos (Devreotes and Janetopoulos, 2003; Parent and Devreotes, 1999) has proposed the Local Excitation Global Inhibition (LEGI) Model. In this model, the leading edge of the cell in a gradient experiences a rapid local excitation and a slower global inhibition whereas the trailing edge experiences the reverse phenomena. This leads to the establishment of an asymmetric phosphoinositol gradient (higher levels of PI(3,4,5)P3) at the front of the cell (Devreotes and Janetopoulos, 2003; Janetopoulos et al., 2004).

Chung *et al.,* have examined how a cell initially establishes polarity by suggesting that initial activation of PI3-kinase at the leading edge of a cell, downstream from receptor activation, could play a role (Chung et al., 2001a; Chung et al., 2001b). Their results indicate that amplification of signals mediated by feedback loops at the leading edge while inhibition at the lateral sides of the cell could lead to the formation of a polarized morphology. They suggest that PI3K partially controls the cytoskeletal components such as myosin II and F-actin that lead to axial polarity.

Most of the data that links phosphoinositols to cell polarity has been focused on PI(3,4,5)P3. Interference with PI3K through different means leads to defects in chemotaxis and polarity (Funamoto et al., 2001; Hirsch et al., 2000; Niggli and Keller, 1997). However there is work from several laboratories that suggests otherwise (Andrew and Insall, 2007; Hoeller and Kay, 2007; Loovers et al., 2006; Takeda et al., 2007).

Dictyostelium as a model system for chemotaxis

One of the most thoroughly used model systems for the study of eukaryotic chemotaxis is the social amoeba *Dictyostelium discoideum.* In the next section, I will describe why it is a suitable system for examining directed motility. While there are over a 100 discovered species of *Dicytostelia* (Jowhar and Janetopoulos, 2013), most of the work on *Dictyostelium* chemotaxis has been focused on *D. discoideum* (Romeralo et al., 2011). It has been more than 75 years since the discovery of this organism by K.B. Raper (Raper, 1935), and there has been a tremendous amount of work performed on this genetically and biochemically tractable system to understand the different behaviors these social amoeba display in response to chemical signals. Non-essential genes in these cells are highly amendable to genetic manipulation, with targeted gene disruptions obtainable in a few weeks. It's relatively small genome is sequenced and RNAi and insertional mutagenesis can be used to identify the function of novel genes (Garcia et al., 2009; Landree and Devreotes, 2004; Parent et al., 1998). Pathways regulating chemotaxis are conserved throughout evolution, as was discovered early on when investigations using *D. discoideum* first showed that eukaryotic cells use serpentine receptors coupled to the heterotrimeric G proteins to undergo chemotaxis (Devreotes, 1994; Parent et al., 1998). It was only after this discovery that a similar signaling cascade was found in mammalian neutrophils during directed migration (Franca-Koh et al., 2009; Kim et al., 1996; Suire et al., 2012). There is

also an online community known as Dictybase (dictybase.org) that is dedicated to exploring the genome, as well as providing tools, strains and plasmids and several other services to fully explore biological processes using *Dictyostelium* (Fey et al., 2006). *D. discoideum* has been very useful in biomedical research and in identifying targets for drugs such as cisplatin (Li et al., 2000), lithium (Williams et al., 1999) and biphosphonates (Grove et al., 2000). It is also proven useful for investigating the mechanisms regulating *Legionalla pneumophila* infection (Williams, 2010) and mitochondrial and neurological diseases (Annesley and Fisher, 2009).

Dictyostelium **development phases**

Dictyostelium cells undergo different morphological and gene expression phases during development, which occurs over a period of about twenty four hours. In the vegetative state, cells feed on bacteria, which secrete a number of factors, including folic acid. *D. discoideum* cells can use folic acid as a guidance cue to find their bacterial prey. When food sources start to deplete, *D. discoideum* undergo a developmental processes that culminates in the formation of a fruiting body. The chemoattractant cyclic adenosine monophosphate (cAMP) plays a critical role in this process and proper management of its secretion and degradation regulates the expression of many developmental genes (Hall et al., 1993; Kessin, 1988) . Propagating waves of cAMP occur approximately every 6 minutes and recruit surrounding cells. This leads to the formation of aggregation centers where hundreds of thousands of cells come together to form large structures known as slugs. Slugs have the capability to move toward an environment conducive to spore dispersal. Their phototactic properties may help in the distribution of spores if the aggregation takes place under a leaf or rock. Slugs can then differentiate into fruiting bodies and can release thousands of spores which remain dormant until favorable environmental conditions allow continuation of the life cycle.

Differences and similarities between folic acid and cAMP chemotaxis

Receptors

Dictyostelium have transmembrane cAMP receptors that belong to the G Protein coupled receptor superfamily (Strader et al., 1995; Xiao et al., 1997). There are four cAMP receptors in *Dictyostelium* (designated cARs 1 – 4) that are expressed at different stages of the developmental program (Klein et al., 1988; Saxe et al., 1991). cAR1 is expressed during early development while cAR3 is expressed later during aggregation and reaches maximal expression during the mound stage of slug formation (Johnson et al., 1993b). cARs 2 and 4 are expressed in the prestalk cells during slug formation, and later fruiting body stages, respectively (Insall et al., 1994; Johnson et al., 1993b; Saxe et al., 1991). The affinities of these receptors for cAMP are also different with cAR1 having the highest affinity and cAR3 having the least affinity (Dormann et al., 2001). cAR3 shares 56% and 69% amino acid sequence identity with cAR1 and cAR2, respectively (Johnson et al., 1993a). The folic acid receptor has not been isolated as to date.

Signaling after receptor activation

The binding of chemoattractants to the receptors catalyzes the exchange of guanosine diphosphate (GDP) for guanosine triphosphate (GTP) and allows both the GTP bound α-subunit and free βγ complexes to signal to downstream effectors (Bourne, 1997; Gilman, 1987). The first in vivo look at G-protein dynamics in response to a stimulus was performed using *D. discoideum* (Janetopoulos et al., 2001). The α2 and βγ-subunits rapidly dissociated and reassociated upon addition and removal of cAMP, respectively. Interestingly, the G proteins appeared to remain in an active conformation in the presence of cAMP, even though responses had declined. This suggested that adaptation must be downstream or independent of heterotrimeric G protein activation. Upon dissociation of the Gβγ subunit from Gα, indirect evidence has shown that Gβγ leads to the activation of the small GTPase Ras (Jin, 2011). Ras

proteins serve as molecular switches whose activity is regulated by Ras GEFs (Guanine nucleotide Exchange Factor) and GAPS (GTPase activating Proteins) (Boguski and McCormick, 1993; Bolourani et al., 2006; Bourne et al., 1991). In addition, Ras activity does not increase in response to chemoattractants in cells lacking functional heterotrimeric subunits (Kae et al., 2004; Sasaki and Firtel, 2006).

Ras is the first marker to show an amplified asymmetric response during migration and is followed closely at the plasma membrane by changes in the level of the enzymes that synthesize and degrade the phosphoinositides (PIPs) that include PI(3,4)P2, PI(3,4,5)P3 and PI(,4,5)P2 (Sasaki et al., 2004; Sasaki et al., 2007; Whitman et al., 1988). In *D.discoideum*, PI 3-kinases and the tumor suppressor PTEN relocate to the front and back of the cell, respectively (Iijima and Devreotes, 2002). See Figure 1 for signaling cascade.

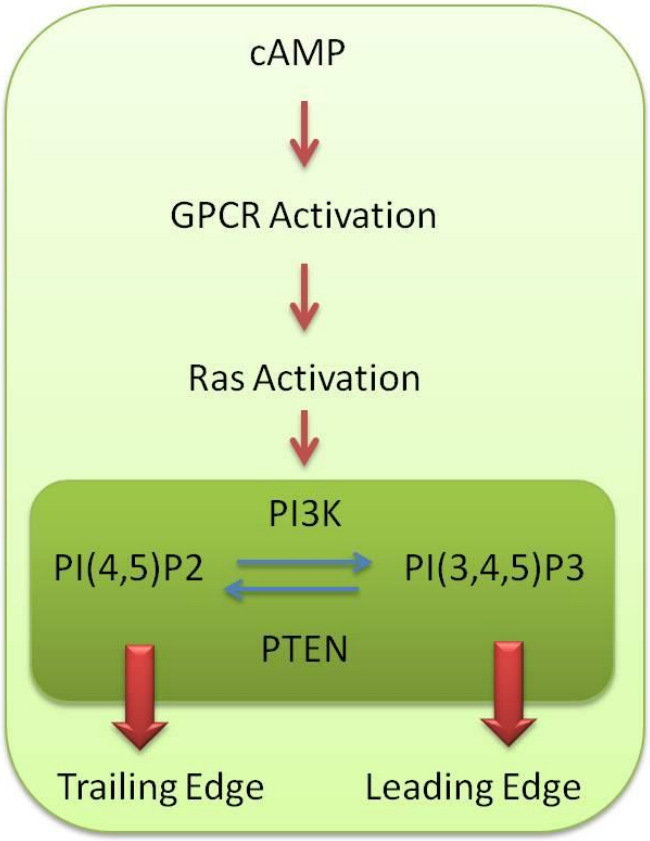

Figure 1. Phosphoinositol distribution after receptor activation When G protein coupled receptors bind cAMP, they become activated. This leads to several downstream events, of which one of the earliest is the activation of Ras. Ras activates PI3K and PI(3,4,5)P3 levels increase at the leading edge, while its antagonist PTEN converts PI(3,4,5)P3 to PI(4,5)P2 and localizes to the trailing edge of the cell. This creates areas of high PI(3,4,5)P3 at the leading edge of the cell and may contribute to high PI(4,5)P2 levels at the trailing edge of the cell.

Dictyostelium heterotrimeric g proteins and functions

The putative folic acid receptor and the *Dictyostelium* cAMP receptors are coupled to heterotrimeric G proteins (Gα, β and γ) which mediate the majority of the signaling responses (Bagorda and Parent, 2008). To date, 14 Gα subunits, one Gβ (although there is another putative Gβ subunit of unknown function) and a single Gγ subunit have been identified in the *D. discoideum* genome (Eichinger et al., 2005). The Gα2 subunit couples to the cAR1 receptor and is essential for development and chemotaxis toward cAMP, while the Gα4 subunit is critical for folic acid-mediated chemotaxis (Hadwiger et al., 1994; Janetopoulos et al., 2001; Kumagai et al., 1991). The Gα4 subunit is homologous to the Gα2 subunit and has 41% amino acid sequence identity (Hadwiger et al., 1991).

Cells lacking Gα2 fail to aggregate or display typical chemoattractant induced responses. In addition, Gα2 is required for receptor G-protein coupling (Wu et al., 1995). Work in the Devreotes lab also investigated the structure and function of the *D. discoideum* Gγ and demonstrated that this subunit is necessary for anchoring Gβ to the membrane. Deletion of a CSVL motif in the carboxy terminal of Gγ leads to the relocation of Gβ to the cytosol. In addition, cells with this truncation were unable to sense a cAMP gradient (Zhang et al., 2001). Biophysical approaches including Förster resonance energy transfer (FRET) and fluorescence recovery after photobleaching (FRAP) showed that the G protein subunits continuously shuttle from a cytosolic pool to the plasma membrane regardless of whether they were active or inactive (Elzie et al., 2009). Interestingly, the Gα2 subunit demonstrated a longer half time on the plasma membrane when cells were in the presence of cAMP. The resident time on the plasma membrane of the Gβγ complex did not change, showing very strong evidence for the complete dissociation of the heterotrimer when in the active state.

It is still unclear whether the Gα2, presumably in an active GTP bound state, is coupled to the receptor or another binding partner at the inner leaflet of the plasma membrane when

cAMP is present (Elzie et al., 2009). These data suggest that the Gα-subunit might locally activate downstream effectors, whereas diffusible Gβγ subunits could potentially act as inhibitory molecules. This fits a model proposed by Levine and colleagues (Levine et al., 2006), which suggested that the G proteins themselves make good candidates for the activator and inhibitor molecules that have been proposed to underlie the large gain seen in the responses at the leading edge during gradient sensing. The data presented in the Elzie paper (Elzie et al., 2009) suggest that the Gα subunit remains local and the Gβγ subunits diffuse away. Further support for this idea comes from single-molecule analysis of cAR1-YFP, which was shown to have two different receptor populations in the absence of signaling. Some were immobile and some were mobile, suggesting that some cAR1 is not precoupled to the G protein (de Keijzer et al., 2008). The authors further found that the immobile fraction was almost identical in chemotaxing cells to that seen at the leading edge of cells lacking the Gα2 subunit. They interpreted this to mean that there was uncoupling of the receptor from the G proteins in response to cAMP. Taken together with the FRAP results, the single molecule results suggest that the Gα2 subunits might be interacting with the receptor directly, but binding the membrane or proteins on the membrane after receptor activation. This local increase of Gα2 subunits at the front of a cell may in turn provide the molecular component for the initial linear amplification that occurs during gradient sensing.

Morphology

When *Dictyostelium* cells are starved, they launch a developmental program during which cells aggregate and form a multicellular fruiting body. In the early stages of this process, starved cells begin to secrete and respond to cAMP, become elongated, and over the course of several hours polarize with a distinct front and rear. Vegetative *Dictyostelium* cells, on the other hand, remain very unpolarized, even while migrating up a folic acid concentration gradient. While the physiological conditions of these two cellular states are fundamentally different, the

signaling mechanisms regulating their directed movement are thought to be very similar (Srinivasan et al., 2013b).

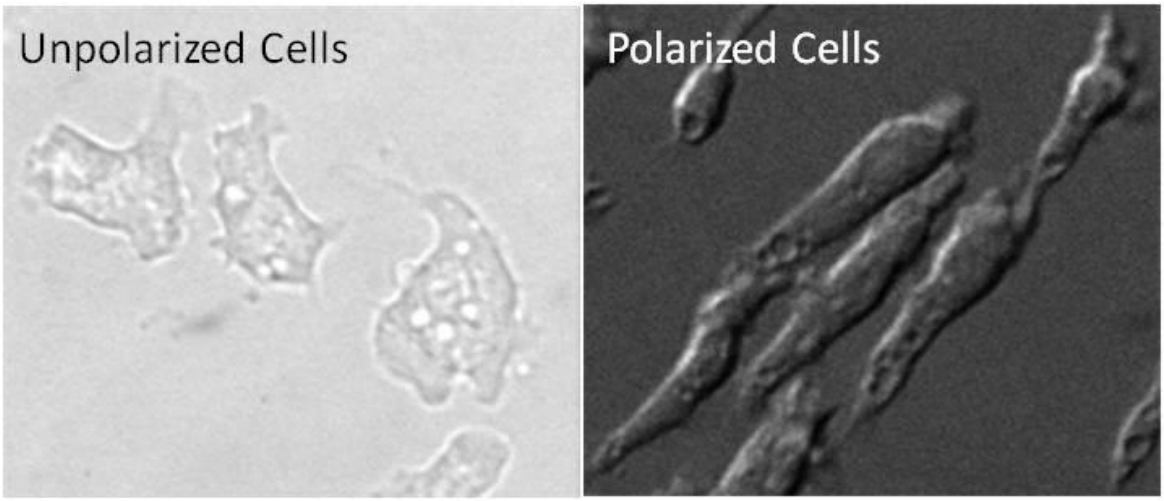

Figure 2. Morphology differences in polarized versus unpolarized cells Unpolarized cells which migrate toward folic acid extend random pseudopods and do not have a distinct front and back (Left). Polarized cells that migrate toward cAMP have an elongated morphology and have a distinct front and back (Right).

I have approached the question of cell polarity from two angles. The first question focuses on the difference in migration between polarized and unpolarized cells and the advantages of having a polarized morphology. In order to address this question, we used unpolarized cells that migrate toward folic acid and polarized cells that migrate toward cAMP and compared the mechanisms regulating their motility in an open microfluidic assay. The second question regarding polarity was focusing on cells that migrate toward cAMP. Since these cells are highly polarized, we wanted to see what events, both cytoskeletal and signaling, contributed to the establishment of polarity. To answer these questions, we developed a more sophisticated open microfluidic system that allowed me to break down and reestablish the polarity of cells expressing known polarity markers. I measured the spatio-temporal localization

of these markers to see the sequence of events that lead to the establishment of polarity after the chemoattractant gradient was inversed. I will compare these findings with some of the currently established models thought to regulate cell polarity. We will also use the findings from our experiments to expand on these models.

Current assays for studying chemotaxis and their limitations

The standard method for visualizing chemotaxing eukaryotic cells, including *D. discoideum*, has been to perform a micropipette assay in an open chamber on an inverted microscope (Parent et al., 1998). William Pfeffer first used a pipette assay to study the chemotaxis of bacteria and flagellates in the late 1880s (Bunning, 1989). Typically, today's devices have a one-micron diameter opening at the tip of a micropipette, which is used to set up a diffusion gradient across a microscope coverslip. Cells then crawl on top of the glass and make their way toward the micropipette. Other methods used for chemotaxis assays make use of devices such as the Boyden chamber (or more recently the Transwell Assay) (Boyden, 1962), Zigmond chamber (Zigmond, 1977), or the Dunn chamber (Zicha et al., 1997). While all three devices are capable of making linear gradients, these gradients change over time and cannot easily be controlled. In addition, only the Zigmond and Dunn chambers allow the viewing of cells during their migration. With the advent of microfluidics, numerous groups are making use of devices that contain microchannels for generating chemical gradients. These channels are on the order of the physical scale of biological cells and have several applications for cell culture as well as single cell analysis (Andersson and van den Berg, 2003; El-Ali et al., 2006; Young and Beebe, 2010). Such devices can provide cells with three-dimensional environments that may be more typical of what they experience in nature (Cukierman et al., 2001; Hegerfeldt et al., 2002; Knight et al., 2000; Wolf et al., 2003).

Microfluidic cell culture environments have been touted as being uniquely suited for achieving a level of quantification and gradient control that is required for correlating observed cell responses with specific gradient characteristics. A thorough review on different gradient generating devices can be found from reviews by (Wu et al., 2013) and (Keenan and Folch, 2008). The two broad categories for microfluidic gradient generating devices are flow-based and flow-free devices (Wu et al., 2013). While their small size gives them certain advantages, flow based devices require constant fluid flow and can often fail to form reproducible gradients in circumstances where air bubbles or other obstructions intrude. Fluid flow subjects cells to confounding or damaging shear and drag forces, and can cause the gradient upstream to differ from the gradient downstream (Keenan and Folch, 2008; Walker et al., 2005). It is possible to avoid shear forces by creating microfluidic devices that rely on passive diffusion to establish a gradient without flow, and these devices can readily include structural elements designed to restrict the motion of cells (Skandarajah et al., 2010). Indeed, several groups have investigated a number of cell types using microfabricated channels that responded to passive gradients (Butler et al., 2010; Taylor et al., 2005). However, closed microfluidic devices often require a complicated cell loading process or are difficult to keep in working condition and free of air bubbles.

Microfluidic devices have also been adapted for the study of *Dictyostelium* by several groups (Amselem et al., 2012; Beta et al., 2007; Fuller et al., 2010; Meier et al., 2011; Wright et al., 2012) to name a few. A more recent device (Meier et al., 2011) that is closest to the signaling cascade as well as polarity studies presented in this thesis uses a flow based setup to study the role of PI3-kinase in cell polarity. The device allows for the generation and switching of a stable gradient, as well as a low flow velocity to provide negligible shear stress on the cells. However, for polarity studies, cells in this experimental setup could also respond to the new gradient either by turning toward it or readjusting their polarity as opposed to completely breaking down and reestablishing it.

One of the goals of my work on polarity studies is to design and build a microfluidic device that allows easy cell loading, generates a stable passive gradient to eliminate shear force effects and provides the ability to confine cells to allow for complete breakdown and reestablishment of their polarity. As such, the Janetopoulos laboratory has developed the Open Microfluidic Device (Jowhar et al., 2010) that uses the combination of both microfluidic and micropipette assays to create an experimental platform that is best suited for polarity studies and that can be adapted for both *Dictyostelium* as well as neutrophil chemotaxis.

Thesis focus

The focus of this thesis is on the study of cell polarity and its role during the directed migration of eukaryotic cells. In order to accomplish this task, we had to develop a novel chemotaxis assay that would allow us to probe the role of polarity in response to chemical gradients. In Chapter II, I will describe the materials and methods used for performing experiments and analyzing the data. I will focus on the development, design, fabrication and analysis of our open microfluidic system for chemotaxis as well as the different quantification tools that we have used to analyze the behavior of the chemical gradient and the response of the cells such as protein localization, signal increase etc. There will also be a strong argument as to how it can be adapted for mammalian chemotaxis. Chapters III and IV will investigate two different aspects of polarity during chemotaxis. In Chapter III, I will look at the role of polarity during chemotaxis, specifically focusing on the difference between unpolarized cells that chemotax toward folic acid and highly polarized cells that chemotax toward cAMP and how polarity affects their behavior. I will use the open microfluidic system that I developed in the Janetopoulos lab to look at the role of polarity played during chemotaxis. In Chapter IV, I will delve deeper into the role of polarity during chemotaxis, particularly by looking at how polarity is established and maintained, the signaling and cytoskeletal components that are responsible for

it and the timeline of these processes. This section will reveal the localization of several fluorescent biomarkers known to localize to certain regions of the cell that are mentioned in the introduction. The molecules and activities that will be focused on are Ras activity, PI(3,4,5)P3 (also known as PIP3), PTEN (a marker for PI(4,5)P2 (also known as PIP2)), F-actin, and labeled tubulin (microtubules). I will examine the role of phosphoinositols in establishing cell polarity during chemotaxis and address the role of PIP3 and PIP2 in establishing polarity. Experiments performed in the open microfluidic system will break down cell polarity and reestablish it. This will allow the observation of the spatiotemporal behavior of these molecules and help elucidate their roles during polarity establishment. Chapter V will have the conclusions and future directions of this project in order to improve our overall understanding of the polarity establishment process during eukaryotic chemotaxis.

*Work for this introductory chapter has been adapted from the following manuscripts.

Jowhar, D., and C. Janetopoulos. 2013. The Chemotactic Compass. *In* Dictyostelids. Springer-Verlag Berlin Heidelberg.

- Jowhar and Janetopoulos wrote manuscript

Jowhar, D., G. Wright, P.C. Samson, J.P. Wikswo, and C. Janetopoulos. 2010. Open access microfluidic device for the study of cell migration during chemotaxis. *Integrative biology : quantitative biosciences from nano to macro*. 2:648-658.

- Janetopoulos and Jowhar devised concept for device. Wikswo and Samson provided input for device design. Jowhar designed and built device. Jowhar, Wright and Janetopoulos designed cell experiments. Experiments and data analysis were performed by Jowhar and Wright. All authors read manuscript and provided input.

CHAPTER II

MATERIALS AND METHODS

In this chapter, I will describe the technical portion of the work on studying cell polarity. In the first portion of chapter II, I will describe how the device was designed, built, characterized and functionalized for chemotaxis. In the second section, I will show how cells are prepared for these assays and convey other technical specifications for this project.

Device design and production

To accomplish the goals for studying cell polarity, I devised a chemotaxis device that makes use of microfluidic and micropipette technology to generate shallow gradients in microchannels which can be tailored to the dimensions of cells that are being assayed. For simple chemotaxis studies, we used a single micropipette to generate variable gradients. For studies involving the breakdown and reestablishment of cell polarity by gradient switching, two micropipettes were used to generate opposing gradients. Both of these devices are easy to use and can be functionalized to perform a variety of studies.

Open microfluidic device for chemotaxis studies

Open-faced channels are microfabricated in PDMS and then plasma bonded to a glass cover slip to form the closed channels (Figure 3A and B). The gradient is formed by a micropipette attached to a micromanipulator and pump. The glass surface forms the bottom of the device where the cells are attached and viewed. The PDMS structure defines the ceiling and the walls of the device. Two devices were created (see Figure 3C–F). One scheme had two

very wide channels (100 µm) while the other device was created with a tandem repeat of four different widths (6, 8, 10 and 12 µm, respectively). The 100 µm width simulated a region where cells could migrate without the confinement of the narrow channels. The ceiling height of both devices was approximately 15 µm. The height of the PDMS (2 mm) was less than that of the fluid depth. The OMD was designed using the AutoCAD software package (Autodesk, San Rafael, CA). Ten channels with an approximate height of 5 µm, width of 6 µm and length of 150 µm were used for the reversal experiments. These dimensions ensure that the cells do not turn when the gradient is reversed but instead break and reestablish their polarity.

Device fabrication processes

The device design was transferred to a chrome mask using a commercial printing process (Advance Reproductions, North Andover, MA). The chrome mask was then used to create a three-dimensional mold using photolithography techniques. In short, a silicon wafer was coated with the negative photoresist polymer SU-8 2010 (Microchem Corp., Newton, MA) which cross-links when exposed to a UV light source. The thickness of the SU-8 coating was controlled by spinning the wafer at the speed and duration recommended by the resist manufacture in order to create the desired height profile of 15 µm. The chrome mask was then placed on top of the coated wafer and exposed to a UV light source (Exfo Novacure 2100 UV). This caused the exposed regions on the resist to crosslink, which, in turn, were the only features that remained on the silicon wafer after a solvent solution of SU-8 developer removed all of the unexposed pre-polymer. The final silicon wafer mold thus consisted of a pattern of 15 µm tall raised structures composed of solidified SU-8. This served as the mold to be used in the microfabrication process. PDMS (Sylgard 184, Dow Corning, Midland, MI) was poured onto the SU-8 and silicon mold and degassed to get rid of air bubbles, and was cured in an oven at a temperature of 65 °C overnight (Camelliti et al., 2006). The cured flexible PDMS device was peeled from the silicon wafer, and the cell loading port was punched out using a hollow punch. The front of the device was cut using a sharp cutter to expose the channels that face the

micropipette. A one-well chamber with a glass bottom (Lab-Tek, Rochester, NY), along with the PDMS slab containing the channels and the cell port, was placed in a plasma cleaner (Harrick Plasma - Plasma Cleaner, Ithaca, NY) for approximately 30 - 40 seconds. After removal from the plasma chamber, the side of the PDMS slab with the channel patterns was pressed onto the bottom of the one-well chamber where it formed a permanent seal. Immediately after the bonding process, the device was wetted using developmental buffer (DB) in order to keep the microchannels hydrophilic and allow for loading of cells for the experiment.

A new device is made for every experiment. Devices were not reused from one day to another. Since experiments that use devices for polarity studies are limited by the number of devices that are made, the number of data points is lower when compared to an experiment that does not use devices such as a micropipette assay.

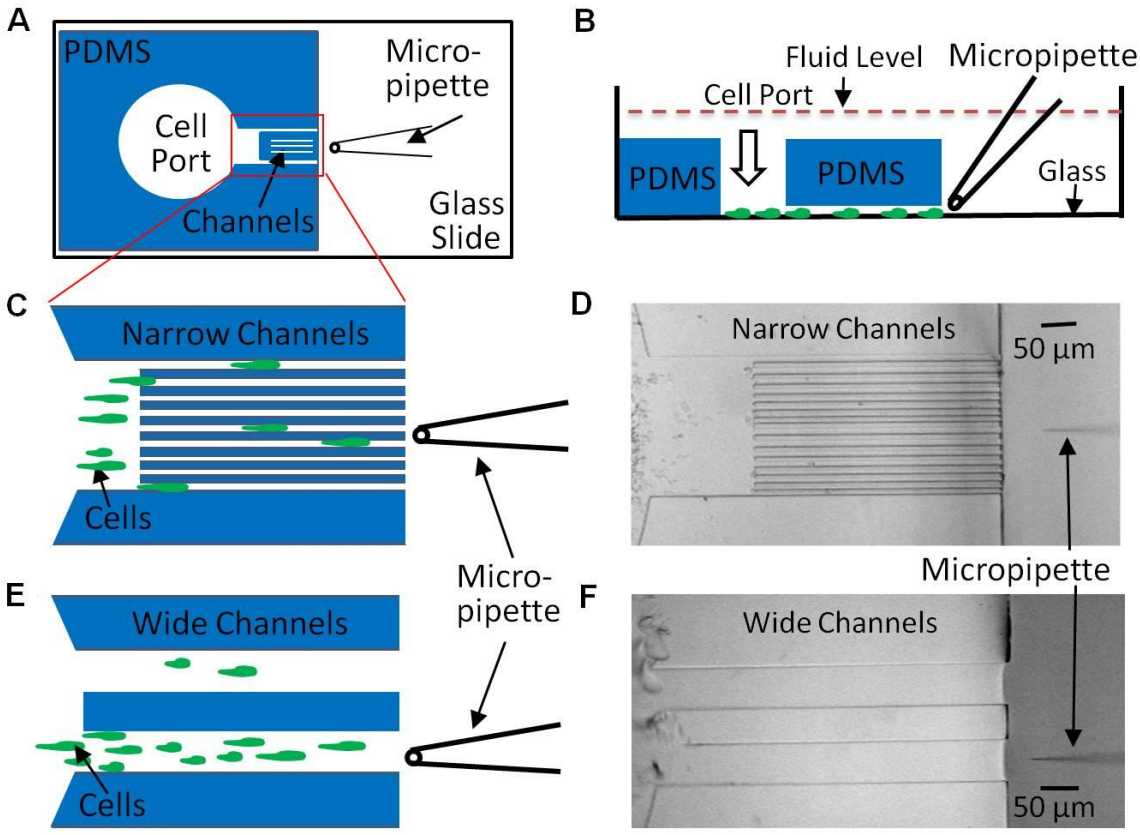

Figure 3. The open microfluidic device (OMD) for studying gradient sensing and cell migration (A) Schematic diagram of an open microfluidic device viewed from the bottom. The PDMS block containing cell port and channels is plasma bonded to the glass cover slip of a one-well chamber. A micropipette filled with chemoattractant is placed in front of the narrow channel region. (B) A side view of the device in 3A depicting cells loaded through the cell port and crawling on the glass surface toward the micropipette. Note that entire device is submerged in buffer solution so that hydrostatic pressure is essentially equivalent on the inside and outside of the device. (C) Magnified cartoon of the narrow channel region with cells crawling between the different-sized channels toward the micropipette placed at the center of the device. In the actual device, there are 16 channels with each size represented 4 times. The channel widths are 6 mm, 6 µm, 8 µm, 8 µm, 10 µm, 10 µm, 12 µm, 12 µm, 6 µm, 6 µm, 8 µm, 8 µm, 10 µm, 10 µm, 12 µm and 12 µm. (D) A bright field image of the device with the narrow channel region described in 1C was obtained using a 10 X objective. (E) Schematic of two wide channel regions with a cartoon that depicts cells crawling toward the micropipette. The width of each wide channel is 100 µm. The micropipette is placed at the center of the bottom wide channel. (F) Bright field image acquired using a 10X objective of the device with the wide channels.

Gradient measurements

The OMD provides a more precisely measured gradient profile when compared to those measured using a micropipette alone since the gradients that cells encountered in the OMD were measured directly without contributions from out-of-focus fluorescence. In an open dish, the observed fluorescence represents a projection into the optical plane of out-of-focus light from a radially-decaying spherical chemoattractant distribution. Hence in the OMD the gradients were approximately linear rather than $1/r^2$ (Gruver et al., 2008).

A micropipette supplying Cy3-cAMP resulted in a stable gradient in both the narrow and wide channel regions within the microfluidic device. A pumping pressure of 50 hecto Pascals (hPa) was applied to the micropipette in these experiments. Using this pressure, a gradient was clearly visible (Figure 4A and D). These gradients were measured in the various channels. Concentration profiles had similar slopes with different mean concentrations (Figure 4B and D). As would be expected from the radial distribution of label around the micropipette tip, the highest fluorescence intensity was measured in the 12 µm channel nearest to the micropipette and gradually decreased for those channels farther away (see Figure 5). This made the OMD useful in that it provided unique experimental conditions that varied in each channel. To demonstrate the differences in gradient profiles that cells might encounter at various points along two channels, we measured the relative changes in pixel intensities (Figure 4B) that 30 µm long cells might encounter in a typical gradient like that depicted in Figure 4A. The change from front to rear of both cells early on was similar (about 11%, cells on right) and later (15% for cell 1 and 16% for cell 2, both on left). The mean concentration eliciting a response, however, was dramatically different (several fold) in the two channels. Yet in our experiments, we detected little difference in speed between cells in channels near and far from the micropipette, suggesting that cells respond to the relative concentration gradient and not the absolute concentration.

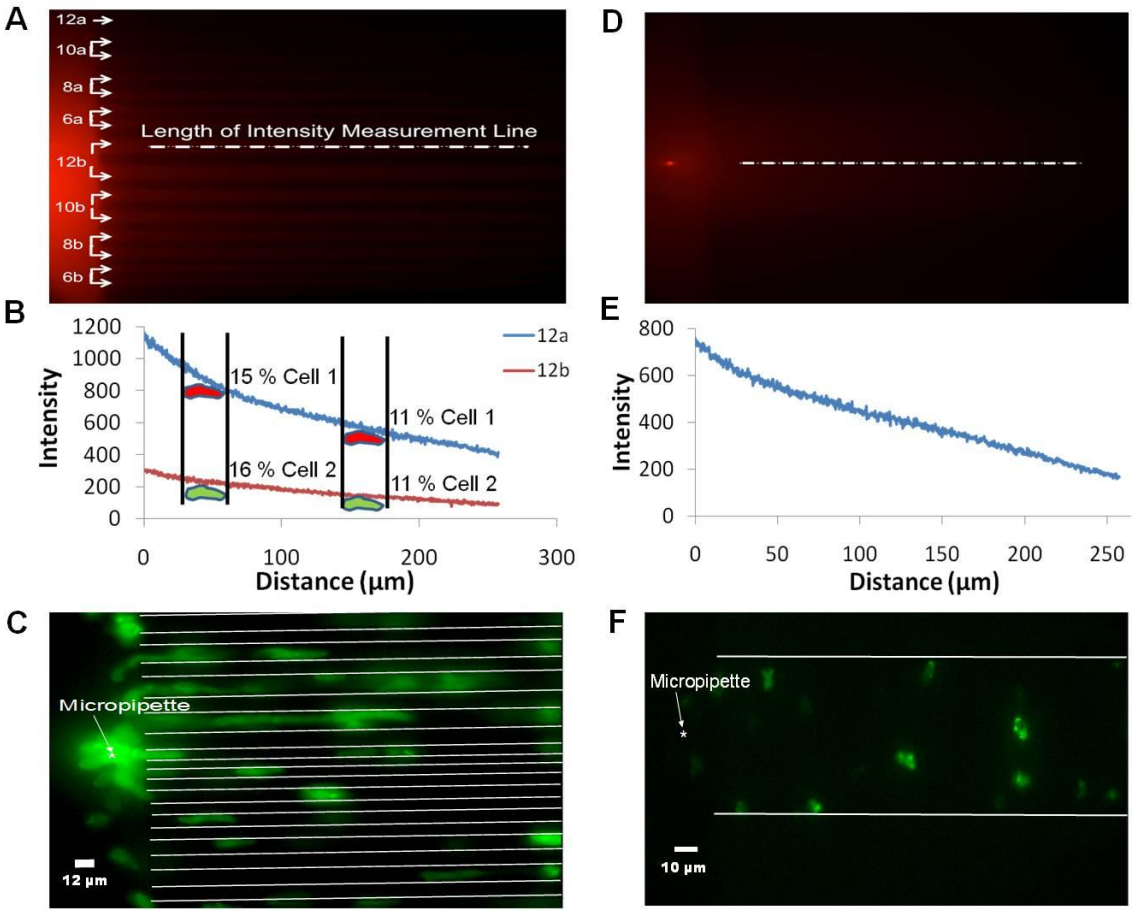

Figure 4. Gradients and cells in the OMD (A) A Cy3-cAMP image of the narrow channel configuration with pumping pressure of 50 hPa. The micropipette was placed in the center of the channel region. The number corresponds to the size of the channel, in microns. For instance, channels labeled 12b are the two middle channels and are both 12 µm wide. The dotted white line drawn across the top 12b channel is representative of where pixel values were obtained for the two channels displayed in 2B. (B) Pixel intensity values as a function of distance for channels 12a and the top 12b are shown in 2A. The intensities were measured along the length of the representative dotted white line as shown in the center of 12b in 2A. Average intensities for the other channels are shown in Figure 5. We measured the relative change in chemoattractant a cell might see if it were at two different points in two different channels. The hypothetical change from front to rear of both cells early on was similar (about 11%, cells on right) and later (15% for cell 1 and 16% for cell 2, both on left). The mean concentration eliciting a response, however, was dramatically different (several fold) in the two channels, suggesting that the mean concentration has little if any effect on migration speeds. (C) Unpolarized and polarized cells crawling toward a micropipette containing both cAMP and FA in the narrow channel configuration. (D) Cy3-cAMP image of the wide (100 µm) channel with pumping pressure of 50 hPa. The micropipette was placed in the center of the wide channel. The white line drawn along the center depicts where the intensities were obtained. (E) Pixel intensities as a function of distance for the 100 µm wide channel region shown in 4D. The intensities were measured along the length of the white line. Five lines were drawn along the wide channel and the average

Gradient characterization

The gradient characterization was done using 1.0 mM of Cy3-cAMP, which was loaded into an Eppendorff femtotip and released in front of the channel structures. Fluorescent images were taken of the region. The intensity profile of the Cy3 fluorescence was measured using Image J's Plot profile feature (U. S. National Institutes of Health, Bethesda, MD) and the intensity values were plotted as a function of distance using Microsoft Excel (Redmond, WA). To measure the gradient in the narrow channels, 1.0 mM Cy3-cAMP was pumped at 50 hPa in front of the narrow channels. The intensity was calculated using SlideBook software after subtracting the background intensity. Figure 5 shows designations of ''a'' and ''b'' after the numbers. ''a'' stands for above and ''b'' stands for below the micropipette. For example, 6 ''a'' represents the average intensity values of the two 6 μm channels that are at the top of the image. The intensities were measured along the same distance for each channel (see Figure 4B and Figure 6). The change in Cy3-cAMP across cells in Figure 4B was calculated as:

$$\text{Percent difference} = \left|\left(\frac{(x1-x2)}{(x1+x2)}\right) \times 100\right|$$

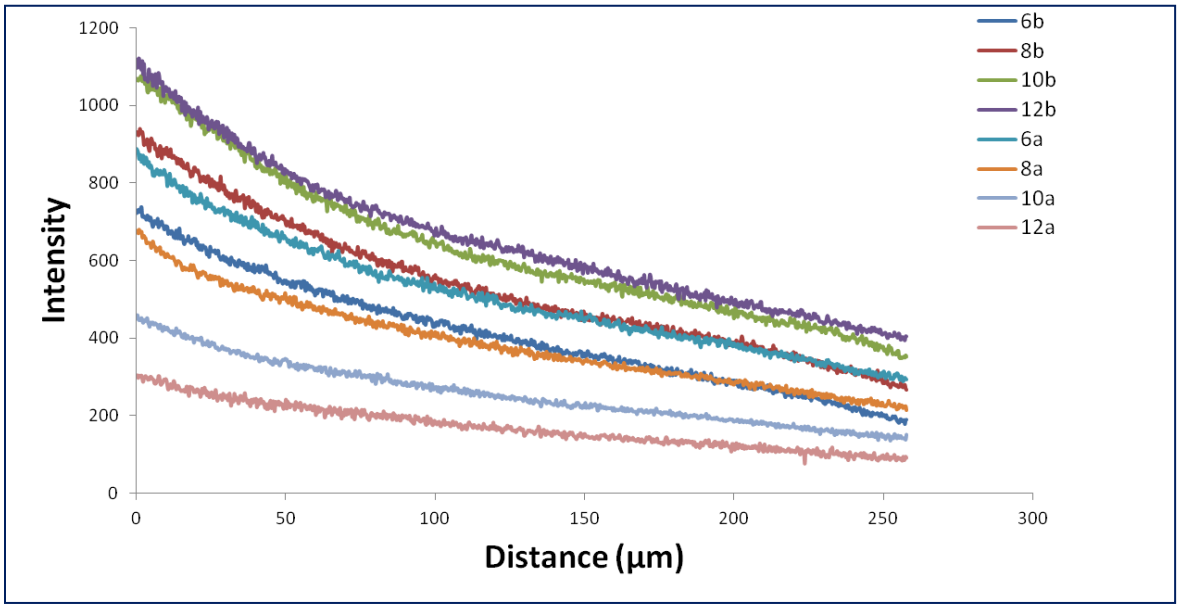

Figure 5. Gradient measurements in different channels Pixel intensity values were measured for all of the channels depicted in Figure 4A. The intensities were measured along the length of the representative dotted white line as shown in the center of 12b in Figure 4A. Each curve represents the average of two channels that are the same size, and right next to each other. The exception is channel 12a, because the other 12 micron channel was outside the captured image and could not be measured.

Gradient stability over time

While typical chemotaxis assays generally only last 20–30 min, we did provide data of cells chemotaxing for several hours. The time limitation in these experiments is typically dependent on the clogging of the micropipette or the channels by the cells. To measure the stability of the gradient, 10 mM fluorescein (FITC) was pumped at 50 hPa in front of the wide channel region. FITC has a mass similar to cAMP (332.306 g mol^{-1} versus 329.06 g mol^{-1}, respectively). Time lapse images were captured every five minutes for over two hours. The gradient was measured by drawing a line and measuring the pixel intensities in the center of the channel for all the time points using software provided by SlideBook. These data are provided in Figure 6.

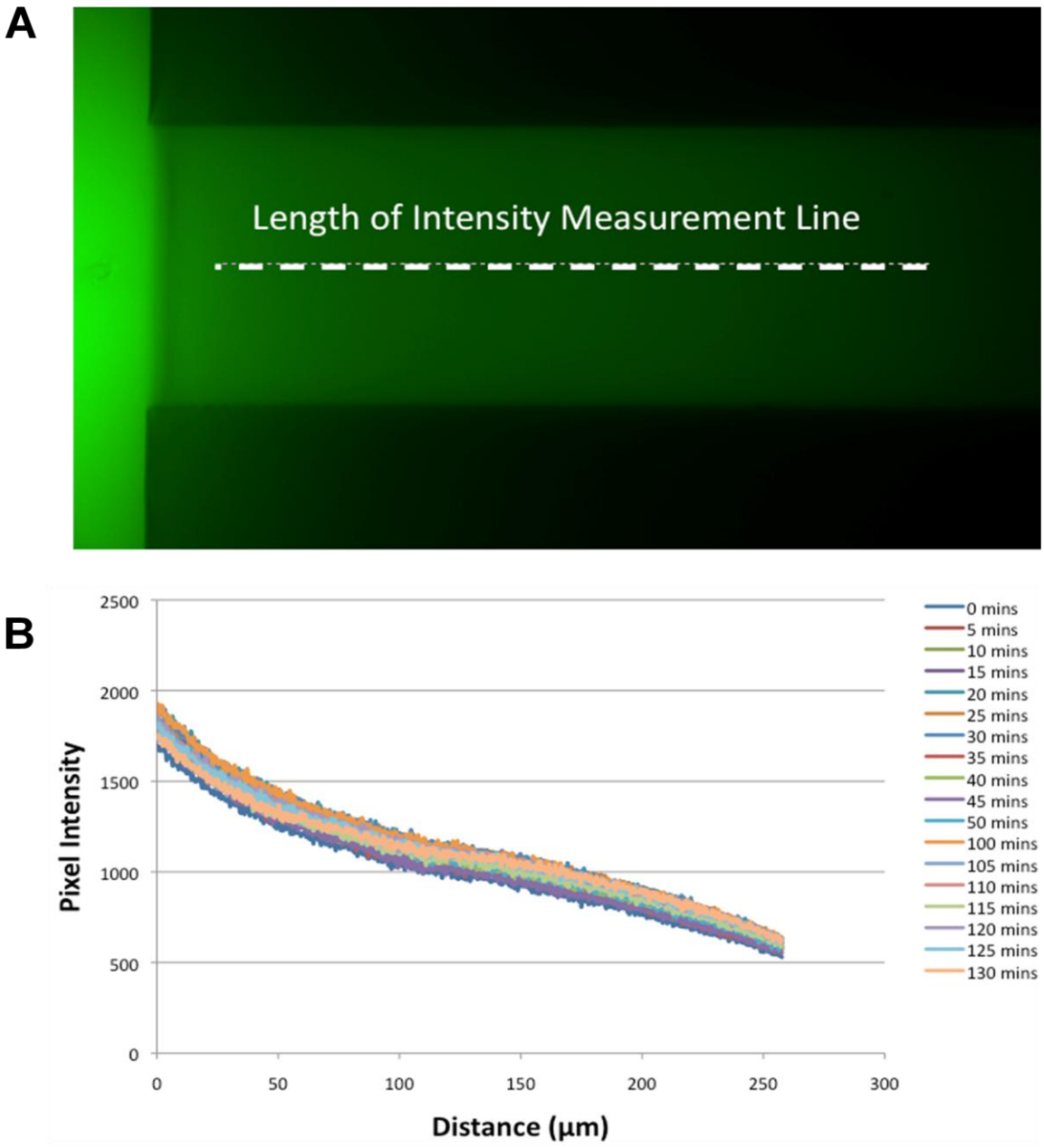

Figure 6. Gradient stability of open microfluidic device A) The stability of the gradient was measured using 10 µM FITC, which was pumped at 50 hPa in front of the wide channel region. FITC has a mass similar to cAMP (332.306 grams/mol versus 329.06 grams/mol, respectively). Time lapse images were captured every 5 minutes for over two hours. B) The gradient was measured by drawing a line and measuring the pixel intensities in the center of the channel for all the time points using software provided by SlideBook.

Experimental setup for polarity reversal experiments

Polarity reversal experiments make use of two micropipettes filled with cAMP and which are connected to a pump. Gradient switching was achieved by turning off the pump that drives the first micropipette and turning on the pump that drives the second micropipette. The pumping pressure can be increased or decreased in order to adjust the gradient. Cells expressing fluorescent biomarkers are lured into microfluidic channels toward the first micropipette. Once the cells are in the channels, the gradient is switched by turning off the first micropipette and turning on the second micropipette.

Device surface coating for HL-60 chemotaxis

In order to functionalize the device for mammalian chemotaxis, I coated the glass portion of the device with Fibronectin which was diluted in Hank's Balanced Salt Solution. Briefly, once the PDMS containing the patterns of the microchannels was bonded to the bottom of the one well chamber, the fibronectin solution was applied. Once it had been incubated at room temperature for an hour, the excess fibronectin was removed by washing with dH_2O two to three times. The entire device was then filled with Hank's Balanced Salt Solution (HBSS). The protocol can be found from the Santa Cruz Biotechnology website at the following web address: (http://datasheets.scbt.com/sc-29011.pdf).

Imaging

Imaging for Chapters III and IV was conducted on a Marianas Workstation equipped with a Cool Snap CCD camera and an Extended QE, high-speed cooled CCD camera (Cascade II 512). We used an inverted, wide-field epifluorescence microscope (Zeiss Axio Observer Z1, Thornwood, NY). Images were taken using SlideBook software (Intelligent Imaging Innovations,

Inc., Denver, CO). Time lapse images were taken every 15 seconds for approximately 2 hours. Confocal Imaging for Chapter IV and V was done on an inverted Nikon spinning disk confocal microscope in conjunction with Metamorph software using a 40 X oil objective. All time lapse images were acquired with a five second interval between frames. Post acquisition image processing was done using FIJI software (Schindelin et al., 2012). Super resolution imaging for Chapter IV was conducted using the Bessel Beam setup at the Betzig Lab as described in (Habib et al., 2013).

Image quantification

Bleach correction

All bleach correction was done in FIJI using Image>Adjust>Bleach Correction. The Simple Ratio algorithm was used. This can be found at the following website: (http://cmci.embl.de/downloads/bleach_corrector#bleach_corrector). The background noise was found by selecting an ROI outside the cell area. The average intensity was measured for the ROI in each frame by using Image>stacks>plot z axis profile. The obtained values were fit into an exponential curve with offset. The background value was determined from the constant in the exponential function.

Cell selection criteria

For all data analysis, only fluorescent cells that were able to reverse their polarity in the field of view were used. The analyzed cells were also not touching one another. There were cells that did not reverse their polarity even though the gradient was switched. These cells were not used for analysis.

Cell speed

The speed of the cells for Chapter III was measured by manually tracking the pixel distance the cells travelled and converting it to microns. The distance was divided by the time it took to capture each frame. This was done using SlideBook software.

Cell length

The average of the image stacks was taken for each frame. A threshold was defined that gave pixel values only to the area defined by the cell. The length of the cell was measured from the left most corner to the right most corner. The distance in pixels was converted to microns.

Kymographs

Image stacks were resliced using FIJI. The average of the generated images was taken to create a kymograph with the Y-axis representing time and the X-axis representing distance. Kymographs were quantified by taking the slope of either the leading edge or the trailing edge and calculating the speed with which they move. Threshold of the images was determined to outline the kymograph and select regions before, during and after polarity reversal were measured.

Signal peak

Automatic thresholding to find the borders of the cell were used to find the length of the cell for each time point. The cell length was divided into 3 equal parts to designate the new cell front, cell middle and cell rear. The fluorescence intensity was measured for each section from the time point of gradient reversal till the end of the experiment. The maximum signal for each time point was plotted as a function of time to measure the peak of signal intensity after gradient reversal.

Cytosol intensity measurement

The RFP and the GFP channels were corrected for bleaching using the Simple Ratio method. A scaling factor between the green and the red channel was found by selecting identical Regions of Interest (ROI)s in both channels. By finding the scaling factor, the Red

channel's pixel values were normalized with the green channel. Three identical ROIs were selected for three different cells expressing RBD-RFP and PTEN-GFP and the cytosolic intensity in these regions was measured as a function of time. It was normalized on a scale of 1 - 0.

Signal at "old" location vs. "new" location

For Ras activity and PIP3 (old front), the bar graphs generated were measured by taking the peak intensity at the old front of the cell at the time point when the gradient was switched. For new front, the first time point when the cell moved forward was used. For PTEN (old back) represents the signal intensity at the old back of the cell at the time point that the gradient was changed. New back represents the signal intensity at the time point where the new back retracted toward the high side of the gradient.

Fold increase

Fold increase was measured by taking the ratio of the signal intensity at the new front: old front at the time points of gradient change and forward movement of the cell front for Ras activity and PIP3. For PTEN new back: old back was taken at the time points of gradient change and new back retraction.

Statistical analysis

Statistical analysis for data points was done using student t test using Microsoft Excel (Redmond, WA). To determine if the increase in signal intensity at the new cell front (for Ras activation and PIP3) or the new cell back (PTEN) was significant, student's t-test was used (Figure 15). First the cell was divided into three equal portions (Front, Middle and Back). Next, for Ras and PIP3, the signal intensity at the back (future front) of the cell was measured at the time point when the gradient was switched. The signal intensity was also measured at the same location (which is now the new front) at the time point when the cell moved forward. The ratio of the two signals were taken to determine the fold increase. For PTEN, the same procedure was applied but in this case the signal intensity for the two time points was measured at the future

back. Since every polarity reversal experiment requires the fabrication of a new device for each day of data collection, the sample numbers are reduced as compared to a micropipette assay in a one well chamber.

Standard error of the mean

All error bars in this thesis are generated from the standard error of the mean. This was calculated by taking the standard deviation of the data points and dividing by the square root of the total number of data points.

Cell reversal

The time point of cell reversal was determined by finding the first frame after gradient reversal where the cell retracted its new back or extended its new front. For Ras activation and PIP3 localization, the time point of leading edge extension toward the new gradient was used. For PTEN, the time point of cell back retraction toward the new gradient was used. Signal intensity at old back/front is measured at the first time point that the gradient is switched whereas signal intensity at the new back/front is measured at the time point when the cell's back retracts toward the new gradient or the cell's front moves forward toward the new gradient.

Cell Line Preparation

Cells lines and plasmids

Wild-type (AX2) cells expressing fluorescent markers were used. The cells were electroporated as described by (Knecht and Pang, 1995). The markers were Raf Ras Binding Domain fused to the Red Fluorescent Protein (RBD_{Raf}-RFP) for Ras activity(Kortholt et al., 2011). PTEN-GFP in PTEN null cells for PTEN as described in (Janetopoulos et al., 2005), PTEN GFP in PLC null cells (Kortholt et al., 2007), α-Tubulin GFP for Microtubules (Octtaviani et al., 2006), PH_{CRAC} for PI(3,4,5)P3 (Parent et al., 1998), LimE RFP for actin polymerization (Clarke et al., 2006), PH CRAC-RFP for PI(3,4,5)P3 from (Chen et al., 2003).

Transformation protocols

Cells were transformed with fluorescent biomarkers using the protocol outlined by (Gaudet et al., 2007). Briefly, cells were pelleted by centrifugation followed by washing with ice-cold H-50 buffer. The cells were pelleted again by centrifugation and resuspended in H-50 buffer. 100 µl of the cell suspension was transferred to a cold 0.1 cm electroporation cuvette containing 10 µg DNA in a volume of approximately 10 µl. The suspension was pipetted up and down to mix the DNA and the cells. Electroporation was done at 0.85 kV and 25 µF twice, waiting for about five seconds between pulses. The cells were then transferred out of the cuvette by adding a few hundred microliters of HL5 from the dish to the cuvette, pipetting up and down to mix and then withdrawing the medium and cells to add them to a Petri dish containing HL5 media. On the next day, the old HL-5 media was changed, and drugs were added to select the cells that have the plasmids containing the fluorescent biomarkers.

Media and buffers

HL-5 and SM Agar were purchased from Formedium. For HL-5 liquid media; 22 g of Formedium HL-5 powder, 10 g of dextrose were added to 1 L of distilled H20 and then autoclaved. For SM media; 41.7 g of Formedium SM agar powder was added to 1 L of distilled H_2O and autoclaved. Development buffer (DB) contained 5 mM Na_2HPO_4, 5 mM KH_2PO_4, 1 mM $CaCl_2$, and 2 mM $MgCl_2$.

cAMP preparation

cAMP was purchased from Sigma. A 10 mM stock solution of cAMP was prepared in dH_2O. For cAMP development the 10 mM stock solution was diluted in 30 ml of development buffer (DB) as described in (http://www.dictybase.org/techniques/media/media.html#DB) to make a 2.5 µM cAMP solution. For cAMP chemotaxis, a 1 mM stock solution was diluted 1:100 in 1 ml of DB to make a 10 µM final concentration.

cAMP development

5 ml of ~ 2 x 10^7 cells / ml of AX2 cells were pulsed with 100 µl of 2.5 µM cAMP every six minutes for six hours with constant agitation. For Figure 13e, 10 ml of 2 x 10^7 cells / ml of AX2 cells were resuspended in 1 ml of DB after washing three times. The solution was then applied to an agar plate and allowed to settle for 30 minutes. Excess DB was removed and the cell was placed upside down for approximately 5.5 hours. Cells were then pipetted with DB from the plate and placed in the 8 well chamber.

Latrunculin-A treatment

Latrunculin-A from Invitrogen dissolved in DB was added to make a final concentration of 5 µM in the cell solution

Uniform cAMP stimulation

For Figure 13 e, a micropipette containing cAMP was pressurized to deliver a bolus of cAMP in the experimental region by using the “clean” feature on the pump that drives the flow out of the micropipette. For Figure 5 E, cells were placed in an 8 well chamber and a drop of cAMP was applied using a P-200 micropipette to create a final concentration of 1 micro molar inside the wells.

Vegetative cells

500 µL of 2 X 10^6 cells ml^{-1} PH-GFP expressing AX2 cells were mixed with ~ 1 X 10^9 cells ml^{-1} *Klebsiella. aerogenes* bacteria from an SM agar plate and the mixture was plated on an SM agar plate. The mixture of cells was allowed to incubate at room temperature overnight. For experiments, the mixture of cells from the SM plate was washed several times in development buffer (DB) to wash off the bacteria. After washing, the *D*. *discoideum* cells were resuspended in 1 ml of DB.

HL-60 cell preparation

Cells were prepared as described in (Sai et al., 2006). For Wortmannin treatment, cells were pretreated at a concentration of 50 nM for 30 minutes at 37°C. During the experiments, the

buffer that the cells were migrating in had the same concentration of Wortmannin during pretreatment.

HL-60 cell experimental setup

Cells were washed twice and resuspended in serum-free RPMI1640 at 2 x 10^6 cells/ml. Cells were then seeded in the device for 5 min at RT. The medium was replaced with 1% BSA/RPMI 1640 medium. The objective used was 40 X oil, with an objective heater set for 37 ° C.

*Work for this chapter has been adapted from the following manuscripts and collaborations.

Jowhar, D., G. Wright, P.C. Samson, J.P. Wikswo, and C. Janetopoulos. 2010. Open access microfluidic device for the study of cell migration during chemotaxis. *Integrative biology : quantitative biosciences from nano to macro*. 2:648-658.

- Janetopoulos and Jowhar devised concept for device. Wikswo and Samson provided input for device design. Jowhar designed and built device. Jowhar, Wright and Janetopoulos designed cell experiments. Experiments and data analysis were performed by Jowhar and Wright. All authors read manuscript and provided input.

Jowhar, Khodadadi, Wright, Rucker, Housman, Wikswo, Chen, Betzig and Janetopoulos, (2013). In preparation.

- Jowhar and Janetopoulos designed concept for experiment setup. Wikswo provided input for data analysis and presentation. Chen and Betzig developed Bessel beam microscopy setup. Experiments and data analysis were performed by Jowhar, Khodadadi, Wright, Rucker, Housman, Chen, Janetopoulos. Janetopoulos, Jowhar and Wright are preparing the manuscript. Janetopoulos, Jowhar and Wright are preparing the manuscript.

Special note for experiments for Chapter IV: All experiments and quantification were performed by Jowhar with the following exceptions.

Experiment for 13e was performed by Janetopoulos and Jowhar
Experiments for Figure 16e were performed by Housman
Experiments and quantification for Figure 19 were performed by Rucker and Khodadadi
Bessel Beam Microscopy (Figure 18c) was performed by Bi-Chang Chen at the Betzig Lab

Collaboration with Richmond Laboratory for HL60 Experiments.

- Dr. Jiqing Sai from the Richmond Laboratory prepared cells and reagents for experiments. Jowhar and Sai performed experiments.

CHAPTER III

POLARIZED VS. UNPOLARIZED CELLS

Introduction

Chemotaxis is a fascinating cellular behavior characterized by the movement of cells up or down a chemical concentration gradient. Directed cell migration plays a critical role in the cell movements that take place during embryo development and are necessary for the day-to-day function of the immune system (Surmi and Hasty, 2010; Thelen, 2001). Chemotaxis also regulates many pathological conditions, including those that involve allergic inflammation and tumor metastasis (Condeelis et al., 2005; De Paepe et al., 2009; Dorsam and Gutkind, 2007; Hansson, 2009; Johnson et al., 2004; Lazennec and Richmond, 2010; Wu et al., 2009). The social amoeba *Dictyostelium discoideum* has played an important role in revealing the mechanisms that control directional sensing and migration. These amoeboid cells are dependent on this process throughout their life cycle, exhibiting chemotaxis toward folic acid during the vegetative state and responding to cyclic adenosine monophosphate (cAMP) during their developmental cycle. Growing *D*. *discoideum* can feed on folic acid secreted by gram-negative bacteria such as *Escherichia coli* and *Klebsiella aerogenes*. When these amoeboid-shaped cells are starved, they launch a developmental program during which cells aggregate and form a multicellular fruiting body. In the early stages of this process, starved cells begin to secrete and respond to cAMP, become elongated, and over the course of several hours polarize with a distinct front and rear.

Vegetative *Dictyostelium* cells, on the other hand, remain very unpolarized, even while migrating up a folic acid concentration gradient. While the physiological conditions of these two cellular states are fundamentally different, the signaling mechanisms regulating their directed

movement are thought to be very similar. Chemotaxing cells can measure and respond to small changes in a chemical gradient, detecting a difference of ~ 5% receptor occupancy over the length of a cell (Ueda et al., 2001).

Studies from a number of research groups have characterized the localization of signaling molecules of *Dictyostelium* cells responding to cAMP gradients. The initial components of the cAMP circuit, such as serpentine receptors and heterotrimeric G-proteins, remain uniformly distributed along the membrane (Janetopoulos et al., 2001; Jin et al., 2000; Xiao et al., 1997). Receptor occupancy and the heterotrimeric G-protein activation mimic the gradient of chemoattractant (Janetopoulos et al., 2001; Ueda et al., 2001). The signaling molecules that regulate phosphoinositide turnover display early signs of a localized response during cAMP gradient sensing (Janetopoulos and Firtel, 2008; Parent et al., 1998).

The small G-protein Ras is critical at this stage and is enriched at the leading edge and promotes the localized activation of key chemotactic effectors, such as PI3-kinase (PI3K) (Kortholt and van Haastert, 2008). PI3K, in turn, is recruited to the anterior plasma membrane of the cell and interacts with its substrate, PI(4,5)P2 (PIP2) and gives rise to PI(3,4,5)P3 (PIP3) (Huang et al., 2003; Merlot and Firtel, 2003). The tumor suppressor PTEN undergoes reciprocal movements and is redistributed to the lateral and posterior membrane of the cell (Funamoto et al., 2002; Iijima and Devreotes, 2002). Moreover, actin polymerization and pseudopod extension preferentially occur in areas where the membrane has high PI3K activity. Positive feedback between the cytoskeleton and the regulators of PIP2 and PIP3 production at the rear and front of the cell, respectively, amplifies these morphological responses, even in the absence of a cAMP gradient (Devreotes and Janetopoulos, 2003; Sasaki et al., 2007). Interestingly, these signaling molecules also are highly regulated during cell division (Janetopoulos et al., 2005), phagocytosis (Cardelli, 2001; Rupper et al., 2001b) and macropinocytosis (Cardelli, 2001; Rupper et al., 2001a). The regulation of the phosphoinositides appears to be a key signaling component for numerous cell processes that regulate changes in the cytoskeleton. These

critical and diverse morphological changes are regulated by a system, which contains a great deal of redundancy, with no one component being required for the circuit to function adequately (Hoeller and Kay, 2007; Insall and Andrew, 2007; Veltman et al., 2008). Recent work has shed new light on the target of rapamycin complex 2 (TORC2), another part of the signaling pathway that is important for *D. discoideum* chemotaxis (Kamimura et al., 2008; Lee et al., 2005). The TORC2 signaling complex is essential for activating mammalian protein kinase B homologs, PKBR1 and PKBA. PKBA contains a Pleckstrin homology (PH) binding domain that triggers the association of the protein with the plasma membrane when PIP3 levels rise. PKBR1 lacks the PH domain and instead has a myristoylation modification and is constitutively localized to the plasma membrane. Recently, the PKB substrates were identified and their phosphorylation states in response to cAMP were analyzed (Kamimura et al., 2008). PKBR1 activation was PIP3-independent and was activated through small G proteins. Recent results suggest that the PKB substrates are phosphorylated by folic acid stimulation in a manner similar to those seen with cAMP addition (Liao et al., 2010).

While there is substantial scientific literature describing the mechanisms that regulate cAMP-mediated chemotaxis, the actual data describing the cellular movements that take place during folic acid-mediated cell migration are quite limited (Korohoda et al., 2002; Laevsky and Knecht, 2001; Sameshima et al., 1988; Veltman et al., 2008). Studies have documented the responses of cells to uniform increments of folate, but little is known about the morphological changes that take place when cells are migrating in a gradient of folic acid (de Wit et al., 1987; Janetopoulos et al., 2005; Kuwayama et al., 1993; Malchow et al., 1981; Rifkin and Goldberg, 2006; Segall, 1988; Wang et al., 1998).

Folic acid appears to bind to a putative seven-transmembrane receptor since cells lacking the heterotrimeric Gα4 subunit are unable to respond to folate (Hadwiger et al., 1994). To aid in the investigation of the cellular properties of cells migrating in response to a gradient of folic acid, a protocol was developed for creating cells that show strong responses to the

chemoattractant folic acid (Srinivasan et al., 2013b). This method will also allow the direct comparison of chemotactic responses between vegetative cells and developed cells to their cognate chemoattractants.

We developed a novel microfluidic device to aid in these experiments. This device allowed the direct, simultaneous observation of both cell types in a highly reproducible and quantitative manner. We wished to compare the relative speeds of cells chemotaxing to either folic acid or cAMP and used this device to study the contributions of cell polarity to the ability of cells to migrate directionally. The effects of microfluidic channel widths on migration rates of unpolarized cells and of developed cells were observed in the presence of folic acid and cAMP respectively. We speculated that the narrow channels might suppress lateral pseudopod extension and increase the probability that anterior pseudopods would extend toward the gradient of folic acid in the unpolarized cells. This, in turn, would increase the chemotactic speed relative to unpolarized cells in wide channels. We also reasoned that the polarized cells within the channels would migrate toward the source of attractant faster than the unpolarized cells in narrow and wide channels. The results suggest that the narrow channels do partially suppress pseudopod extension in unpolarized cells but do not increase the migration speed of the cell relative to cells in wide channels. Polarized cells migrate significantly faster than unpolarized cells toward their respective chemoattractants. These elongated cells are also highly sensitive to chemoattractants at their anterior end. Our experimental results suggest that the anterior of the cell, alone, has the capacity to sense the gradient and direct the cell up the concentration gradient.

Results

Migration speeds of polarized cells versus unpolarized cells within channels

Chemoattractant delivery using a micropipette pressure of 50 hPa created a concentration gradient that can cause cells to migrate rapidly in both narrow and wide channels (Figure 4C and F). This delivery setting, in conjunction with the OMD channel geometry, created controlled experimental conditions where cells could be ‘‘raced’’ against each other. For these assays, wild-type cells expressing PH-GFP, a biosensor for PI(3,4,5)P3, and LimE, a marker for actin polymerization (Clarke et al., 2006), were starved and developed for 7 hours and raced against wild-type, unpolarized cells expressing PH-GFP alone (Parent and Devreotes, 1999). The developed cells were polarized and responded to cAMP, while the unpolarized cells were grown in the presence of bacteria and responded to the chemoattractant folic acid. Fluorescent cells were mixed and loaded into the cell chamber within the OMD. A single micropipette was loaded with a 1:1 ratio of 10 µM cAMP and 10 µM folic acid and was lowered on one side of the channels as depicted in Figure 3C. Individual cells were tracked and their migration speed determined within the various channels (Figure 7A). The polarized cells migrated to cAMP at 17.75 µm min^{-1} (± 1.41 µm min^{-1}) while the vegetative cells moved toward folic acid at 6.79 µm min^{-1} (± 0.67 µm min^{-1}). Thus, the polarized cells migrated significantly faster than the vegetative cells in identical gradients of their respective chemoattractants.

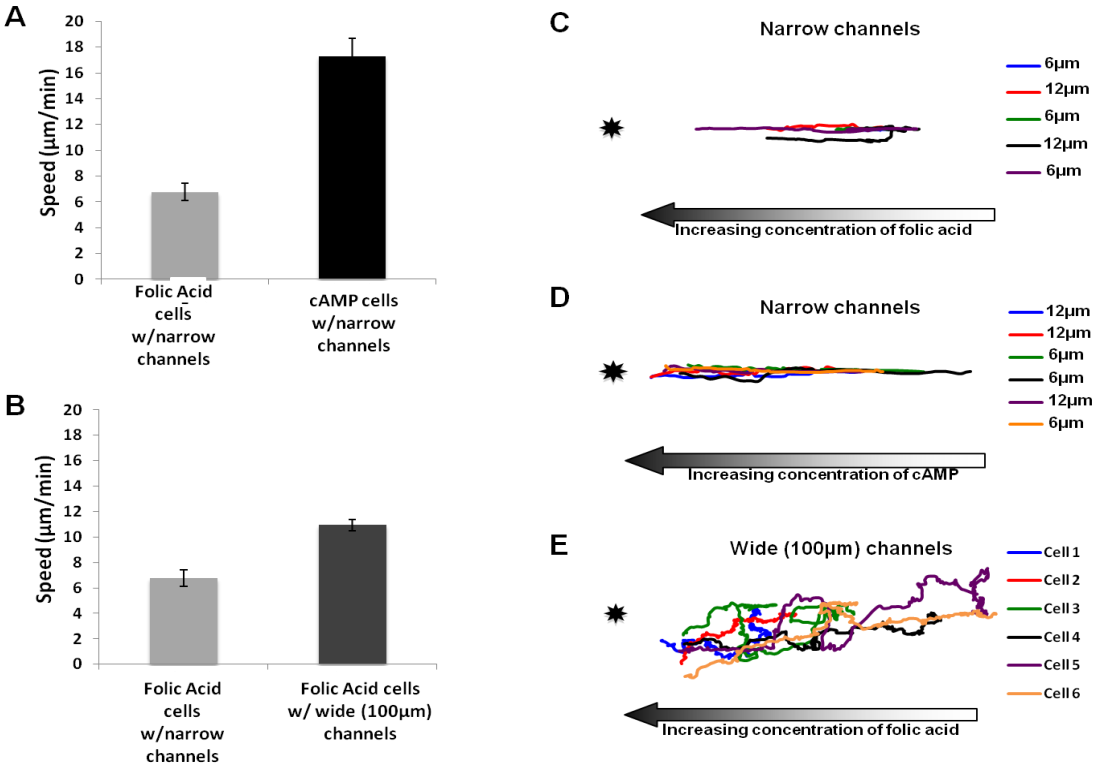

Figure 7. Analysis of cell migration in the OMD (A) Migration speeds of unpolarized cells within narrow channels are significantly slower than polarized cells within narrow channels toward the chemoattractant source ($p<0.001$) (two tailed Student's t test). The migration speed (µm min^{-1}) was measured from a mixture of unpolarized and polarized cells toward a micropipette loaded with 10 µM cAMP and folic acid. The error bars represent the standard error of the mean where n = 30. (B) Unpolarized cells in the presence of narrow channels migrate slower than folic acid cells in the 100 µm wide channels toward folic acid ($p<0.001$) (two tailed student's t test). The migration speed (µm min^{-1}) was measured for the vegetative cells in a device containing narrow channels and a device containing 100 µm wide channels toward 10 µM folic acid. n = 30 for folic acid cells with narrow channels and n = 17 for folic acid cells in wide channels (2 different days). The error bars represent the standard error of the mean. (C) Representative unpolarized cells within the narrow channels migrate in a relatively straight line toward the attractant source. Cells from the two innermost 6 and 12 µm channels in the device were analyzed. The cells moved with an average speed of 7 µm min^{-1} (± 0.6 µm min^{-1}). (D) Representative polarized cells within the narrow channels migrate in a straight line toward the attractant source. Cells from the two innermost 6 and 12 µm channels in the device were tracked. (E) Representative unpolarized cells in the wide channels migrate in a biased random walk toward the attractant source. The unpolarized cells moved at a speed of 11 µm min^{-1} (± 0.4 mm min^{-1}).

Migration speeds of unpolarized cells within and in the absence of channels

Unpolarized cells extend random pseudopods quite often even when migrating up a concentration gradient of folic acid. To determine whether confinement in the narrow channels would affect migration speeds, unpolarized cells were assayed as described above toward folic acid in the presence of narrow channels (Figure 7C) and in wide channels (Figure 7E). Cells in the wide channels moved at an average speed of 10.95 μm min^{-1} (± 0.42 μm min^{-1}) while those with narrow channels migrated at 6.79 μm min^{-1} (± 0.67 μm min^{-1}) (Figure 7B). Surprisingly, these data indicate that the confinement of the narrow channels did not increase the migration speed of the unpolarized cells.

The migration path of cells under three different conditions was determined by cell tracking. Polarized cells moving toward cAMP and unpolarized cells migrating toward folic acid were tracked when confined within the middle 12 μm and 6 μm channels (Figure 7C and D). These two channels were chosen since the mean concentration and slope most closely resembled those of the other device, which had wide channels. The polarized cells migrated in a relatively straight line (Figure 7D). The unpolarized cells in narrow channels exhibited a migration path with a greater number of lateral movements and more path reversals when compared to the polarized cells migrating to cAMP (Figure 7C). Lastly, the unpolarized cells in the absence of channels meandered toward the pipette rather than taking a direct route, as described above for both the polarized cells and the vegetative cells within the channels (Figure 7E). Cells in the wide channels clearly strayed off course, yet they migrated faster than cells confined to narrow channels.

We also investigated whether the size of a narrow channel (6 μm versus 12 μm channels) would have an effect on the cell migration speed of unpolarized cells. The migration speeds of the unpolarized cell in 6 μm and 12 μm channels were measured (Figure 8A). Unpolarized cells in the 6 μm and 12 μm channels had an average speed of 8.82 μm min^{-1} (± 0.74 μm min^{-1}) and 8.18 μm min^{-1} (± 0.94 μm min^{-1}), respectively. A time lapse video of polarized

cells was also recorded. Cells in each of the channels exhibited similar relative speeds during an 18 minute experiment (Figure 8 B–D). These data suggested that the size of the channel did not improve or impede relative migration speeds of the cells observed. They also provided further evidence that cells respond to the relative change in concentration of chemoattractant since the outer channels would have several fold lower mean concentrations.

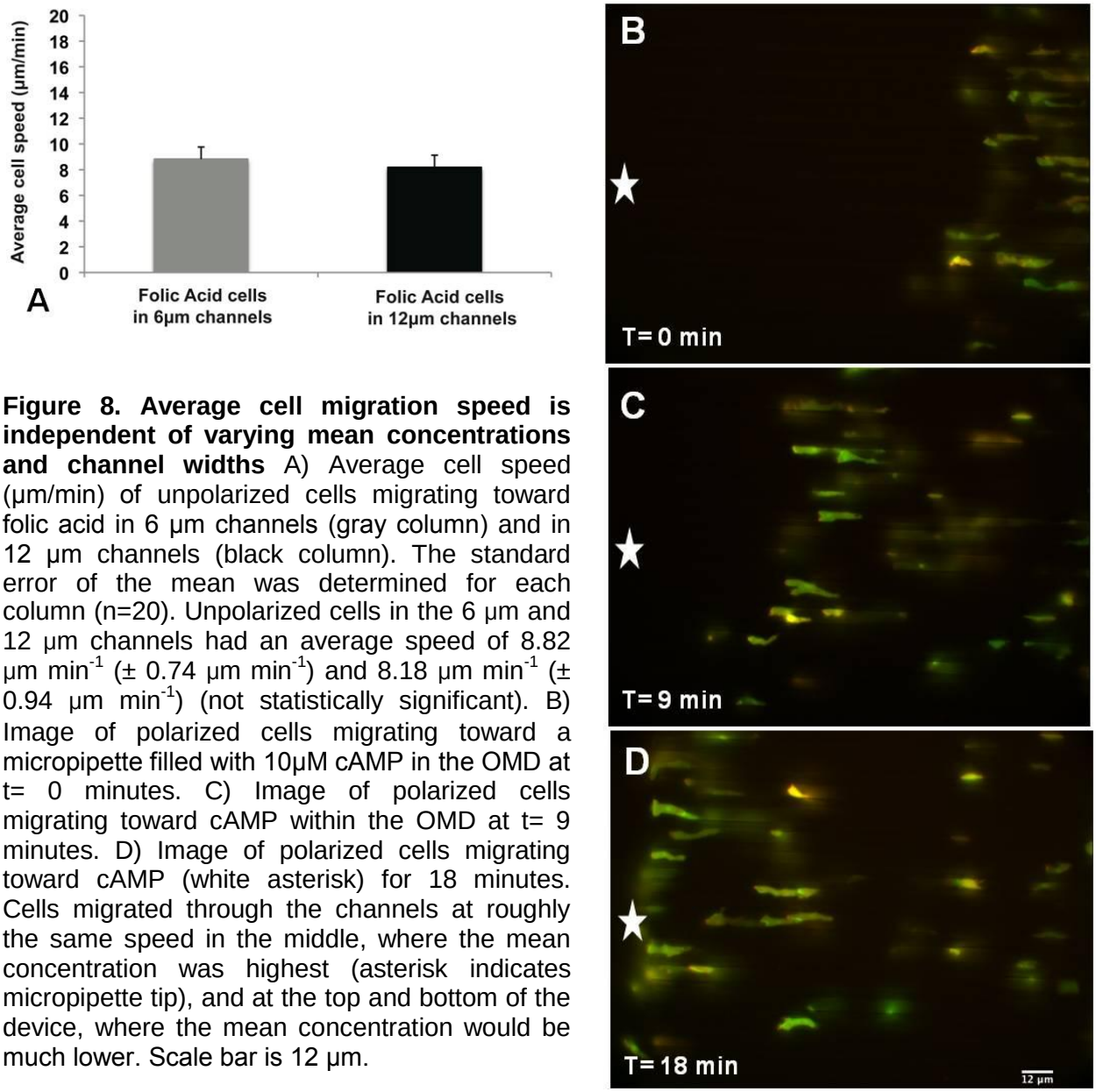

Figure 8. Average cell migration speed is independent of varying mean concentrations and channel widths A) Average cell speed (μm/min) of unpolarized cells migrating toward folic acid in 6 μm channels (gray column) and in 12 μm channels (black column). The standard error of the mean was determined for each column (n=20). Unpolarized cells in the 6 μm and 12 μm channels had an average speed of 8.82 μm min^{-1} (± 0.74 μm min^{-1}) and 8.18 μm min^{-1} (± 0.94 μm min^{-1}) (not statistically significant). B) Image of polarized cells migrating toward a micropipette filled with 10μM cAMP in the OMD at t= 0 minutes. C) Image of polarized cells migrating toward cAMP within the OMD at t= 9 minutes. D) Image of polarized cells migrating toward cAMP (white asterisk) for 18 minutes. Cells migrated through the channels at roughly the same speed in the middle, where the mean concentration was highest (asterisk indicates micropipette tip), and at the top and bottom of the device, where the mean concentration would be much lower. Scale bar is 12 μm.

Spatial gradient sensing occurs primarily at the leading edge

Polarized cells moved rapidly toward the micropipette while in the channel and also once they exited the channel on the side facing the micropipette. In fact, an interesting observation was made that demonstrated that cells could sense the change in the cAMP profile before fully exiting the channel (Figure 9A). We determined the percentage of cells that turned toward the chemoattractant source while less than 50% of the cell was outside the channel. The thirty cells observed were divided into two classes: (1) cells that turned directly toward the attractant loaded micropipette with less than 50% of their cell bodies outside of the channels, and (2) cells that turned away from, or did not turn directly toward the micropipette with less than 50% of their cell bodies outside of the channels. Out of the 30 cells that were analyzed, 21 cells meeting the first criteria turned directly toward the cAMP-loaded micropipette (Figure 9B). Additionally, PH-GFP and LimE-RFP localized to the fraction of the leading edge that was facing the cAMP-loaded micropipette (Figure 9A). These results demonstrated that the leading edge of the cell could sense a change in the concentration gradient across the midline of the cell without the help of the rear of the cell.

Discussion

The OMD apparatus was created for studying the migration of cells in response to a passive chemical gradient. Two- and three-dimensional patterns within this device can be designed to study various properties of migrating cells to further our understanding of gradient sensing and the mechanical properties that regulate cell motility up or down a concentration gradient. While other groups have shown the migration of cells through channels in response to a passive gradient (Butler et al., 2010; Taylor et al., 2005), this device produces stable gradients by using a micropipette. In addition, the cell loading and gradient generation in the OMD are completely independent of one another. Cells can be readily introduced into this system through

an open well. The micropipette is a high-impedance controlled source of chemoattractant whose instantaneous position and flow rate can be readily controlled by the experimenter, whereas the devices that utilize reservoirs and multiple channels are generally subject to convective flows driven by small differences in hydrostatic pressure between the various reservoirs. The device by Butler et al. (Butler et al., 2010) avoids the convection problem by using closed channels, but this eliminates the possibility of changing the local gradient, for example, at the opening to the migration channel, and limits the ability to load cells into the channel from the low side of the gradient. While these other devices are not capable of the rapid changes in gradients or concentrations that we can achieve, their geometries may be better suited for the study of cells that move or grow slowly. The OMD is ideal for rapidly moving cells, and is not subject to the hydrodynamic forces associated with flow gradient mixers (Lin et al., 2004; Walker et al., 2005).

The OMD generated gradients of varying profiles and mean concentrations and quantified the responses of *D. discoideum* amoebae toward folic acid or cAMP. For these biological assays, a mixed population of cells, as well as a combination of the chemoattractants cAMP and folic acid, was used to provide a direct comparison of migration rates while cells were under identical experimental conditions. The micropipette was positioned at the very center of the device and produced a gradient in all of the channels. The concentration of chemoattractant entering the channels nearest the micropipette had a mean concentration that was higher than those farther away. While the absolute amount of chemoattractant differed between the channels, the relative change in concentration that a cell would experience varied very little, and the cells migrated with similar speeds. The experimental design allowed us to directly test the effects of cell confinement on migration rates, since the channels were alternated and similarly sized channels had both low and high mean concentrations. By varying the micropipette pumping pressure, different profiles were generated and their effects on chemotaxis were observed.

The OMD was used to measure the migration speed of unpolarized vegetative cells and of polarized developed cells. We hypothesized that the narrow channels within the OMD would suppress lateral pseudopod extension in the unpolarized cells and as a result cause the cells to migrate toward the source of attractant faster than unpolarized cells in the wide channels. This was not observed. The migration speed of the unpolarized cells in the narrow channels was significantly less than that seen for both the unpolarized cells in the wide channels and the polarized cells responding to cAMP. We speculate that this result occurred because pseudopods from unpolarized cells were extinguished if they encountered a wall in the channel. Since the cells appeared to bias their pseudopods in the direction of the concentration gradient, only those pseudopods that randomly formed directly up the gradient, and in the center of the channel, lead to motility. This resulted in an overall decrease in motility to folic acid. This explanation was further supported when the cell migration tracks were measured for each of the cell conditions. The vegetative and cAMP-developed cells within the channels migrated in a relatively straight line. However, the vegetative cells in the absence of channels migrated in a much more random fashion. The gradient sensing system regulates the spatiotemporal localization of signaling molecules at the front and rear of the cells (Janetopoulos and Firtel, 2008). With the OMD, the micropipette formed a gradient via radial diffusion. As a consequence, the cells were exposed to a gradient vector that was parallel to the channels within the channels and a gradient vector that was perpendicular to the channels when the cells exit the channels.

Analysis of polarized cells exiting the channels demonstrated that the leading edge of the cell was capable, by itself, of sensing a gradient (Figure 9A and B). In addition, the sensing mechanism localized PI3K activity, leading to higher PIP3 levels and ultimately actin polymerization as shown by cells expressing PH-GFP and LimE-RFP, respectively. This demonstrated that the front of the cell could respond to the gradient independent of ligand binding at the rear of the cell. This is a unique finding since most reports on gradient sensing focus on the differences in attractant concentration and signaling responses between the front

and the back of the cell (Janetopoulos and Firtel, 2008; Janetopoulos et al., 2004; Kimmel et al., 2004; Korohoda et al., 2002).

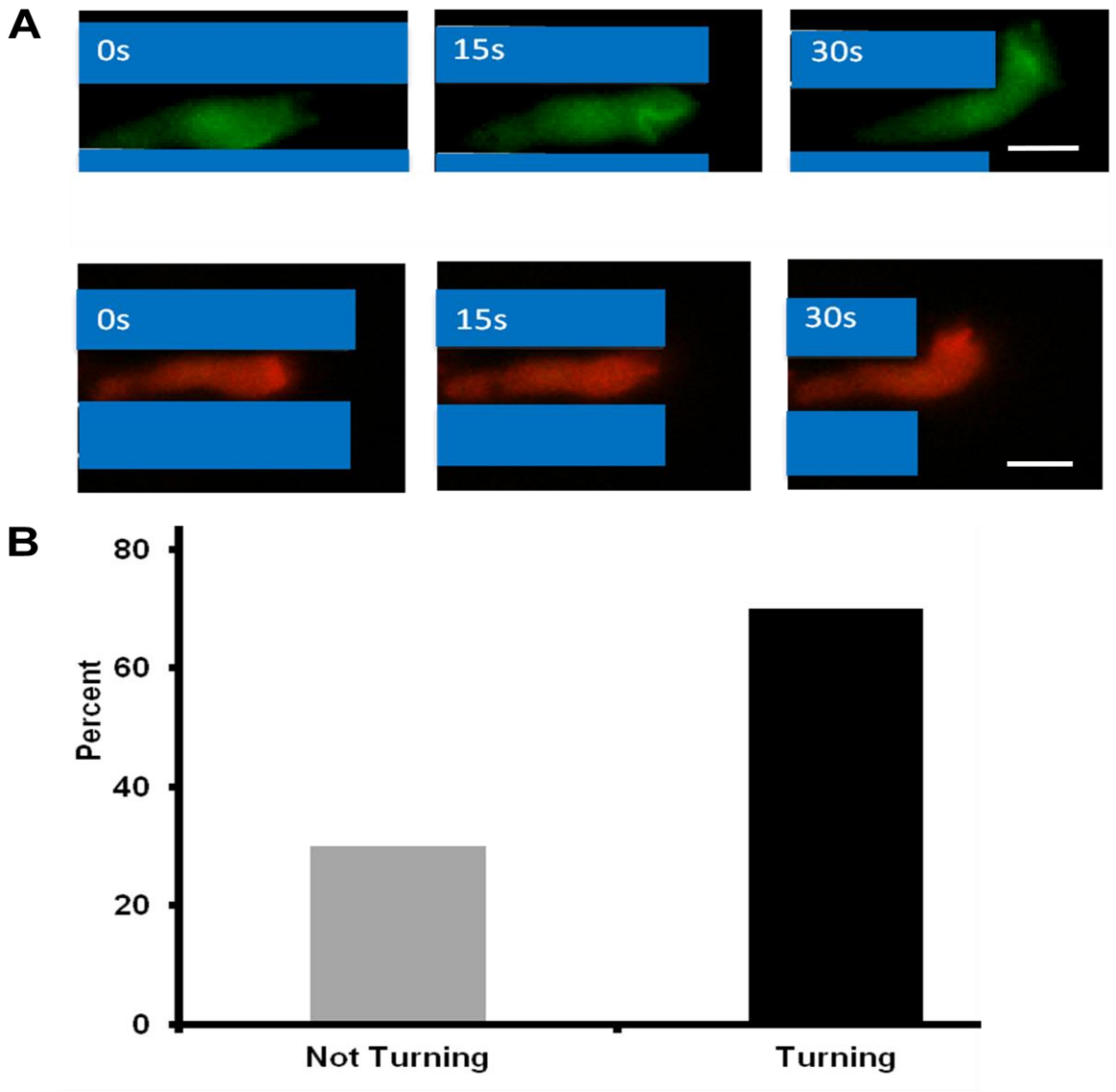

Figure 9. The turning behavior of cells as they exit the narrow channels. (A) The leading edge of a cell has the capacity to sense a cAMP gradient across the midline and turn toward the attractant source. Depicted is a representative cell that exhibited turning behavior toward the cAMP-loaded micropipette. This cell was expressing PH-GFP (green) and LimE-RFP (red). The snapshots in A, B and C were three consecutive frames 15 s apart. Scale bar is 10 μm. (B) 70% of polarized cells turned their leading edge toward the micropipette as the cells exited the channels. Thirty cells (10 cells each from 3 different days) were analyzed. For a positive turning result to be scored, the cells were not in contact with other cells and had at least 50% or less of the cell body outside of the channel.

Previous studies in *Dictyostelium* have also shown that cells are more sensitive at the front than the rear (Devreotes and Janetopoulos, 2003; Parent and Devreotes, 1999), and that immobile cells can respond to multiple stimuli simultaneously (Janetopoulos et al., 2004). Cells in a gradient will display stable, localized responses, but when given a global stimulus will show a uniform response and adapt (Parent et al., 1998). Numerous models, many containing feedback mechanisms, have been proposed to help explain these results and the ability of cells to amplify their response when in a chemoattractant gradient (Devreotes and Janetopoulos, 2003; Fuller et al., 2010; Levine et al., 2006). One scheme, the Local Excitation and Global Inhibition (LEGI) model, provides a potential mechanism for these spatial temporal sensing responses (Devreotes and Janetopoulos, 2003; Janetopoulos et al., 2004; Parent and Devreotes, 1999). The LEGI model has two main components, a fast excitation process, and a slower global inhibitor. In a uniform stimulus of chemoattractant the fast local excitation processes increase proportionally to receptor occupancy. The inhibitory processes increase slowly as a function of the average ligand binding and eventually turn off the response. In a steady state gradient, the excitatory processes along the length of the cell are higher in the front of the cell than the back, while the inhibitory processes are proportional to the mean receptor occupancy and exceed excitatory signals in the rear (Janetopoulos and Firtel, 2008; Janetopoulos et al., 2004; Ma et al., 2004). This will allow a persistent directional response toward a spatial gradient. The results reported here demonstrate that cells can abruptly turn toward the chemoattractant source as they are exiting the channels. This suggests that the LEGI mechanism is capable of providing localized responses by measuring the gradient difference across the leading edge of the cell. This is consistent with previous data which showed that a cell can elicit amplified responses at opposing ends (Janetopoulos et al., 2004).
In this report, however, it is important to note that the rear of the cell does not see a change in the gradient concentration across the short axis of the cell. This is quite different from previously reported micropipette assays where cells turn and chase the change in gradient concentration.

The turning behavior reported here is depicted in Figure 10, where the cartoon also displays several paths that the cell could have taken. The majority of cells observed in these experiments made an approximate 90° turn toward the micropipette upon exiting the channel. These results suggest that the leading edge of a cell, in addition to being more responsive to incremental changes in chemoattractant when exposed to a uniform stimulus, is also very sensitive to changes in the gradient concentration. In addition to similar questions outlined in this report using the model system *D. discoideum*, the open microfluidic device could be used for addressing many biological questions related to directional sensing and cell migration in a wide range of prokaryotic and eukaryotic organisms.

The OMD is very easy to use, with setup times on the order of a few minutes. Cells were loaded into an open chamber and allowed to settle. During this time the micropipette was loaded and positioned. Since there were no valves, flow or tubing within the PDMS device, there was very little that could go wrong, including no leaks, air bubbles or evaporation issues. The device allowed cells to chemotax toward a passive gradient without encountering shear forces. Future chemotaxis experiments can custom design the PDMS channels and alter the shape and size of the channels to observe the migratory properties of cells when confined by a number of different surfaces. These devices, combined with imaging techniques such as total internal reflection fluorescence microscopy (TIRFM), will help elucidate the basic principles by which cells orient and move directionally.

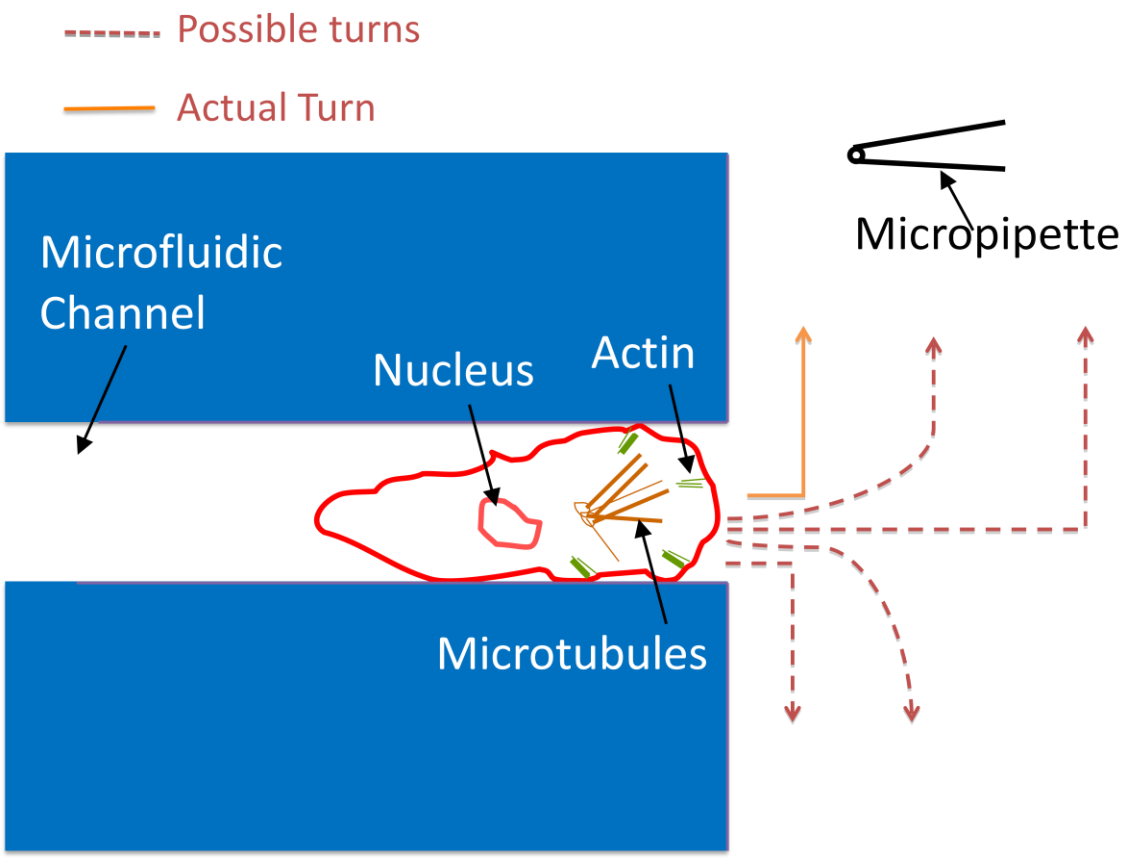

Figure 10. Turning strategy of cells exiting the channel Cells that exited the channels had a number of possible directions to follow as they made their way toward the micropipette. Cells could have continued in a straight line, turned in the correct direction, or migrated 1801 in the opposite direction. They could have also made more shallow turns in the correct or incorrect direction. They mostly migrated directly toward the micropipette, even while their trailing edge was still not exposed to the gradient that was perpendicular to the cell. Since the cells did not make a shallow turn, as might be expected if you averaged the proportion of the cell's outer surface that is normally exposed to the chemoattractant, the rear of the cell contributed little or no spatial information to the turning profile of the cell.

*Work for this chapter has been adapted from the following manuscript.

Jowhar, D., G. Wright, P.C. Samson, J.P. Wikswo, and C. Janetopoulos. 2010. Open access microfluidic device for the study of cell migration during chemotaxis. *Integrative biology : quantitative biosciences from nano to macro*. 2:648-658.

- Janetopoulos and Jowhar devised concept for device. Wikswo and Samson provided input for device design. Jowhar designed and built device. Jowhar, Wright and Janetopoulos designed cell experiments. Experiments and data analysis were performed by Jowhar and Wright. All authors read manuscript and provided input.

CHAPTER IV

POLARITY REVERSALS REVEAL THE ROLE OF PI(4,5)P2 IN SIGNALING RESPONSES AND POLARIZED MORPHOLOGY

Introduction

Migrating cells typically exhibit a polarized morphology, which includes the development of a distinct cell front and rear and the asymmetric distribution of plasma membrane (PM) and cytoskeletal molecular components required for both cell signaling and motility (Devreotes and Janetopoulos, 2003). This spatial localization occurs when cells are in a chemical gradient, but can also occur during a uniform stimulus, where the cells undergo chemokinesis, and migrate randomly (Becker, 1977; Bourne and Weiner, 2002; Kriebel et al., 2003; Wilkinson, 1990). A polarized morphology permits the cell to respond robustly to gradients of chemoattractant and sets up feedback loops that inhibit pseudopodial projections in the wrong direction, and reinforce leading edge formation towards the high side of the gradient (Srinivasan et al., 2013a). The social amoeba *Dictyostelium discoideum* has proven to be an excellent model organism for understanding the polarity circuits that control polarized morphologies and eukaryotic chemotaxis (Bagorda et al., 2006; Devreotes and Janetopoulos, 2003; Janetopoulos and Devreotes, 2006; Kay, 2002; Kimmel and Firtel, 2004; King and Insall, 2009).

The distribution of many of the molecules critical for cell migration has been well documented in *D. discoideum*. The chemoattractant cAMP binds to serpentine receptors that are coupled to the heterotrimeric G proteins (Johnson et al., 1992; Louis et al., 1994; Strader et al., 1995; Sun and Devreotes, 1991) and are uniformly localized on the membrane of polarized cells (Xiao et al., 1997). The binding of cAMP to the receptor results in the exchange of GDP for GTP in the Gα2 subunit and the complete dissociation of the Gα2$\beta\gamma$ heterotrimer (Elzie et al.,

2009). The continuous activation of the heterotrimeric G-proteins in a uniform stimulus suggests that heterotrimeric G-protein activity likely mirrors the cAMP gradient (Janetopoulos et al., 2001) and experimental evidence supports this premise (Xu et al., 2007). The first documented asymmetric response occurring downstream of the heterotrimeric G-proteins is at the level of Ras activation (Sasaki et al., 2004), followed shortly by the recruitment of PI3-Kinase (Sasaki et al., 2004) which phosphorylates PI(4,5)P2 to PI(3,4,5)P3, and contributes to the polymerization of F-actin (Funamoto et al., 2001; Iijima and Devreotes, 2002; Merlot and Firtel, 2003; Sasaki et al., 2004). A positive feedback loop is thought to occur between F-actin and PI3K which can facilitate the extension of the leading edge towards increasing concentrations of cAMP (Sasaki and Firtel, 2006; Sasaki et al., 2007).

The tumor suppressor and phosphatase PTEN regulates PI(3,4,5)P3 and PI(4,5)P2 levels and does so by another positive feedback loop, since PTEN directly binds to PI(4,5)P2 on the plasma membrane (Chen et al., 2003; Iijima and Devreotes, 2002; Iijima et al., 2004). Cells lacking PTEN have an extended PI(3,4,5)P3 and F-actin response and are unpolarized. This inability to polarize likely occurs since PTEN contributes to the suppression of the formation of lateral pseudopods during chemotaxis (Iijima and Devreotes, 2002; Wessels et al., 2007). The PI(4,5)P2 binding motif at the N-terminus of PTEN serves a dual role of localizing PTEN to the membrane and regulating its enzymatic activity (Iijima et al., 2004). The anchoring of PTEN to PI(4,5)P2 on the inner leaflet of the plasma membrane (PM) has also been shown in mammalian cells, where PTEN redistributed to the cytosol from the PM after PI(4,5)P2 depletion by the forced translocation to the PM of a PI(4,5)P2-specific phosphatase, inositol polyphosphate-5-phosphatase (Rahdar et al., 2009).

PI(4,5)P2 levels are also regulated by the activity of phospholipase C (PLC), which hydrolyzes PI(4,5)P2 to create the secondary messengers inositol triphosphate (IP3) and diacylglycerol (DAG) (Berridge and Irvine, 1984; Van Dijken et al., 1994; Van Haastert and Devreotes, 2004). PLC null cells can still display a polarized morphology during aggregation and

PTEN dissociates from the membrane upon uniform stimulation with cAMP, with kinetics similar to those seen in wild type cells (Srinivasan et al., 2013a). However, PTEN does localize more strongly to the PM in cells lacking PLC and fails to redistribute to the cytosol when stimulated with the weaker chemoattractant folic acid. Furthermore, cells overexpressing PLC have less PTEN on the PM (Kortholt et al., 2007; Srinivasan et al., 2013a). This data suggests that PLC is not necessary for the regulation of PTEN, but can regulate PI(4,5)P2 levels which in turn directly influence PTEN localization. The activity of these enzymes likely creates an asymmetric distribution of phospholipids and effector molecules at the front and rear of the cell.

Interestingly, the role of PI(4,5)P2 has mostly taken a back seat to understanding how or if PI(3,4,5)P3 generates actin polymerization and contributes directly to motility (Ganesan et al., 2006; Hoeller and Kay, 2007; Vedham et al., 2005; Xu et al., 2003). After over 15 years of being in the limelight, there are very few pieces of evidence directly linking PI(3,4,5)P3 to actin polymerization and in fact numerous papers suggesting that it does not link to PI(3,4,5)P3 (Andrew and Insall, 2007; Park et al., 2008).

The role of microtubules has also been examined during chemotaxis in *D. discoideum* by imaging GFP tagged tubulin in normal and drug-treated cells. Both trimethyltin and nocodazole treatment, which disrupt microtubules, caused an inhibition of chemotaxis (Sroka et al., 2001)**.** *D. discoideum* contain a nucleus-associated centrosome that serves as the microtubule-organizing center (MTOC). Microtubules appear to serve as anchoring structures for the nucleus, and are largely absent from pseudopods (Rubino et al., 1984) and the location of the nucleus and the MTOC during cell migration likely plays a role in determining the stability of the pseudopod in random motility (Ueda et al., 1997), but there has been limited work showing the role that microtubules play in overall polarity of the cell.

In this study, we were able to observe the redistribution of signaling and cytoskeletal components during the complete reorganization of a cell's morphological polarity. We reset the cell's polarity 180º using a microfluidic device and protocol, so that the old front became the new

rear of the cell and vice versa. This gave us the unprecedented opportunity to watch the breakdown of the cell's polarity and the emergence of polarity in the opposite direction. During these events, we visualized and performed the quantification of a number of signaling and cytoskeletal markers. We have previously developed several "open" microfluidic devices (OMDs) that permitted the quantitative analysis of cell migration in confined channels using a passive gradient under the control of a micropipette (Jowhar et al., 2010; Wright et al., 2012). The system described here uses a similar platform; however a pair of micropipettes allows the gradient to be rapidly reversed once the cells enter the channel. We observed the localization of several polarity markers which include a Ras activity biomarker, the Ras binding domain fused to the red fluorescent protein (RBD-RFP) (Sasaki et al., 2004); a PI3-kinase activity marker, the Pleckstrin Homology domain fused to green fluorescent protein (PH-GFP) that monitors PI(3,4,5)P3 levels (Parent et al., 1998); the tumor suppressor and phosphatase PTEN fused to GFP (PTEN-GFP, which is also a marker for PI(4,5)P2) (Iijima and Devreotes, 2002; Iijima et al., 2004; Rahdar et al., 2009); LimE-RFP, a marker for F-actin polymerization (Clarke et al., 2006); and Tubulin-GFP, which marks microtubules (Octtaviani et al., 2006) and quantified the time it takes for redistribution of these fluorescently tagged molecules during polarity reversal.

When highly polarized cells are exposed to a gradient at their rear, they typically do a U-turn (Devreotes and Janetopoulos, 2003; Srinivasan et al., 2013a). The assay described here confines individual cells in 3 dimensions (3D) to prevent U-turns when the gradient of chemoattractant is reversed 180º. This gave us the unique ability to visualize the collapse of cellular polarity and the reestablishment of polarity in the new gradient direction. We also gained insight from stimulating cells at metaphase to further support our model for the role of PI(4,5)P2 in signaling responses. These results show the dominant role that PI(4,5)P2 and "backness" plays in polarity and also elucidate the interactions of signaling molecules and cytoskeletal elements with one another.

Results

Experimental design

We developed a procedure that used passive cAMP gradients to direct cells into confined channels (Figure 11a). This cell migration device was developed based on a previous OMD that used a micropipette to produce passive chemical gradients and polydimethylsiloxane (PDMS)-based technology to form the 3D channels (Jowhar et al., 2010). The device is essentially a wall with channels running through it that are adjacent to the coverslip. The channels open to reservoirs that both contain a cAMP-filled micropipette. Polarized cells migrate through the channel and toward one of the micropipettes. The gradient can be reversed by removing the first pipette and lowering a second pipette at the rear of the cells (Figure 11b).The dimensions of the channels were designed so that they were small enough that cells had to invert their polarity and were prevented from making U-turns (Figure 11c).

Figure 11. Experimental Setup for polarity reversal experiments. A) Actual setup of experiment. Top image shows a top down view of device chamber mounted on a microscope stage flanked by two micropipettes that secrete cAMP. Bottom image shows a side view of the same setup. 40 X oil objective was used for these experiments. B) Cells expressing fluorescent biomarkers are lured into microfluidic channels toward a gradient of cAMP secreted from a micropipette. Once the cells are in the channels, the micropipette is removed and a second micropipette containing cAMP is introduced at the rear of the cell. The changes in cell morphology and protein localization are measured while the cell reverses its polarity in response to the change in gradient direction. C) DIC Image of a highly polarized cell undergoing the polarity reversal process while in the microfluidic channels (*) indicates the location of the micropipette.

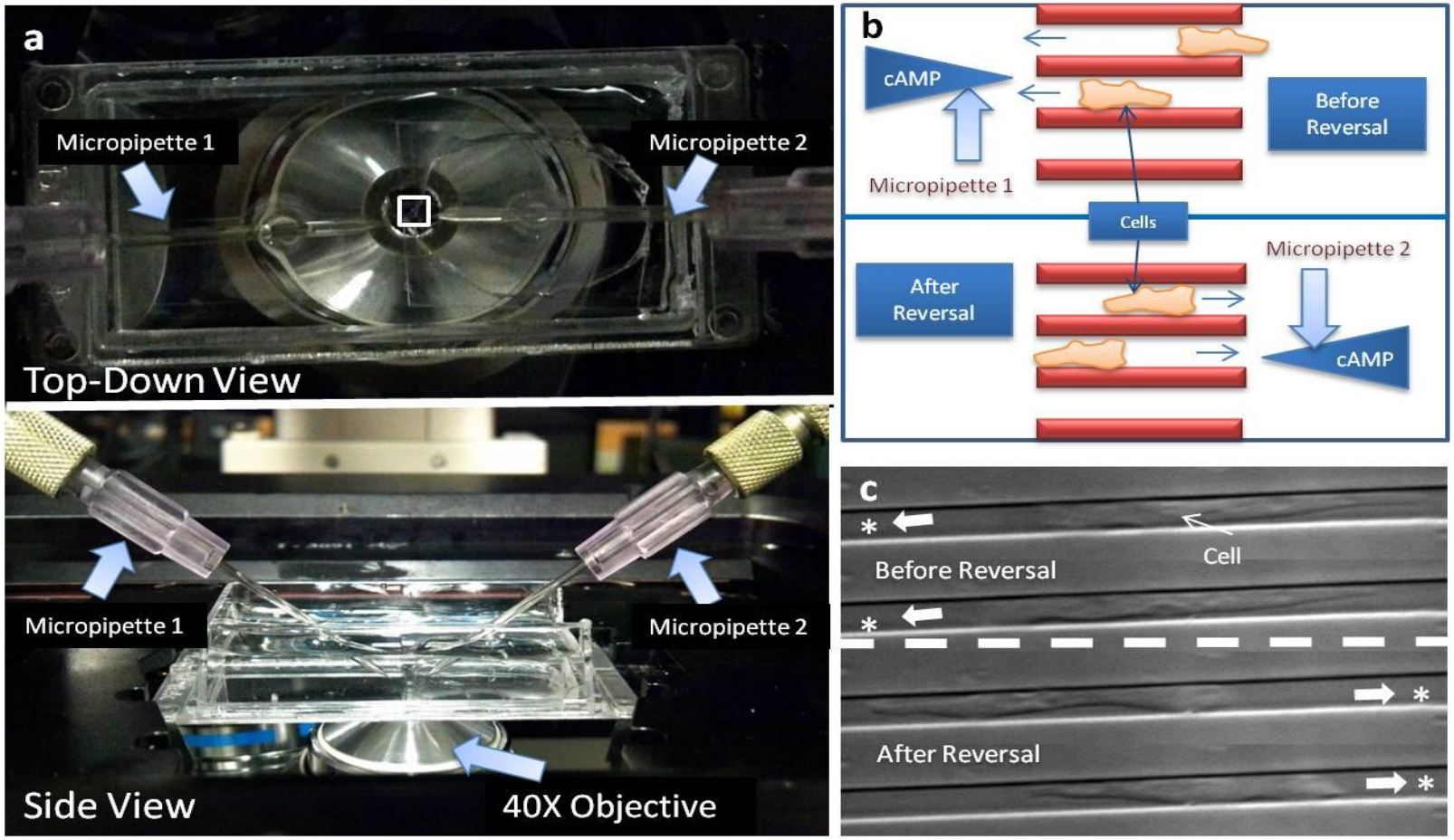
a
Micropipette 1
Micropipette 2
Top-Down View
Micropipette 1
Micropipette 2
Side View
40X Objective
b
cAMP
Micropipette 1
Before Reversal
Cells
Micropipette 2
After Reversal
cAMP
c
Before Reversal
Cell
After Reversal

Ras activation occurs as the leading edge forms and only does so where PI(4,5)P2 levels are low

Highly polarized cells expressing RBD-RFP, one of the first signaling components known to be activated, were lured into channels and were observed during the reversal process (Figure 12). It takes approximately one minute for a cell to have overall net movement in the opposite direction when the gradient is reversed. Some cells responded quickly and switched directions faster, while others continued moving without ever reversing. Kymograph analysis and intensity quantification revealed that Ras activation occurred at the new front of the cell prior to an increase in PI(3,4,5)P3 levels (Figure 12a and see below). In addition, in 8/11 cases, new pseudopod extension only occurred when levels of Ras activation were higher at the new leading edge than the residual activity at the old front (Figure 12b, 12c). In some instances, Ras activity could be visualized moving along the periphery of the cell to the other end of the cell (see Figure 13a).

The kymograph analysis also revealed that back retraction could occur prior to front extension. We quantified the length of these cells immediately before and just after the gradient reversal and found a vast majority of cells (>70%) shortened prior to changing directions. The decrease in cell length can also be visualized in the two kymographs below. PI3K activity was monitored by measuring PH-GFP (Figure 12d-f). PI3K activity was present at the old leading edge prior to gradient reversal, and appears again after pseudopod extension at the new leading edge. Cells were unable to extend a new front and move forward until the PTEN-GFP levels dropped substantially from the “old” back (see Figure 12g, h). Interestingly, it was not necessary for there to be PI(3,4,5)P3 or PTEN at the new front or rear, respectively, for new front or rear extension to occur (Fig 12d,g, time zero). A drop in leading edge PTEN levels corresponds with a dramatic increase in front extension and a rapid increase in PTEN levels at the new rear. In some instances, PTEN or PH-GFP were present on both ends of the cell simultaneously during the polarity reversal (Figure 12c and see Figure 14). When this occurred,

the cells appeared to be “locked” in place. The presence of PI(3,4,5)P3 at the “old” leading edge was not sufficient for the cell to continue extending in the “old” direction.

Quantification of signal increases by taking ratios of the new cell fronts to old cell fronts indicates that Ras activity is the first marker to increase after gradient reversal (Figure 15a). Ras activity also reaches a maximal level before both PI(3,4,5)P3 and PI(4,5)P2 (Figure 15b). However, Ras activity by itself was also not sufficient to produce pseudopod extension. PTEN redistributes both through the cytosol and along the periphery of the cell during polarity reversals (see Figure 12h). Once PTEN levels rise at the rear, they are stable, whereas RBD and PI3K activity oscillate as the cell migrates.

a
-25"
-7.0"
Ras Activity
RBD-RFP 140"
b
-15"
-10"
50"
75"
125"
140"
Ras activation
RBD-RFP
c
Ras activity at new front
Ras activity at old front
Signal Intensity
Cell Number
d
PI3K Activity
-170"
0"
Pseudopod Extension
PH-GFP
270"
e
-110"
-15"
175"
180"
215"
225"
PI3K Activity
PH-GFP
f
PIP3 at new front
PIP3 at old front
Signal Intensity
Cell Number
g
-380"
0"
Pseudopod Extension
Back Retraction
PTEN-GFP
360"
h
-380"
-80"
PTEN
-170"
265"
420"
795"
PTEN-GFP
i
PTEN at new back
PTEN at old back
Signal Intensity
Cell Number

Figure 12. Ras activation, PIP3 and PIP2 localization during polarity reversal a) Kymograph indicating polarity reversal of a representative cell. Areas of Ras activity are shown by arrow heads. Solid block arrows indicate the high side of the gradient. Dashed line indicates time point of gradient switch (0 seconds). b) Still images of the cell in A as it undergoes polarity reversal. There is Ras activity at the leading edge of the cell as indicated by solid arrows. c) Signal intensity of RBD RFP as measured at the new front and old back of the cell indicates that in 5/11 cases Ras activity is higher at the new front than the old front when the cell starts to move forward. d) Kymograph indicating polarity reversal of a representative cell. Areas of PI3K activity are shown by arrow heads. Pseudopod extension is indicated by solid arrows. e) Still images of the cell in A as it undergoes polarity reversal. There is PI3K activity at the leading edge of the cell which increases after the cell has reversed as indicated by solid arrows. f) Signal intensity of PH-RFP as measured at the new front and old back of the cell indicates in 8/9 cases PIP3 is higher at the old front than the new front when the cell starts to move forward. g) Kymograph indicating polarity reversal of a representative cell. Areas of PTEN localization are shown by arrow heads. Solid arrows indicate front extension after PTEN dissociates from the new front of the cell. Dashed arrows indicate back retraction while PTEN is still at the old back of the cell. h) Still images of the cell in g) as it undergoes polarity reversal. There is PTEN localization at both the front and the rear of the cell (Time Point 170 seconds). PTEN also appears to be moving along the sides of the cell as indicated by arrow heads. h) Signal intensity of PTEN-GFP as measured at the old from and new back indicate that in all cases (8/8), PTEN is higher at the old back than the new back (old front of the cell) when the cell begins to retract its new back. Bar graphs are for individual cells. (11 cells for Ras activity (4 different days), 9 cells for PI(3,4,5)P3 (2 different days) and 8 cells for PTEN (2 different days)). Scale bar in cell images is 10 μm.

To examine the relationship between Ras activity and PI(4,5)P2 levels, we examined cells that co-expressed RBD-RFP and PTEN-GFP (Figure 13). Ras activity and PI(4,5)P2 levels did not co-localize during cell migration. Furthermore, new pseudopod extension only occurred when PI(4,5)P levels dropped and PTEN dissociated from the membrane (Figure 13a). To determine if the actin cytoskeleton influenced the localization of these two markers, we examined cells responding to a moving cAMP-filled micropipette in the absence of an actin cytoskeleton and again found Ras activity and PI(4,5)P2 levels to be reciprocally regulated (Figure 13b). We also monitored RBD-RFP and PTEN-GFP in highly polarized cells stimulated with a uniform stimulus of cAMP. Interestingly, we again did not see the co-localization of Ras activity in areas where PI(4,5)P2 was high (Figure 13c). To examine this localization at higher spatial and temporal resolution, we performed Bessel Beam microscopy of cells expressing these two biomarkers (Habib et al., 2013). This gave us the unprecedented ability to monitor the plasma membrane of the entire cell with 300 nm x, y, and z resolution. These 3D volumes again show the reciprocal regulation of Ras activity and PI(4,5)P2 (Figure 13d). Since Ras activity has been shown to occur prior to PI3K activity, we speculated that RBD-RFP should translocate to the PM prior to PTEN-GFP moving to the cytosol in cells that were unpolarized. Ras activity reached a maximum within a few seconds after uniform cAMP stimulus, whereas PTEN-GFP moved to the cytosol a few seconds later. Therefore, Ras activity can occur while PI(4,5)P2 levels are high if cells are exposed to a rapid increase in saturating cAMP, but Ras activity diminishes as PTEN-GFP returns to the PM and PI(4,5)P2 levels reach prestimulus levels (Figure 13 e,f).

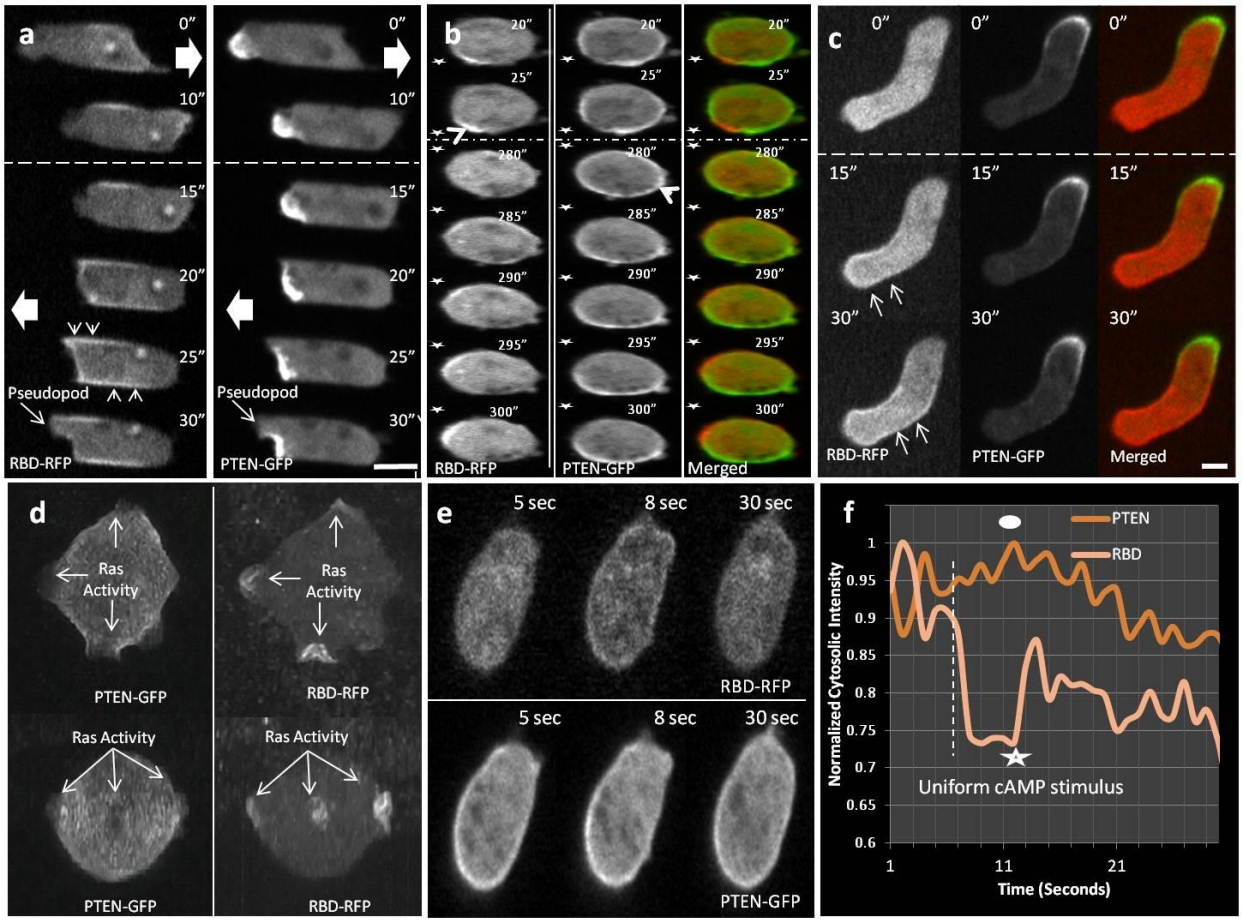

Figure 13. Ras activity occurs in regions that have low PIP2 levels a) A polarized cell undergoing a polarity reversal after a gradient switch has Ras activation at the new front of the cell, but is not able to extend a pseudopod until PTEN GFP comes off the new front of the cell (Time point 30 seconds). Arrow heads indicate Ras activity moving along the edges of the cell b) Cells treated with Latrunculin A do not show colocalization between Ras activity and PTEN in the absence of polymerized actin. Star indicates location of micropipette. Arrow heads indicate areas of Ras activity and PTEN localization c) Polarized cells exposed to a uniform dose of cAMP do not sow colocalization between Ras activity and PTEN as observed in time point 15 and 30 seconds. Arrows indicate areas of Ras activation that do not have PTEN localization. d) Super Resolution Bessel Beam image of cells expressing both RBD and PTEN. Arrows indicate regions where Ras activity is present while PTEN is absent. e) Cells that have been starved for 5.5 hours are treated with a uniform dose of cAMP as shown in time point 8 seconds. Image is of a representative cell. Ras activity is shown by solid arrows. f) Quantification of Ras activity and PTEN intensity (PIP2 localization) measured in the cytosol of cells shown in (e). Graph is an average of 3 different cells in the same field of view. Ras activity starts to go down immediately prior to PIP2 levels increasing at the membrane. cAMP stimulus was added at 8 seconds as indicated by the dotted line. Solid circle shows PTEN peak, while white star shows lowest Ras activity peak in the cytosol due to the recruitment of Ras activity to the cell membrane. Scale bar is 10 µm.

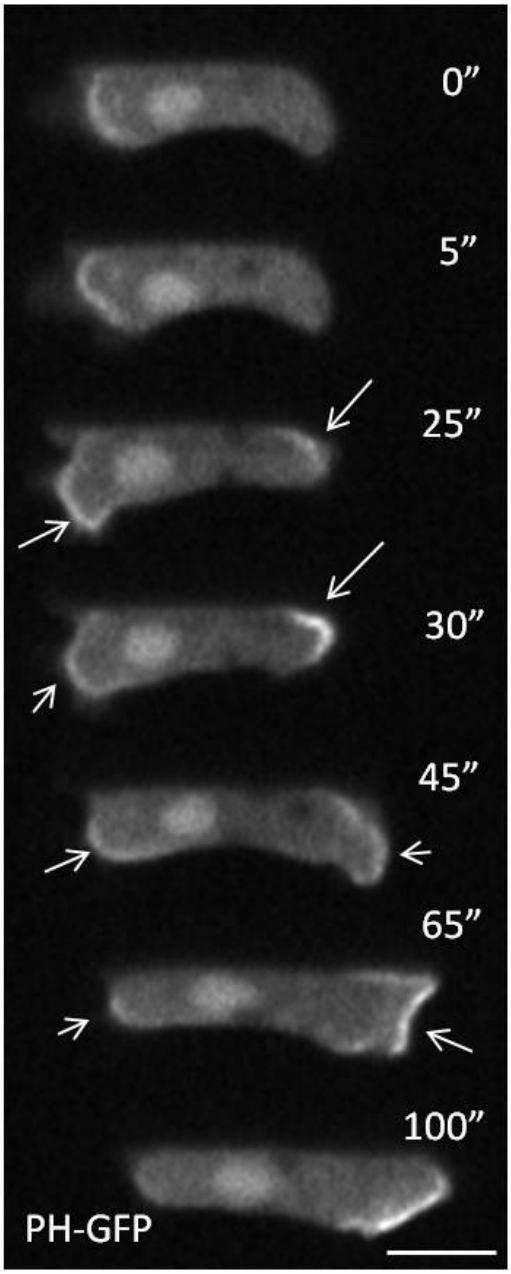

Figure 14. PIP3 is not sufficient to direct actin polymerization A cell expressing the PIP3 marker (PH-GFP) has its crescent at the leading edge of the cell during migration. When the cell senses the new gradient, it localizes PIP3 at the new front (old back) at time point 25 seconds. Even though there are high levels of PIP3 at the old front (new back) of the cell, it moves towards the new gradient. Eventually, the new front of the cell has high PIP3 levels compared to the new back. Scale bar is 10 μm.

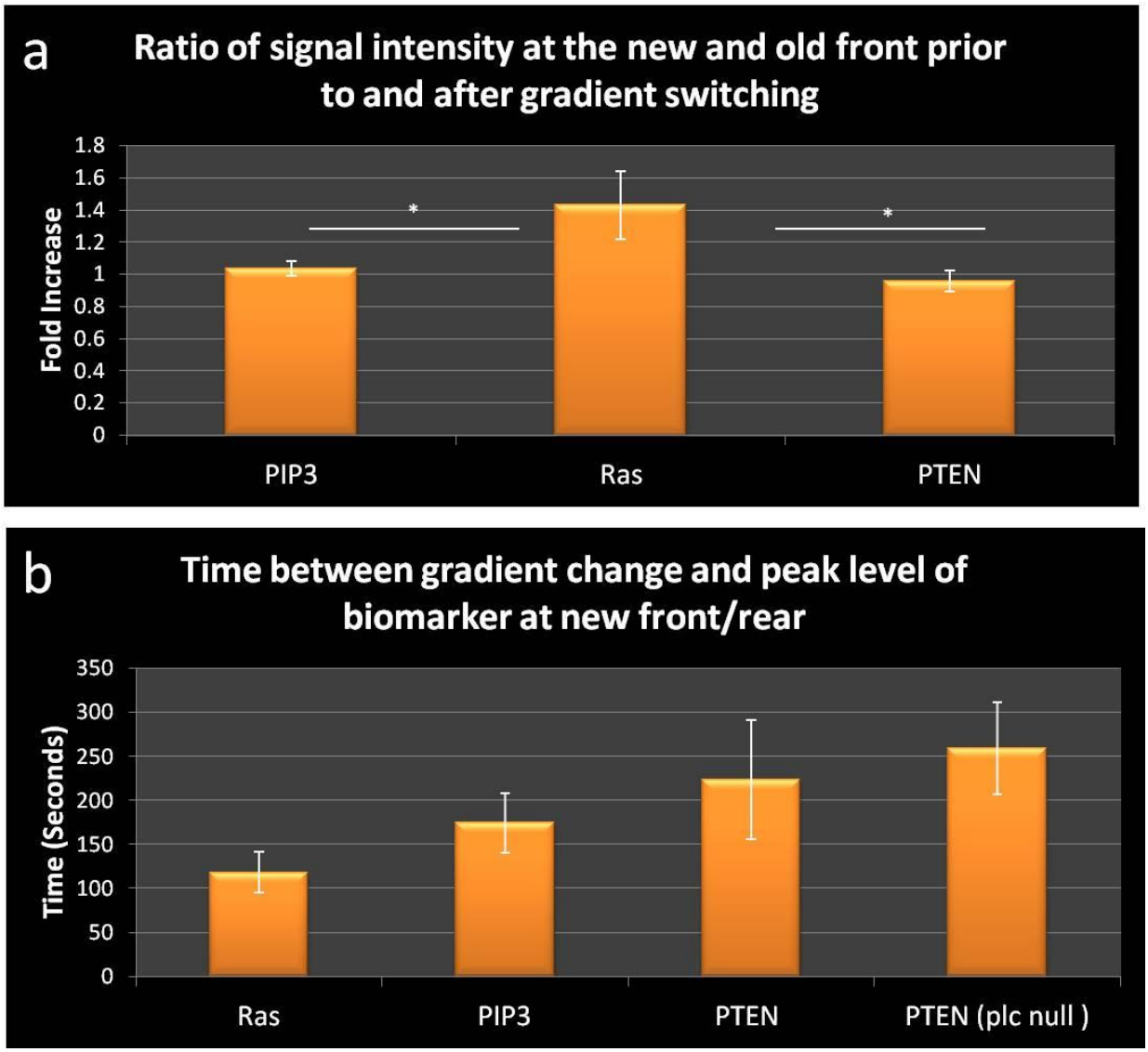

Figure 15. Ras activation increases significantly and quickly at the leading edge of a cell a) When measuring the ratio of Ras activation, and PIP3 at the new front vs. the old back) and PIP2 (old back vs. new front), we find that Ras activity has a significantly higher fold change. There were 11 cells used for Ras activity (4 different days), 9 cells for PIP3 (2 different days)and 8 cells for PTEN (2 different days). A one tailed student t test with type two sample unequal variance was used to determine if the fold increases for Ras, PIP3 and PTEN were statistically different from each other. It was determined that Ras activity increase was statistically significant than PIP3 (p value < 0.012) at the new front and PTEN (p value $<.00809$) at the new back. b) The time it takes for Ras activity to reach its peak at the new front of the cell is smaller compared to PIP3 (new front) and PIP2 (new back) of the cell. 9 cells were used for Ras activity (3 different days), 10 cells for PIP3 (2 different days), 9 cells for PTEN (2 different days), and 10 cells for PTEN plc null (3 different days).

PLC null cells still reverse polarity and PTEN forms vesicles at the rear of the cell when cells reverse.

In order to investigate the role of PI(4,5)P2 during polarity break down and reestablishment, we expressed PTEN-GFP in PLC null cells. Cells lacking PLC have been shown to influence PI(4,5)P2 levels (Kortholt et al., 2007; Srinivasan et al., 2013b) and also have trouble responding during chemorepellant stimulation (Keizer-Gunnink et al., 2007). Prior to the reversal, cells were polarized and migrating towards the high side of the gradient. As seen in wild-type cells, high levels of PI(4,5)P2 at the old back blocked the establishment of "frontness" and pseudopod extension (Figure 16a). On the other hand, rear retraction clearly begins before the redistribution of PTEN-GFP to the new back. Much of the PTEN in PLC null cells appeared to redistribute to the back of the cell by diffusing along the plasma membrane, but there was also PTEN diffusion through the cytosol (Figure 16b). These PTEN-GFP decorated vesicles appeared to break away from the rear of the cell in small patches and reassociate with the new rear side of the cell (Figure 16 a,b). Similar vesicular structures were also present when PLC nulls were imaged during random migration (Data not shown). On average, cells lacking PLC retracted their "new" rear more quickly than wild-type cells after gradient switching (Figure 16c) but there no detectable difference in the ability of cells to ramp up the PI(4,5)P2 levels in the new backs (Figure 17).

It has been suggested that other regulators that use PI(4,5)P2 as a substrate, should also influence overall PI(4,5)P2 levels (Kortholt et al., 2007; Srinivasan et al., 2013a). To test the ability of cells to regulate PI(4,5)P2 levels in the absence of PI3K activity, PLC nulls were stimulated in the absence and presence of the PI3K inhibitor LY 294002. Untreated cells showed a very strong redistribution of PTEN-GFP to the cytosol in response to a uniform stimulus of cAMP (Data not shown). Treated cells had very little loss of PTEN-GFP on the plasma membrane (Figure 16e). Wild-type cells in the same field expressing PH-GFP and a marker for actin polymerization, showed no increase in PI(3,4,5)P3 levels, but displayed a very

strong actin response. These results show that PI3K activity contributes to the lowering of PI(4,5)P2 levels, but there is still yet another regulator of PI(4,5)P2 levels. Interestingly, these cells were still able to move in the direction of the micropipette, and lowered their PI(4,5)P2 levels on the pseudopods that were extending outward. It is worth noting that the wild-type cell also extended an actin-filled projection in the absence of PI3K activity (Figure 16e) (Housman).

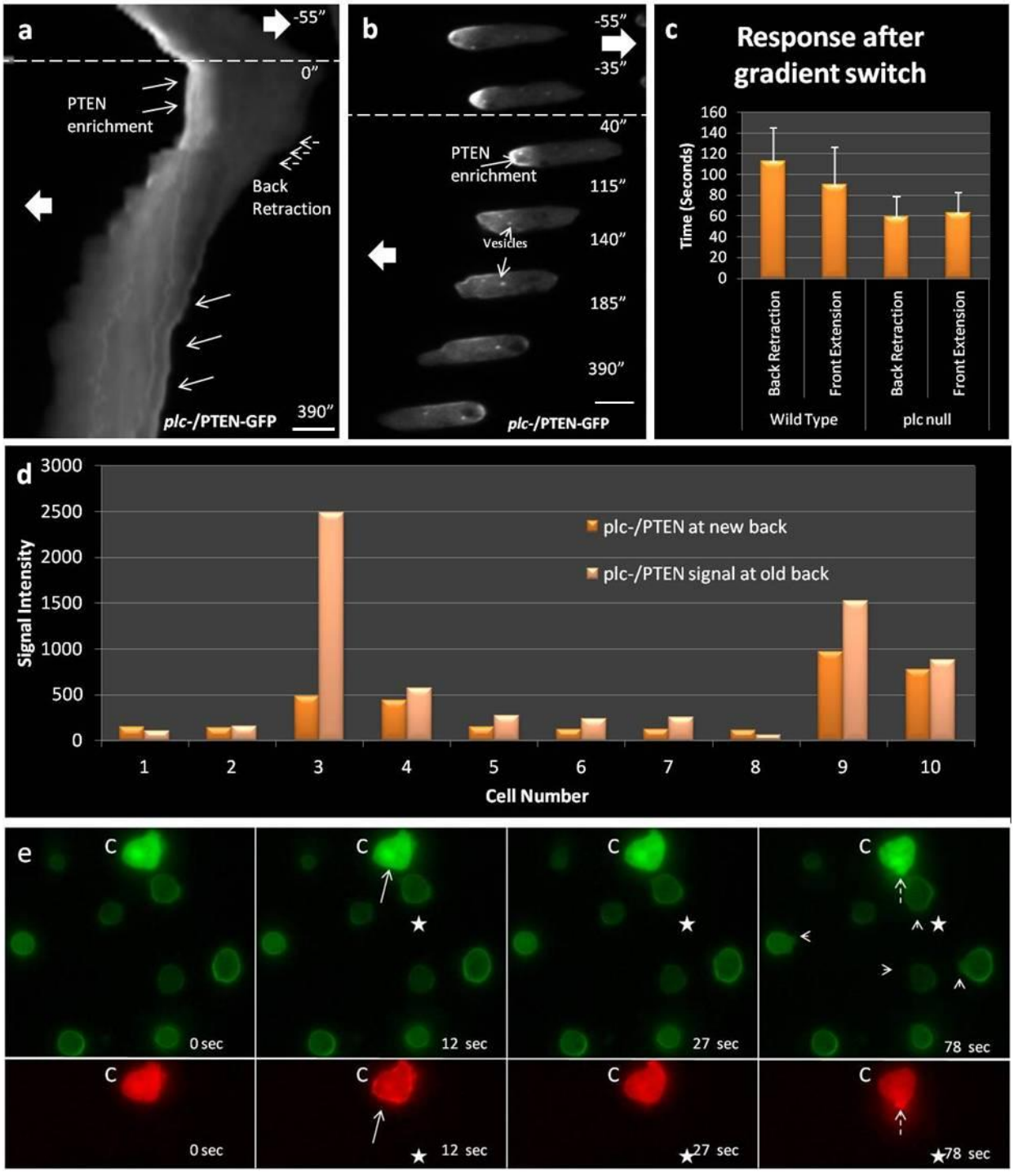
a
-55″
0″
PTEN
enrichment
Back
Retraction
plc-/PTEN-GFP
390″
b
-55″
-35″
40″
PTEN
enrichment
115″
Vesicles
140″
185″
390″
plc-/PTEN-GFP
c
Response after
gradient switch
Time (Seconds)
160
140
120
100
80
60
40
20
0
Back Retraction
Front Extension
Back Retraction
Front Extension
Wild Type
plc null
d
Signal Intensity
3000
2500
2000
1500
1000
500
0
plc-/PTEN at new back
plc-/PTEN signal at old back
1
2
3
4
5
6
7
8
9
10
Cell Number
e
C
0 sec
12 sec
27 sec
78 sec

Figure 16. *plc*-/PTEN-GFP cells can reverse their polarity after a gradient switch a) Kymograph indicating polarity reversal of a representative cell. PTEN enrichment is shown by arrows. Back retraction before PTEN localization at the new rear is indicated by dashed arrows. b) Still images of the cell in A as it undergoes polarity reversal. There is an enrichment of PTEN at the rear of the cell as indicated by solid arrows. Vesicles containing PTEN GFP are also observed. c) Comparison of the time it takes to extend the new front and retract the new back between wild type and plc null cells. 8 cells (2 different days) were used for Wild type data set and10 cells (3 different days) were used for PLC null data set. See text for actual values. Error bars show standard error of the mean. See Chapter II for Methods. d) Signal intensity of PTEN GFP measured at the new back of the cell at the time point of gradient change and at the time point of initial back retraction shows that in 8/10 cells, PTEN is higher at the old back of the cell when the back starts to retract. Bars represent data for each individual cell. Experiments are from 3 different days. e) plc- cells expressing PTEN GFP are exposed to cAMP at time point 12 seconds (solid arrow). Cell Labeled C is a control cell that expresses both PH-GFP (top panel) and LimE RFP (bottom panel). Star indicates micropipette location. Solid Arrow indicated the time point of the uniform stimulation (12 seconds). Arrow heads indicate pseudopod extensions that do not have PTEN (78 seconds). Dashed arrow indicates pseudopod extension with LimE (bottom panel). Scale bar is 10 µm.

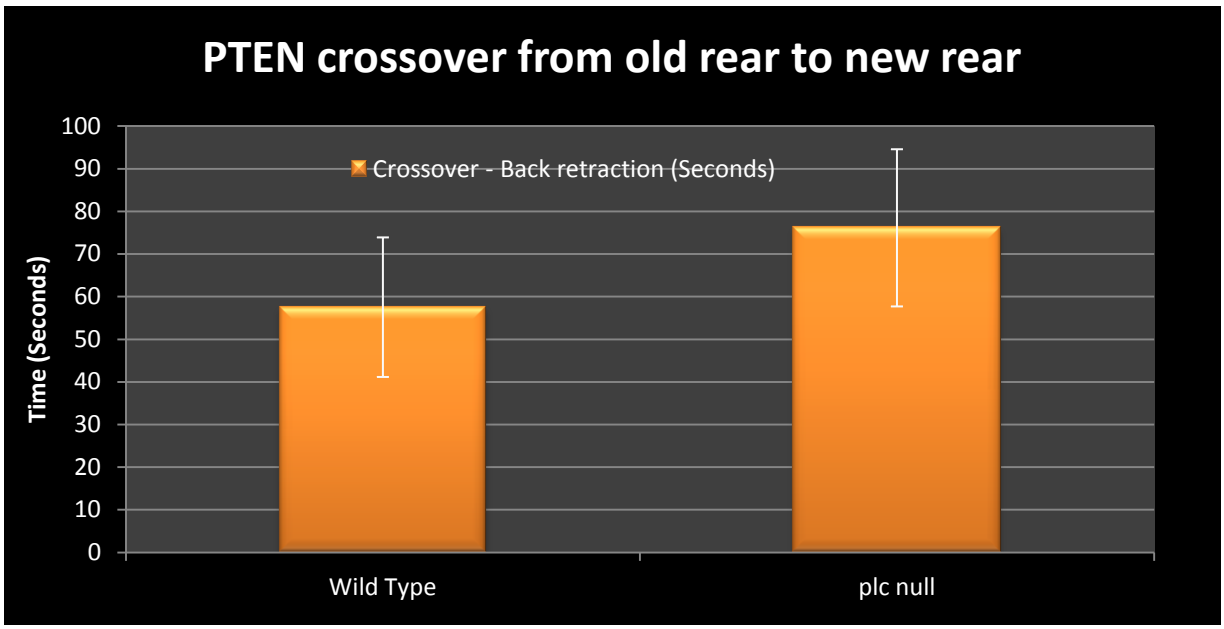

Figure 17. PLC null cells take longer to accumulate PTEN at the new rear of the cell compared to wild type cells The intensity of PTEN-GFP at the old back and new back were measured. The graph indicates the average time it takes for the new back of the cell to have more PTEN than the old back of the cell after the cell has started to retract its new back. The average time was taken for 6 cells (2 different days) for wild type and 9 cells for PLC null cells (3 different days). Error bars are for standard error of the mean.

Microtubule interaction with the plasma membrane at the poles is inversely correlated with the presence of F-actin.

We monitored the dynamic localization of microtubules during *D. discoideum* chemotaxis toward a gradient of cAMP and after gradient reversal. Microtubules initially at the rear of the cell, maintained their positioning at the new front of the cell until a new leading edge formed and a pseudopod extended (Figure 18 a and 18 d). Once the cell extended these pseudopods, microtubules were excluded from this region. We speculated that F-actin filled projections were somehow excluding the microtubules from these regions. To test this, we examined cells that were expressing both GFP-tubulin and LimE-RFP, a marker for actin polymerization. As can be seen from Figure 18B, the GFP-tubulin and LimE-RFP do not co-localize. To explore this localization further, this phenomenon was also confirmed in cells undergoing random migration using Bessel Beam microscopy (Figure 18c). There is a complete lack of GFP-tubulin from F-actin filled pseudopods and macropinosomes, while in areas where there is little LimE-RFP signal, GFP-tubulin can often be seen interacting with the plasma membrane. As has been previously been reported, we found that the nucleus oriented towards the front, with the MTOC at the rear during directed migration. Microtubules originating from the MTOC were found mainly on the sides and the rear of the cell and were absent from the leading edge (Figure 18b and c). Cells expressing GFP-tubulin were also observed during the reversal process. Microtubules reach the new rear of the cell, prior to a PIP3 crescent at the new front of the cell (Data not shown). In cells treated with Latrunculin-A, it was also found that the microtubules are very active and can be seen interacting with the inner portion of the plasma membrane for short periods of time. During these time periods, the MTOC/nucleus also appears to move slightly as if it is temporarily connected to the plasma membrane via the microtubules (Figure 18d).

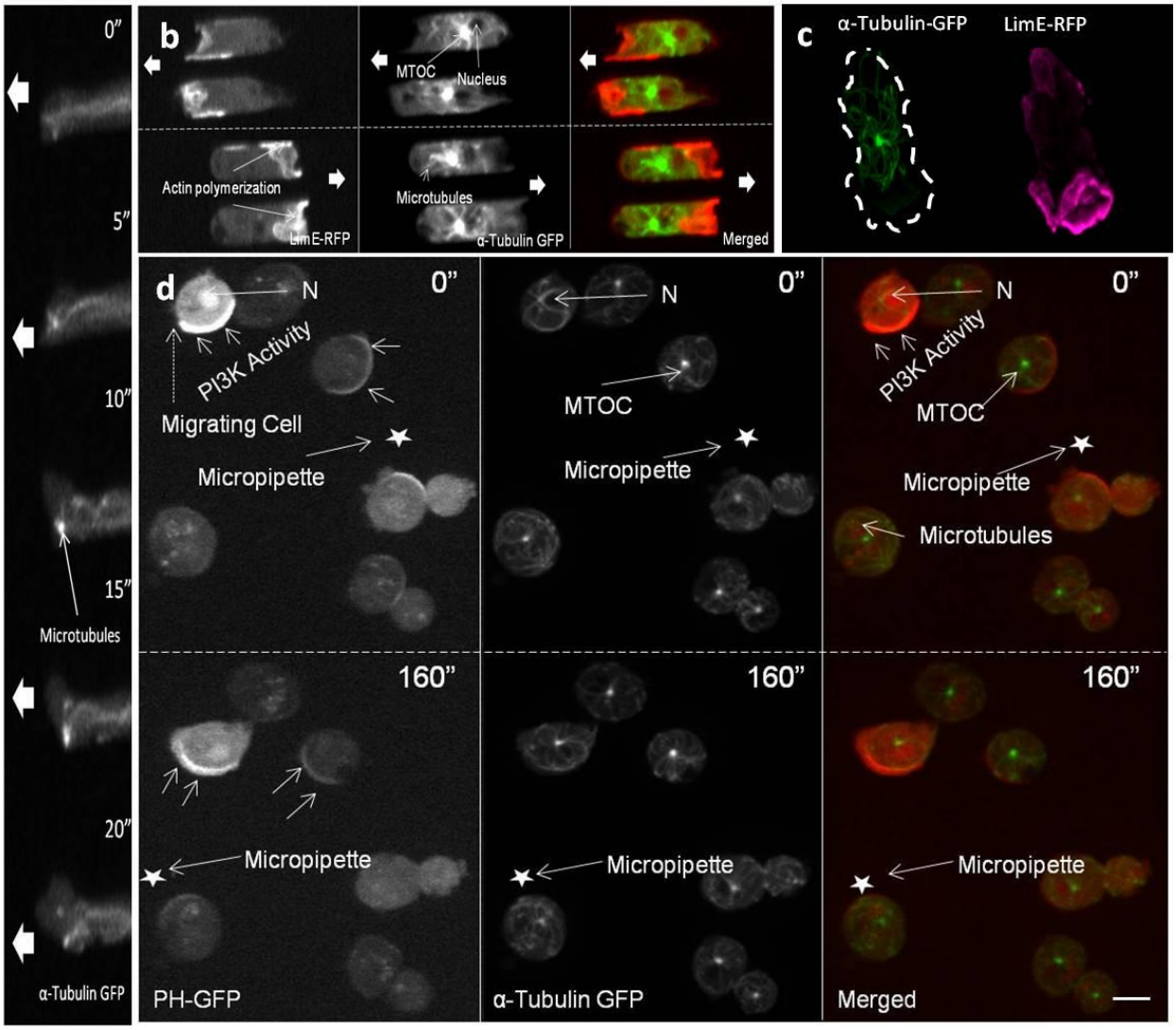

Figure 18. Areas of actin and microtubule polymerization are mutually exclusive a)The extension of a pseudopod at the new front of the cell dislodges microtubules b) Microtubules and polymerized actin are spatially segregated. c) Similar segregation was found during random movement by Bessel Beam microscopy d) Cells treated with Latrunculin-A to dissociate the actin cytoskeleton have microtubules present all over the cell and can sense the gradient indicated by the PH-CRAC signal as indicated by arrows. The migrating cell has not fully depolymerized its actin cytoskeleton. N - Nucleus, MTOC – Microtubule Organizing Center. Projection Images of 5 planes. Scale bar is 10 µm.

To pursue the role that high levels of PI(4,5)P2 have on chemoattractant-mediated responses, we decided to stimulate cells at the onset of metaphase. Cells typically round up at the onset of metaphase prior to cell division. It has been shown in *D. discoideum* that the PM levels of PI(4,5)P2 are uniformly high along the entire periphery of the PM at metaphase (Janetopoulos et al., 2005). This mirrors the localization of myosin II and presumably cortexilln I, which also binds to PI(4,5)P2. Presumably, the cell resets it's polarity prior to anaphase when the spindle re-establishes asymmetry (Janetopoulos and Firtel, 2008). Vegetative cells expressing PH-GFP were stimulated with the chemoattractant folic acid at metaphase. These cells showed no response, while surrounding control cells in other stages of the cell cycle showed robust PI(3,4,5)P3 responses (Figure 19a and 19b). When we stimulated cells expressing PTEN-GFP at metaphase, PTEN did not redistribute to the cytosol (data not shown). Presumably, the feedback loops that maintain the high levels of PI(4,5)P2 at metaphase are hard to break at this stage of the cell cycle

We wondered whether cells were incapable of responding to chemoattractants during metaphase, so we stimulated metaphase cells expressing RBD-GFP. To our surprise, cells gave a strong response, suggesting that the upstream components were intact (Figure 19b). This finding suggested that PI(3,4,5)P3 responses were inhibited due to the large amount of PTEN on the PM. To test this, we stimulated PTEN null cells expressing PH-GFP with folic acid. Metaphase cells gave a very robust PI(3,4,5)P3 response (Figure 19c). The PI(3,4,5)P3 response was largely confined to the poles of the dividing cell and persisted through the latter stages of cytokinesis. Interestingly, the response of PTEN null cells at metaphase and at other stages of the cell cycle were completely the opposite of wild-type cells at metaphase or at other stages of the cell cycle. PTEN null cells gave strong responses at metaphase, while wild type cells showed no response (Figure 19b). PTEN null cells at other stages of the cell cycle showed little or no response since their PMs were already highly decorated with PH-GFP as vegetative cells are highly sensitive to stochastic signaling fluctuations (Srinivasan et al.,

2013b). Wild-type cells at other stages of the cell cycle in the same field had robust PI(3,4,5)P3 responses. Note that PTEN null cells have very little PI(3,4,5)P3 at the furrow. This is not surprising given that migrating PTEN null cells only have PI(3,4,5)P3 on the side of the cell facing the higher concentration of chemoattractant (Iijima and Devreotes, 2002) and suggests that other regulators maintain elevated PI(4,5)P2 levels in the furrow of dividing and in the rear of migrating PTEN null cells. Lastly, the PI(3,4,5)P3 response in metaphase PTEN null cells display kinetics similar to those seen to wild-type cells.

Given that RBD was active, but PTEN did not redistribute in metaphase cells, we examined cells expressing PI3K2-GFP (Janetopoulos et al., 2005) and LimE-RFP (Clarke et al., 2006) to see whether they responded to folic acid stimulation. PI3K2 and LimE responded rather weakly, while control cells showed robust responses (Figure 19e) (Rucker and Khodadadi). We stimulated cells at metaphase and also again later at anaphase. Responses at metaphase were uniform, while those at anaphase were limited to the poles, as has been previously described (Janetopoulos et al., 2005). Cells at metaphase were still activating Ras, PI3K and had an actin response, yet the cells hardly showed any morphological change as compared to cells in other phases of the cell cycle (Data not shown).

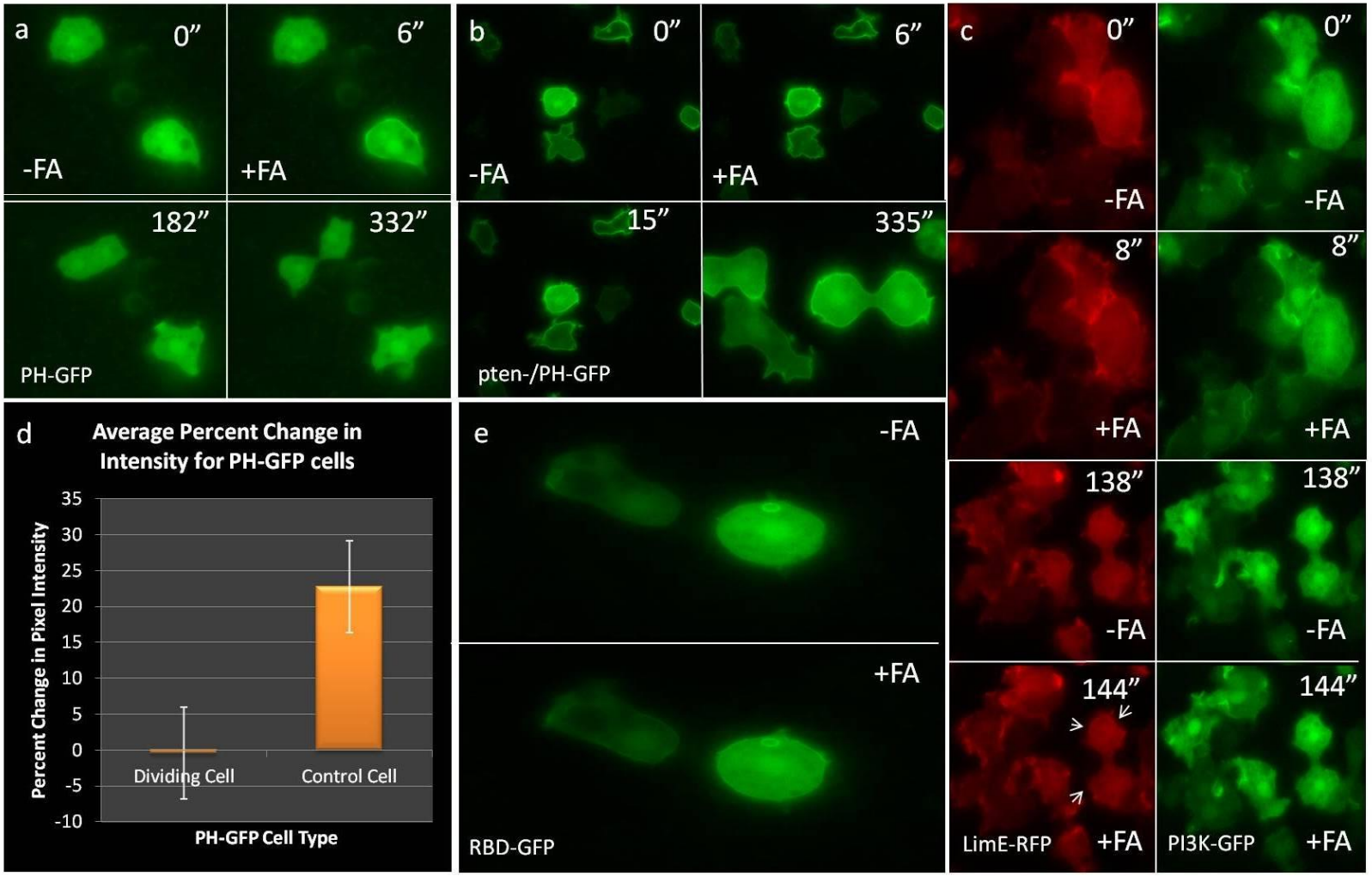
a
0”
6”
-FA
+FA
182”
332”
PH-GFP
b
0”
6”
-FA
+FA
15”
335”
pten-/PH-GFP
c
0”
0”
-FA
-FA
8”
8”
+FA
+FA
138”
138”
-FA
-FA
144”
144”
LimE-RFP
+FA
PI3K-GFP
+FA
d
Average Percent Change in Intensity for PH-GFP cells
Percent Change in Pixel Intensity
35
30
25
20
15
10
5
0
-5
-10
Dividing Cell
Control Cell
PH-GFP Cell Type
e
-FA
+FA
RBD-GFP

Figure 19. High PIP2 levels reduce response after uniform stimulation by chemoattractant a) Cells undergoing mitosis do not have PH-GFP membrane localization under uniform stimulus of folic acid. b) pten-/PH-GFP cells undergoing mitosis have low PH-GFP at the membrane after uniform FA stimulation (6 seconds) and also have low PH-GFP at the furrow. c) Cells that express LimE RFP and PI3K GFP have weak PI3K localization after uniform folic acid stimulus. d) Quantification of PH-GFP in dividing cells vs. control cells shows that the PH-GFP signal does not change in dividing cells after stimulation. The p-value for this data set is 1.48E-06. e) RBD localization before and after stimulation with Folic Acid at Metaphase shows that Ras activity localizes to the membrane after uniform stimulation. +FA = 10 μm uniform Folic Acid.

DISCUSSION

Advantages of using the open microfluidic system for cell polarity studies

There have been many studies performed using *D. discoideum* cells to look at the responses of cells exposed to rapidly shifting gradients by moving a micropipette filled with chemoattractant to either the front or the rear of the cell in order to induce cells to change directions (Chen et al., 2003; Dalous et al., 2008; Devreotes and Janetopoulos, 2003; Srinivasan et al., 2013a). Microfluidic experiments in a flow based bidirectional gradient generator that changed the gradient of unconfined cells have also looked at cells in varying gradients (Meier et al., 2011). Here, we described a protocol that uses two micropipettes eliciting passive cAMP gradients and confines cells to individual channels to prevent the cells from doing U-turns and which forces them to invert their polarity and completely reorganize their cytoskeleton. This technique allowed us to study individual cells as well as quantify the spatial and temporal redistribution of signaling and cytoskeletal components during polarity loss and reestablishment in the opposite direction.

Kymograph analysis reveals distinct features of polarity establishment

As can be seen from the kymographs in (Figures 12 a,d,g and Figure 16a), the rear of the cell typically begins retracting before front extension. Front extension did not occur until redistribution of PTEN from the PM of the old rear. Measurement of PI(4,5)P2 and PI(3,4,5)P3 accumulation during polarity reversals indicate that PI(4,5)P2 accumulation is slightly slower at the new rear of the cell compared to PI3K activity at the new front of the cell. The generation of PI(3,4,5)P3 likely occurs rapidly since Ras activity is upregulated very quickly. On the other hand, PTEN-GFP has to make its way across the length of the cell before it can set up a feedback loop in the developing rear.

Interestingly, our data shows that neither “frontness” nor “backness” seems sufficient for overall cell motility. Net movement of the cell requires the proper balance of the two. Additionally, cells

having PTEN on both ends do not retract on both ends and shorten, while cells having high PM levels of PI(3,4,5)P3 do not have two leading edges and do not stretch out and elongate. The latter case is reminiscent of dividing cells, where there is some extension in opposite directions of PI(3,4,5)P3-labeled poles, but has one critical difference since there is still polarity driven by the developing furrow, which contains high levels of PI(4,5)P2 during cytokinesis (Janetopoulos et al., 2005).

Relationship between microtubules and the actin cytoskeleton

The role of microtubules during chemotaxis has been studied in various cell types such as *D. discoideum* and mammalian cells. Early work showed that microtubules in moving cells are excluded from the leading pseudopod (Rubino et al., 1984). Moreover, the microtubule network is associated with the MTOC and helps maintain the nucleus in a fixed position. In migrating amoebae, it was shown that nuclei can be found in the frontal region of the cell but more preferentially following the MTOC (Schliwa et al., 1999). Our experiments indicate that front extension as well as back retraction during polarity re-establishment was observed prior to MTOC and nucleus repositioning. These results suggest that the initial positions of the MTOC and nucleus are not mandatory for initially establishing cell polarity during chemotaxis but are likely important for the maintenance of polarity as it is being established. The position of the MTOC could determine where the microtubules are localized in the cell. Molecules transported along the microtubules may contribute to reinforcement of “backness” and may also interact with PI(4,5)P2 (Klopfenstein et al., 2002).

Interestingly, cells naturally disassemble their entire microtubule cytoskeleton at metaphase. Based on the localization of the microtubules during motility, one would expect PI(4,5)P2 levels to drop, yet they rise along the entire PM and the cells become all “back”. Then, during anaphase, astral microtubules extend and contribute to activation at the poles, which has components analogous to the leading edge of the cell. This suggests either that microtubules have no role in establishing membrane asymmetry or that the microtubules during cytokinesis

interact differently with the PM than they do during the rest of the cell cycle. Our work at metaphase shows that an intact microtubule network is not necessary for signaling responses or actin polymerization. Interesting questions persist: Does the loss of polymerized microtubules contribute to the rise in PI(4,5)P2 levels and backness?. In any case, understanding the mechanism at this stage should be of high priority since it would potentially make a very good drug target for silencing overactive cells such as those seen during metastasis.

Antagonistic role between PI(4,5)P2 and Ras

While the reciprocal relationship between PTEN and PI3K has been well documented, this is the first report showing the antagonistic spatial localization of Ras activity and PM PI(4,5)P2 levels. There was no colocalization of activated Ras and PTEN in both migrating polarized cells as well as in Latrunculin treated cells that were exposed to rapidly changing cAMP gradients.

High levels of PM PI(4,5)P2 put the brakes on actin polymerization and contribute to "backness"

We have recently expanded on what was apparent to some in the motility and polarity fields. Signaling molecules that translocate to the plasma membrane in response to a chemoattractant stimulus largely localize to the front of a migrating cell or to the poles of a dividing cell. Conversely, signaling molecules that interact with PI(4,5)P2 are largely on the plasma membrane prior to a stimulus, and redistribute to the cytosol. Such PI(4,5)P2 markers like PTEN or cortexillin I are also localized to the rear of a migrating cell and furrow of a dividing cell.

The link between the actin cytoskeleton and the phosphoinositols has not been shown directly. One of the best pieces of evidence to show this link used cells that have a disruption in the PTEN gene. These cells are expected to have high PI(3,4,5)P3 levels due to the absence of PTEN. Experiments have shown that the PIP3 response as well as the actin response is elongated and also highly coordinated in the absence of PTEN (Iijima and Devreotes, 2002;

Janetopoulos and Firtel, 2008). This has been used as a premise to link PI(3,4,5) levels to actin polymerization. However, it may be that is not just because of high PI(3,4,5) levels, but also because of low PI(4,5)P2 levels that actin polymerizes. It may be that PI(3,4,5)P3 does support the generation of actin polymerization (Ganesan et al., 2006; Vedham et al., 2005; Xu et al., 2003). However, we speculate that it is also critical for PI(4,5)P2 levels to be lowered. PI3-kinase activity contributes to lower levels by using PI(4,5)P2 as a substrate, as does PLC. Both are activated in response to chemoattractants. Loss of PTEN means both a sustained level of PI(3,4,5)P3 and lower PI(4,5)P2 levels after a uniform stimulus. We propose that it is these low levels of PI(4,5)P2 that provide access to effector molecules that drive F-actin polymerization (Figure 20). This model would explain why there can often be F-actin polymerization in the absence of PI3K activity. Work in the mammalian system has also shown that lowering of PI(4,5)P2 levels is critical for cofilin activation, and thus a similar mechanism is likely at work in higher eukaryotes (Bravo-Cordero et al., 2013), although we would speculate that there is much evidence to suggest that other mechanisms also regulate the polymerization of actin filaments during migration (Chen and Pollard, 2013; Choi et al., 2013; Insall et al., 2001).

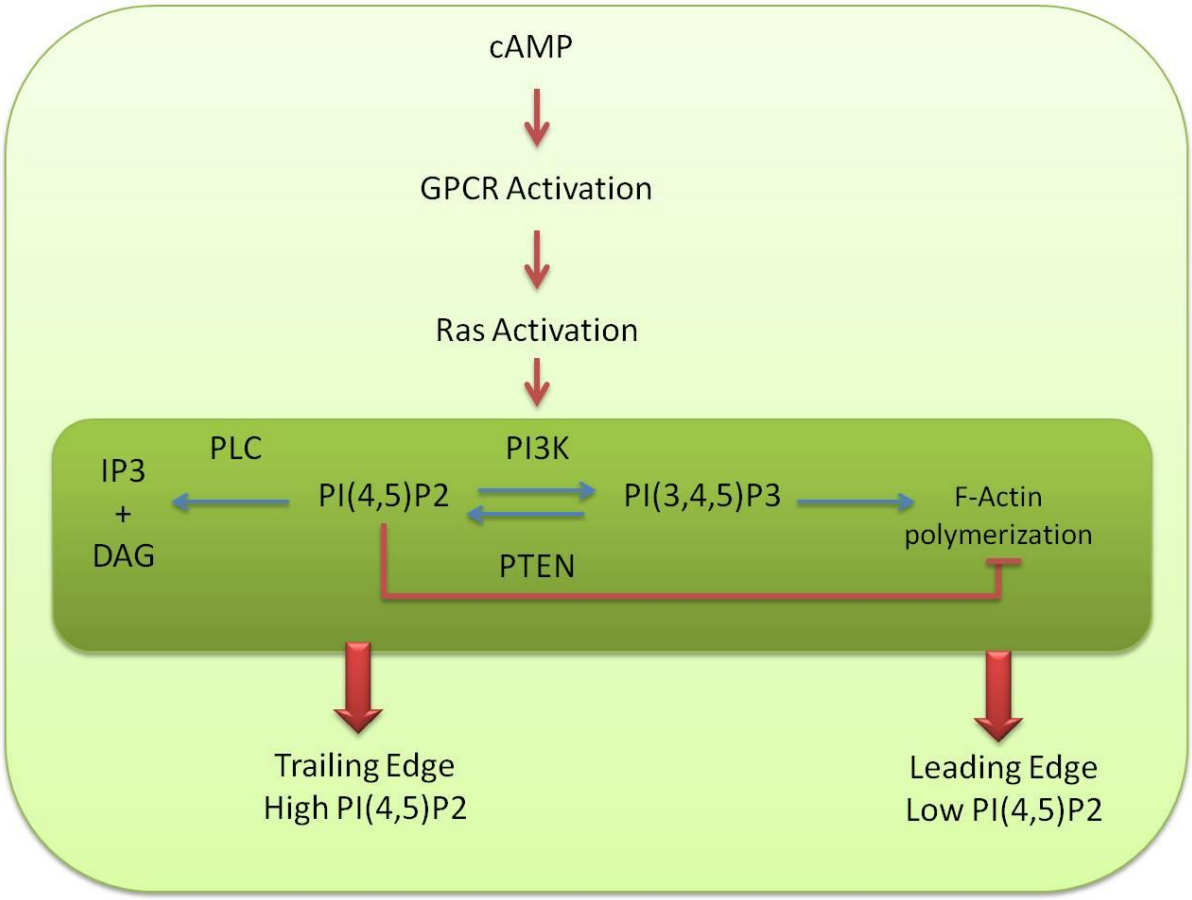

Figure 20. Model for defining "frontness" and "backness" via PI(4,5)P2 Once a cell senses a cAMP gradient, it activates the G protein coupled receptors which lead to other events downstream such as Ras activation followed by PI3K activity at the leading edge to convert PI(4,5)P2 to PI(3,4,5)P3. PI(4,5)P2 is also converted to IP3 + DAG by PLC. The combined efforts of PI3K and PLC help to lower PI(4,5)P2 levels at the leading edge of the cell which allows for the leading edge to form by enabling F-actin based protrusion. The sides and rear of the cell have high PI(4,5)P2 levels which promote actomyosin and rear constriction. The balance between high and low PI(4,5)P2 levels determines "frontness" and "backness"

What else supports this model? PLC overexpressing cells lower PI(4,5)P2 levels, and morphologically resemble PTEN null cells in a cAMP gradient. These cells also trigger very strong PI(3,4,5)P responses when given a uniform stimulus (Kortholt et al., 2007). It may be that in both cases, lower PI(4,5)P2 levels initiate positive feedback loops which allow “frontness” and branched F-actin polymerization to occur. We suggest that just the opposite occurs at metaphase where the cell membrane becomes quiescent prior to the taking over of cell polarity by the spindle apparatus. Metaphase cells have a high PI(4,5)P2 levels and a higher threshold to activate branched F-actin polymerization.

We propose a model where high PI(4,5)P2 levels can block membrane protrusion and contributes to “backness”, which helps maintain and stabilize the rear or furrow of the cell. While careful measurements of the PM levels of PI(4,5)P2 have not been done, the loss of PTEN (and cortexillin I) from the PM in response to uniform stimulation of chemottractants in wild-type cells suggests that PI(4,5)P2 levels drop considerably and then rapidly rise as the PI(3,4,5)P3 response terminates. We suggest that it is a possibility that the low levels of PI(4,5)P2 provide access of GEFs to excitatory components (like activated heterotrimeric G proteins and small GTPases). When PI(4,5)P2 levels are high, the local environment favors activators of “backness” and blocks excitatory signaling molecules like Ras. This rise in PI(4,5)P2 may be the elusive “inhibitor” that several models have proposed as regulating chemoattractant-mediated responses (Janetopoulos et al., 2004), and many other modeling papers (Levchenko and Iglesias, 2002; Meinhardt, 1999). We would not say PI(4,5)P2 is actually an inhibitor, but more specifically is associated with “backness”, which is typically the quiescent state of a cell.

However, several pieces of data argue against such a simple model. First of all, PI3K and Ras would be predicted to have extended time courses in PTEN nulls, but their time courses are normal (Iijima and Devreotes, 2002; Sasaki et al., 2004). In addition, it would be predicted that since PTEN nulls lack phosphatase activity, PI(,4,5)P2 levels in these cells would take longer to recover. Expression of a phosphatase dead PTEN (ptenG123E) construct in a

PTEN null background might be expected to result in PTEN staying in the cytosol. This phosphatase dead PTEN displays normal kinetics and moves back onto the PM after a uniform stimulus. Interestingly, PTEN null cells still have “backness”, suggesting that PI(4,5)P2 levels still increase in the rear of the cell.

PTEN null cells stimulated during cytokinesis demonstrate that PI(4,5)P2 levels still regulate cytokinesis even in the absence of PTEN. PI(3,4,5)P3 responses at metaphase in wild-type cells resembles the lack of a folic acid response in PLC nulls. These data all suggest that another regulator, possibly a kinase (PI4 and 5-kinase), is active in the furrow and during the adaptation phase of the response. Evidence for their activity is well documented (Mao and Yin, 2007; Sorensen et al., 1998; Sorensen et al., 1999; Zhu et al., 2013). This can be tested by treating the cells with drugs such as Wortmannin to inhibit PI4-kinase activity and monitoring the response.

Polarized morphologies manifest themselves during migratory processes in many cell types and throughout the lifecycle of metazoan organisms. The spatial and temporal regulation of signaling molecules and the cytoskeletal rearrangements that occur are highly conserved across species and also display themselves during random cell motility and cytokinesis (Janetopoulos and Devreotes, 2006; Janetopoulos and Firtel, 2008; Muthuswamy and Xue, 2012; Panbianco and Gotta, 2011; Vorotnikov, 2011). The studies described here have elucidated key signaling events and have given us insight into the regulation that occurs during the establishment and maintenance of cellular polarity in response to chemoattractant gradient switching. Similar studies can be conducted that investigate other proteins or lipids to generate a detailed time line of the sequence of events that lead to polarity establishment, gradient sensing and motility. This system has also been adapted for mammalian cell chemotaxis and can be used as a powerful tool to observe cell polarity establishment as well as other cellular interactions that were formerly not possible to observe using standard chemotaxis assays.

*Work for this chapter is adapted from the following manuscript currently in preparation.

Jowhar, Khodadadi, Wright, Rucker, Housman, Wikswo, Chen, Betzig and Janetopoulos, (2013). In preparation.

- Jowhar and Janetopoulos designed concept for experiment setup. Wikswo provided input for data analysis and presentation. Chen and Betzig developed Bessel beam microscopy setup. Experiments and data analysis were performed by Jowhar, Khodadadi, Wright, Rucker, Housman, Chen, Janetopoulos. Janetopoulos, Jowhar and Wright are preparing the manuscript.

Special note for experiments for Chapter IV: All experiments and quantification were performed by Jowhar with the following exceptions.

Experiment for 13e was performed by Janetopoulos and Jowhar
Experiments for Figure 16e were performed by Housman
Experiments and quantification for Figure 19 were performed by Rucker and Khodadadi
Bessel Beam Microscopy (Figure 18c) was performed by Bi-Chang Chen at the Betzig Lab

CHAPTER V

FUTURE DIRECTIONS

The study of cell polarity in model organisms provides us with a valuable tool to understand the mechanisms and pathways regulating cell migration and provide insight into the migratory processes in higher organisms, particularly those involved in disease states. In this work, we have looked at cell polarity from two different angles. The first was the role of polarity during cell migration and the second was the mechanism of polarity establishment. It was shown in Chapter III that cells that are polarized are very efficient in chemotaxis as measured by their higher chemotactic speed. In addition, the leading edge of a polarized cell can not only sense a chemical gradient but also mobilize its cytoskeleton to respond to the gradient, all without input from the rear of the cell. In Chapter IV, we elucidated the process of polarity establishment by forcing polarized cells to extinguish their polarity and reestablish it in the opposite direction. We looked at several known markers of polarity and the spatial and temporal response that takes place during polarity establishment. We have found that polarity, as defined by the presence of a distinct front and back, is established by the coordinating efforts of both signaling and cytoskeletal components.

Our results show that PI(4,5)P2 levels at the plasma membrane serve as inhibitors to several downstream events after receptor activation and specify “backness”. By lowering PI(4,5)P2 levels using PI3K, PLC and potentially other regulators, the cell can activate Ras (and likely other GTPases) which drive actin polymerization at the leading edge of the cell. While our measurements and studies by others (Sasaki et al., 2004) have shown that Ras activation is one of the first events downstream of receptor activation that leads to polarity establishment, we find that PIP2 levels have to be lowered in these regions for Ras activity to initiate the leading edge of the cell. Ras activity is closely followed by the activity of PI3K to increase PI(3,45)P3

levels (while simultaneously lowering PI(4,5)P2 levels) to lower membrane PTEN levels. This will allow for pseudopod extension via actin polymerization at the side of the cell facing the chemoattractant. At the same time, there is an accumulation of PIP2 toward the sides and rear of the cell which serves as a binding site for PTEN. This allows for the prevention of lateral pseudopods at the side and rear of the cell and also helps to create a defined cell rear.

Using our cell polarity reversal assay, we have been able to clearly observe that cell rear retraction can initiate in the absence of PTEN. We speculate that levels of PI(4,5)P2 may rise in the absence of PTEN while PTEN is “tied up” at the old rear. Once PI(4,5)P2 levels drop in the old rear, they rapidly rise in the new rear. We have observed this in both wild type and PLC null cells. We have not seen colocalization with activated Ras and PTEN in both polarized and Latrunculin-A treated cells which indicates that Ras activation typically only happens when plasma membrane levels of PI(4,5)P2 are low.

In addition, we have seen that regions that have actin polymerization are devoid of microtubules. We speculate that either the actin filaments block the interaction of the microtubules with the plasma membrane or that the microtubules have a higher affinity for the new back. We favor the latter mechanism. The microtubules may then transport molecules that support “backness”. We have also observed that the positioning of the nucleus and the MTOC is not a prerequisite to the establishment of cell polarity.

These observations were possible using our polarity reversal assay which creates a highly quantifiable and reproducible platform for understanding the mechanisms involved in the establishment of cell polarity. Even though our focus was on known regulators of cell polarity in *D. discoideum* chemotaxis, this system could be applied to study several other processes involved in chemotaxis.

While other groups have attempted to reestablish cell polarity or look at cellular responses in the absence of an actin cytoskeleton using a micropipette assay, the Open Microfluidics Method provides a controlled environment for examining signaling responses. This

setup coupled with the analysis method outlined in Chapter II, can provide a useful platform to screen for mutants as well as correlate localization of biomolecules and their effects on cell chemotaxis. For example, there have been several microtubule associated proteins that have certain functions during cell migration. By observing the relocalization of movement of these motors or their cargo, their role in biasing transport toward the rear of the cell can be observed and measured. The sensitivity of the front or rear of the cell can also be assayed using this setup by generating gradients of different steepness and correlating it to the response time of the cell. This assay can also be used to study the polarity establishment during the chemotaxis of neutrophils and other mammalian cells.

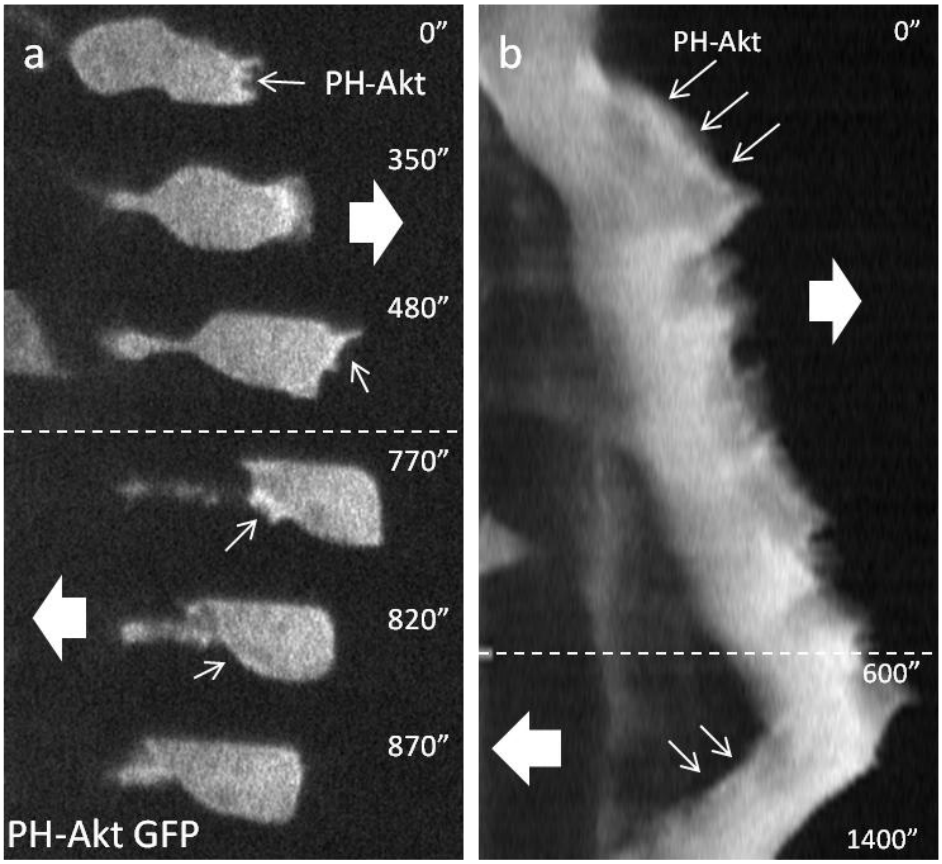

Figure 21. HL-60 cells during polarity reversal a) A representative cell expressing fluorescent PH-Akt can reverse polarity after the gradient is switched. The white block arrows indicate the direction of the high side of the gradient. The small white arrows show PH-Akt localization at the leading edge of the cell. b) Kymograph of the cell shown in “a”. PH-Akt can be seen at the leading edge of the cell and once the cell reverses its polarity, it can be visualized at the new leading edge (white arrows).

We have shown previously (Rachakonda et al., 2010) that microfluidic systems that have maze designs can be used to study the migration of cancer cells, particularly as they migrate through tight spaces. This can be coupled with fluorescent biomarkers to delineate the roles played by different cellular components in gradient sensing and mobilization of the cytoskeleton. We have already used this setup to study the migration of HL-60 cells. By pre-coating the device with fibronectin, which provides a suitable substrate for cell migration, we have been able to observe the migration and reversal of cell polarity of these cells and have determined the appropriate channel dimensions that allow this process to occur.

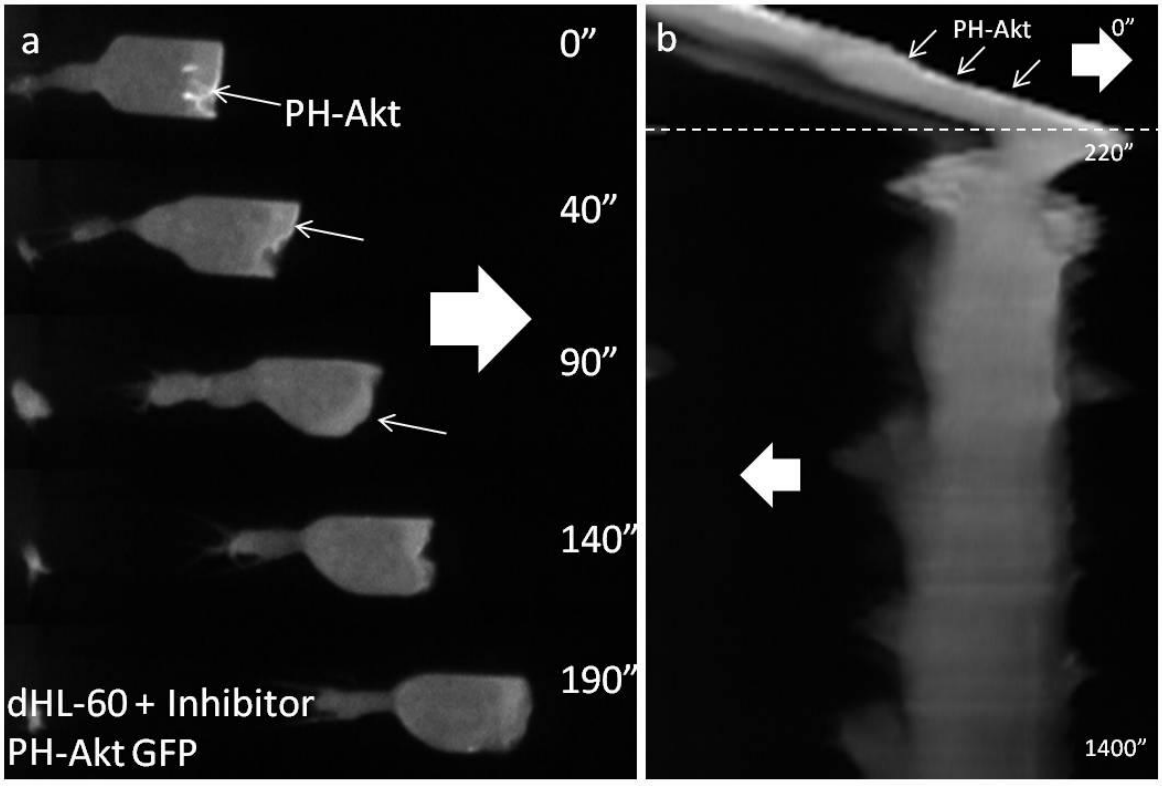

Figure 22. Polarity reversal of Hl-60 cells treated with Wortmannin a) A representative cell treated with the PI3K inhibitor Wortmannin migrating toward the high side of the gradient. PH-Akt is localized to the leading edge of the cell. These cells can perform chemotaxis, but have defects in reversing after a gradient switch. b) Kymograph of the same cell indicates that chemotaxis is toward the high side of the gradient, but once the gradient is switched (dotted line) the cell cannot move toward the new direction indicating that cell polarity reversal behavior is inhibited.

Since these cells migrate in small regions that are on the order of or smaller than the size of our microfluidic channels, this type of assay can be used to observe and quantify the localization and redistribution of molecules involved in gradient sensing and cell polarity establishment. For example, we have been able to test the effects of Wortmannin, a PI 3K inhibitor, on the turning behavior of Hl-60 cells. Cells that have not been treated with the inhibitor can respond to the gradient by extending a pseudopod and moving toward the new side of the gradient (Figure 21), whereas cells treated with Wortmannin have difficulty responding to the new gradient and cannot mobilize their cytoskeleton (Figure 22).

This setup can be used to study the chemotaxis of mutant cell lines as well as cells treated with different drugs/inhibitors to assay the effect it has on chemotaxis, cell polarity and gradient sensing. The width of the microchannels can be modified and the surface of the channels can be treated with different proteins to create an ideal and more realistic microenvironment than conventional experimental setups that use only micropipette systems. In addition, the confined channels allow the complete reversal of polarity. Our finding using *D. discoideum* has led to a major breakthrough in our understanding of cell polarity. We expect to elucidate the functions of signaling molecules in mammalian cells that might have been missed or overlooked using conventional assays.

This experimental setup can help improve our understanding of the mechanism regulating mammalian gradient sensing and may elucidate pathways which can be affected or targeted by therapeutics to alter the chemotaxis process. There are an unlimited number of combinations that can be tested using the biomarkers that are already available or new ones as they come along. These can be tested in mutant backgrounds or in cell lines treated with various signaling or cytoskeletal inhibitors. This system has a lot of potential to identify and measure the behavior of cells and their spatiotemporal response in defined and highly reproducible chemical gradients .

* Experiments for this chapter were performed in collaboration with the Richmond Laboratory and the Janetopoulos laboratory. Sai prepared cells and provided reagents. Jowhar and Sai performed experiments.

REFERENCES

Amselem, G., M. Theves, A. Bae, E. Bodenschatz, and C. Beta. 2012. A stochastic description of Dictyostelium chemotaxis. *PloS one*. 7:e37213.

Andersson, H., and A. van den Berg. 2003. Microfluidic devices for cellomics: a review. *Sensors and Actuators B: Chemical*. 92:315-325.

Andrew, N., and R.H. Insall. 2007. Chemotaxis in shallow gradients is mediated independently of PtdIns 3-kinase by biased choices between random protrusions. *Nature cell biology*. 9:193-200.

Annesley, S.J., and P.R. Fisher. 2009. Dictyostelium discoideum--a model for many reasons. *Molecular and cellular biochemistry*. 329:73-91.

Bagorda, A., V.A. Mihaylov, and C.A. Parent. 2006. Chemotaxis: moving forward and holding on to the past. *Thrombosis and haemostasis*. 95:12-21.

Bagorda, A., and C.A. Parent. 2008. Eukaryotic chemotaxis at a glance. *Journal of cell science*. 121:2621-2624.

Becker, E.L. 1977. Stimulated neutrophil locomotion: chemokinesis and chemotaxis. *Archives of pathology & laboratory medicine*. 101:509-513.

Bennett, N.T., and G.S. Schultz. 1993. Growth factors and wound healing: biochemical properties of growth factors and their receptors. *American journal of surgery*. 165:728-737.

Berridge, M.J., and R.F. Irvine. 1984. Inositol trisphosphate, a novel second messenger in cellular signal transduction. *Nature*. 312:315-321.

Beta, C., D. Wyatt, W.J. Rappel, and E. Bodenschatz. 2007. Flow photolysis for spatiotemporal stimulation of single cells. *Analytical chemistry*. 79:3940-3944.

Boguski, M.S., and F. McCormick. 1993. Proteins regulating Ras and its relatives. *Nature*. 366:643-654.

Bolourani, P., G.B. Spiegelman, and G. Weeks. 2006. Delineation of the roles played by RasG and RasC in cAMP-dependent signal transduction during the early development of Dictyostelium discoideum. *Molecular biology of the cell*. 17:4543-4550.

Bourne, H.R. 1997. How receptors talk to trimeric G proteins. *Current opinion in cell biology*. 9:134-142.

Bourne, H.R., D.A. Sanders, and F. McCormick. 1991. The GTPase superfamily: conserved structure and molecular mechanism. *Nature*. 349:117-127.

Bourne, H.R., and O. Weiner. 2002. A chemical compass. *Nature*. 419:21.

Boyden, S. 1962. The chemotactic effect of mixtures of antibody and antigen on polymorphonuclear leucocytes. *The Journal of experimental medicine*. 115:453-466.

Bravo-Cordero, J.J., M.A. Magalhaes, R.J. Eddy, L. Hodgson, and J. Condeelis. 2013. Functions of cofilin in cell locomotion and invasion. *Nat Rev Mol Cell Biol*. 14:405-417.

Bunning, E. 1989. Ahead of His Time: Wilhelm Pfeffer. Carlton University Press.

Butler, K.L., V. Ambravaneswaran, N. Agrawal, M. Bilodeau, M. Toner, R.G. Tompkins, S. Fagan, and D. Irimia. 2010. Burn injury reduces neutrophil directional migration speed in microfluidic devices. *PloS one*. 5:e11921.

Camelliti, P., J.O. Gallagher, P. Kohl, and A.D. McCulloch. 2006. Micropatterned cell cultures on elastic membranes as an in vitro model of myocardium. *Nature protocols*. 1:1379-1391.

Cardelli, J. 2001. Phagocytosis and macropinocytosis in Dictyostelium: phosphoinositide-based processes, biochemically distinct. *Traffic (Copenhagen, Denmark)*. 2:311-320.

Chen, L., C. Janetopoulos, Y.E. Huang, M. Iijima, J. Borleis, and P.N. Devreotes. 2003. Two phases of actin polymerization display different dependencies on PI(3,4,5)P3 accumulation and have unique roles during chemotaxis. *Molecular biology of the cell*. 14:5028-5037.

Chen, Q., and T.D. Pollard. 2013. Actin Filament Severing by Cofilin Dismantles Actin Patches and Produces Mother Filaments for New Patches. *Current biology : CB*.

Choi, C.H., P.A. Thomason, M. Zaki, R.H. Insall, and D.L. Barber. 2013. Phosphorylation of actin-related protein 2 (Arp2) is required for normal development and cAMP chemotaxis in Dictyostelium. *The Journal of biological chemistry*. 288:2464-2474.

Chung, C.Y., S. Funamoto, and R.A. Firtel. 2001a. Signaling pathways controlling cell polarity and chemotaxis. *Trends in biochemical sciences*. 26:557-566.

Chung, C.Y., G. Potikyan, and R.A. Firtel. 2001b. Control of Cell Polarity and Chemotaxis by Akt/PKB and PI3 Kinase through the Regulation of PAKa. *Molecular cell*. 7:937-947.

Clarke, M., A. Muller-Taubenberger, K.I. Anderson, U. Engel, and G. Gerisch. 2006. Mechanically induced actin-mediated rocketing of phagosomes. *Molecular biology of the cell*. 17:4866-4875.

Comer, F.I., and C.A. Parent. 2002. PI 3-kinases and PTEN: how opposites chemoattract. *Cell*. 109:541-544.

Condeelis, J., and J.E. Segall. 2003. Intravital imaging of cell movement in tumours. *Nature reviews. Cancer*. 3:921-930.

Condeelis, J., R.H. Singer, and J.E. Segall. 2005. The great escape: when cancer cells hijack the genes for chemotaxis and motility. *Annual review of cell and developmental biology*. 21:695-718.

Cukierman, E., R. Pankov, D.R. Stevens, and K.M. Yamada. 2001. Taking cell-matrix adhesions to the third dimension. *Science*. 294:1708-1712.

Dalous, J., E. Burghardt, A. Muller-Taubenberger, F. Bruckert, G. Gerisch, and T. Bretschneider. 2008. Reversal of cell polarity and actin-myosin cytoskeleton reorganization under mechanical and chemical stimulation. *Biophysical journal*. 94:1063-1074.

de Keijzer, S., A. Serge, F. van Hemert, P.H. Lommerse, G.E. Lamers, H.P. Spaink, T. Schmidt, and B.E. Snaar-Jagalska. 2008. A spatially restricted increase in receptor mobility is involved in directional sensing during Dictyostelium discoideum chemotaxis. *Journal of cell science*. 121:1750-1757.

De Paepe, B., K.K. Creus, and J.L. De Bleecker. 2009. Role of cytokines and chemokines in idiopathic inflammatory myopathies. *Current opinion in rheumatology*. 21:610-616.

de Wit, R.J., R. Bulgakov, T.A. Bominaar, and T.F. Rinke de Wit. 1987. Differential effects of stimulus termination on excitation and desensitization of folic acid receptors and guanylate cyclase in Dictyostelium discoideum. *Biochimica et biophysica acta*. 930:1-9.

Devreotes, P., and C. Janetopoulos. 2003. Eukaryotic chemotaxis: distinctions between directional sensing and polarization. *The Journal of biological chemistry*. 278:20445-20448.

Devreotes, P.N. 1994. G protein-linked signaling pathways control the developmental program of Dictyostelium. *Neuron*. 12:235-241.

Di Gennaro, A., and J.Z. Haeggstrom. 2012. The leukotrienes: immune-modulating lipid mediators of disease. *Advances in immunology*. 116:51-92.

Dormann, D., J.Y. Kim, P.N. Devreotes, and C.J. Weijer. 2001. cAMP receptor affinity controls wave dynamics, geometry and morphogenesis in Dictyostelium. *Journal of cell science*. 114:2513-2523.

Dorsam, R.T., and J.S. Gutkind. 2007. G-protein-coupled receptors and cancer. *Nature reviews. Cancer*. 7:79-94.

Eichinger, L., J.A. Pachebat, G. Glockner, M.A. Rajandream, R. Sucgang, M. Berriman, J. Song, R. Olsen, K. Szafranski, Q. Xu, B. Tunggal, S. Kummerfeld, M. Madera, B.A. Konfortov, F. Rivero, A.T. Bankier, R. Lehmann, N. Hamlin, R. Davies, P. Gaudet, P. Fey, K. Pilcher, G. Chen, D. Saunders, E. Sodergren, P. Davis, A. Kerhornou, X. Nie, N. Hall, C. Anjard, L. Hemphill, N. Bason, P. Farbrother, B. Desany, E. Just, T. Morio, R. Rost, C. Churcher, J. Cooper, S. Haydock, N. van Driessche, A. Cronin, I. Goodhead, D. Muzny, T. Mourier, A. Pain, M. Lu, D. Harper, R. Lindsay, H. Hauser, K. James, M. Quiles, M. Madan Babu, T. Saito, C. Buchrieser, A. Wardroper, M. Felder, M.

Thangavelu, D. Johnson, A. Knights, H. Loulseged, K. Mungall, K. Oliver, C. Price, M.A. Quail, H. Urushihara, J. Hernandez, E. Rabbinowitsch, D. Steffen, M. Sanders, J. Ma, Y. Kohara, S. Sharp, M. Simmonds, S. Spiegler, A. Tivey, S. Sugano, B. White, D. Walker, J. Woodward, T. Winckler, Y. Tanaka, G. Shaulsky, M. Schleicher, G. Weinstock, A. Rosenthal, E.C. Cox, R.L. Chisholm, R. Gibbs, W.F. Loomis, M. Platzer, R.R. Kay, J. Williams, P.H. Dear, A.A. Noegel, B. Barrell, and A. Kuspa. 2005. The genome of the social amoeba Dictyostelium discoideum. *Nature*. 435:43-57.

El-Ali, J., P.K. Sorger, and K.F. Jensen. 2006. Cells on chips. *Nature*. 442:403-411.

Elzie, C.A., J. Colby, M.A. Sammons, and C. Janetopoulos. 2009. Dynamic localization of G proteins in Dictyostelium discoideum. *Journal of cell science*. 122:2597-2603.

Engelmann, T. 1883. Bakterium photometricum. Ein Beitrag zur vergleichenden Physiologie des Licht- und Farbensinnes. *Pflügers Arch Gesamte Physiol Menschen Tiere*. 42.

Fey, P., P. Gaudet, K.E. Pilcher, J. Franke, and R.L. Chisholm. 2006. dictyBase and the Dicty Stock Center. *Methods in molecular biology (Clifton, N.J.)*. 346:51-74.

Franca-Koh, J., S.S. Willard, and P. Devreotes. 2009. G-Protein Signaling in Chemotaxis. *In* Handbook of Cell Signaling. Vol. 2. 1705-1712.

Franciszkiewicz, K., A. Boissonnas, M. Boutet, C. Combadiere, and F. Mami-Chouaib. 2012. Role of chemokines and chemokine receptors in shaping the effector phase of the antitumor immune response. *Cancer research*. 72:6325-6332.

Frost, E.E., Z. Zhou, K. Krasnesky, and R.C. Armstrong. 2009. Initiation of oligodendrocyte progenitor cell migration by a PDGF-A activated extracellular regulated kinase (ERK) signaling pathway. *Neurochemical research*. 34:169-181.

Fuller, D., W. Chen, M. Adler, A. Groisman, H. Levine, W.J. Rappel, and W.F. Loomis. 2010. External and internal constraints on eukaryotic chemotaxis. *Proceedings of the National Academy of Sciences of the United States of America*. 107:9656-9659.

Funamoto, S., R. Meili, S. Lee, L. Parry, and R.A. Firtel. 2002. Spatial and temporal regulation of 3-phosphoinositides by PI 3-kinase and PTEN mediates chemotaxis. *Cell*. 109:611-623.

Funamoto, S., K. Milan, R. Meili, and R.A. Firtel. 2001. Role of phosphatidylinositol 3' kinase and a downstream pleckstrin homology domain-containing protein in controlling chemotaxis in dictyostelium. *The Journal of cell biology*. 153:795-810.

Ganesan, L.P., T. Joshi, H. Fang, V.K. Kutala, J. Roda, R. Trotta, A. Lehman, P. Kuppusamy, J.C. Byrd, W.E. Carson, M.A. Caligiuri, and S. Tridandapani. 2006. FcgammaR-induced production of superoxide and inflammatory cytokines is differentially regulated by SHIP through its influence on PI3K and/or Ras/Erk pathways. *Blood*. 108:718-725.

Garcia, G.L., E.C. Rericha, C.D. Heger, P.K. Goldsmith, and C.A. Parent. 2009. The group migration of Dictyostelium cells is regulated by extracellular chemoattractant degradation. *Molecular biology of the cell*. 20:3295-3304.

Gaudet, P., K.E. Pilcher, P. Fey, and R.L. Chisholm. 2007. Transformation of Dictyostelium discoideum with plasmid DNA. *Nature protocols*. 2:1317-1324.

Gilman, A.G. 1987. G proteins: transducers of receptor-generated signals. *Annual review of biochemistry*. 56:615-649.

Grove, J.E., R.J. Brown, and D.J. Watts. 2000. The intracellular target for the antiresorptive aminobisphosphonate drugs in Dictyostelium discoideum is the enzyme farnesyl diphosphate synthase. *Journal of bone and mineral research : the official journal of the American Society for Bone and Mineral Research*. 15:971-981.

Gruver, J.S., J.P. Wikswo, and C.Y. Chung. 2008. 3'-phosphoinositides regulate the coordination of speed and accuracy during chemotaxis. *Biophysical journal*. 95:4057-4067.

Habib, S.J., B.C. Chen, F.C. Tsai, K. Anastassiadis, T. Meyer, E. Betzig, and R. Nusse. 2013. A localized Wnt signal orients asymmetric stem cell division in vitro. *Science*. 339:1445-1448.

Hadwiger, J.A., S. Lee, and R.A. Firtel. 1994. The G alpha subunit G alpha 4 couples to pterin receptors and identifies a signaling pathway that is essential for multicellular development in Dictyostelium. *Proceedings of the National Academy of Sciences of the United States of America*. 91:10566-10570.

Hadwiger, J.A., T.M. Wilkie, M. Strathmann, and R.A. Firtel. 1991. Identification of Dictyostelium G alpha genes expressed during multicellular development. *Proceedings of the National Academy of Sciences of the United States of America*. 88:8213-8217.

Hall, A.L., J. Franke, M. Faure, and R.H. Kessin. 1993. The role of the cyclic nucleotide phosphodiesterase of Dictyostelium discoideum during growth, aggregation, and morphogenesis: overexpression and localization studies with the separate promoters of the pde. *Developmental biology*. 157:73-84.

Hansson, G.K. 2009. Inflammatory mechanisms in atherosclerosis. *Journal of thrombosis and haemostasis : JTH*. 7 Suppl 1:328-331.

Hawkins, O.E., and A. Richmond. 2012. The dynamic yin-yang interaction of CXCR4 and CXCR7 in breast cancer metastasis. *Breast cancer research : BCR*. 14:103.

Hegerfeldt, Y., M. Tusch, E.B. Brocker, and P. Friedl. 2002. Collective cell movement in primary melanoma explants: plasticity of cell-cell interaction, beta1-integrin function, and migration strategies. *Cancer research*. 62:2125-2130.

Hirsch, E., V.L. Katanaev, C. Garlanda, O. Azzolino, L. Pirola, L. Silengo, S. Sozzani, A. Mantovani, F. Altruda, and M.P. Wymann. 2000. Central role for G protein-coupled phosphoinositide 3-kinase gamma in inflammation. *Science*. 287:1049-1053.

Hoeller, O., and R.R. Kay. 2007. Chemotaxis in the absence of PIP3 gradients. *Current biology : CB*. 17:813-817.

Huang, Y.E., M. Iijima, C.A. Parent, S. Funamoto, R.A. Firtel, and P. Devreotes. 2003. Receptor-mediated regulation of PI3Ks confines PI(3,4,5)P3 to the leading edge of chemotaxing cells. *Molecular biology of the cell*. 14:1913-1922.

Iijima, M., and P. Devreotes. 2002. Tumor suppressor PTEN mediates sensing of chemoattractant gradients. *Cell*. 109:599-610.

Iijima, M., Y.E. Huang, H.R. Luo, F. Vazquez, and P.N. Devreotes. 2004. Novel mechanism of PTEN regulation by its phosphatidylinositol 4,5-bisphosphate binding motif is critical for chemotaxis. *The Journal of biological chemistry*. 279:16606-16613.

Insall, R., and N. Andrew. 2007. Chemotaxis in Dictyostelium: how to walk straight using parallel pathways. *Current opinion in microbiology*. 10:578-581.

Insall, R., A. Muller-Taubenberger, L. Machesky, J. Kohler, E. Simmeth, S.J. Atkinson, I. Weber, and G. Gerisch. 2001. Dynamics of the Dictyostelium Arp2/3 complex in endocytosis, cytokinesis, and chemotaxis. *Cell motility and the cytoskeleton*. 50:115-128.

Insall, R.H., R.D. Soede, P. Schaap, and P.N. Devreotes. 1994. Two cAMP receptors activate common signaling pathways in Dictyostelium. *Molecular biology of the cell*. 5:703-711.

Janetopoulos, C., J. Borleis, F. Vazquez, M. Iijima, and P. Devreotes. 2005. Temporal and spatial regulation of phosphoinositide signaling mediates cytokinesis. *Developmental cell*. 8:467-477.

Janetopoulos, C., and P. Devreotes. 2006. Phosphoinositide signaling plays a key role in cytokinesis. *The Journal of cell biology*. 174:485-490.

Janetopoulos, C., and R.A. Firtel. 2008. Directional sensing during chemotaxis. *FEBS letters*. 582:2075-2085.

Janetopoulos, C., T. Jin, and P. Devreotes. 2001. Receptor-mediated activation of heterotrimeric G-proteins in living cells. *Science*. 291:2408-2411.

Janetopoulos, C., L. Ma, P.N. Devreotes, and P.A. Iglesias. 2004. Chemoattractant-induced phosphatidylinositol 3,4,5-trisphosphate accumulation is spatially amplified and adapts,

independent of the actin cytoskeleton. *Proceedings of the National Academy of Sciences of the United States of America*. 101:8951-8956.
Jin, T. 2011. GPCR-controlled chemotaxis in Dictyostelium discoideum. *Wiley interdisciplinary reviews. Systems biology and medicine*. 3:717-727.
Jin, T., N. Zhang, Y. Long, C.A. Parent, and P.N. Devreotes. 2000. Localization of the G protein betagamma complex in living cells during chemotaxis. *Science*. 287:1034-1036.
Johnson, R.L., C.L. Saxe, 3rd, R. Gollop, A.R. Kimmel, and P.N. Devreotes. 1993a. Identification and targeted gene disruption of cAR3, a cAMP receptor subtype expressed during multicellular stages of Dictyostelium development. *Genes Dev*. 7:273-282.
Johnson, R.L., C.L. Saxe, R. Gollop, A.R. Kimmel, and P.N. Devreotes. 1993b. Identification and targeted gene disruption of cAR3, a cAMP receptor subtype expressed during multicellular stages of Dictyostelium development. *Genes & Development*. 7:273-282.
Johnson, R.L., P.J. Van Haastert, A.R. Kimmel, C.L. Saxe, 3rd, B. Jastorff, and P.N. Devreotes. 1992. The cyclic nucleotide specificity of three cAMP receptors in Dictyostelium. *The Journal of biological chemistry*. 267:4600-4607.
Johnson, Z., C.A. Power, C. Weiss, F. Rintelen, H. Ji, T. Ruckle, M. Camps, T.N. Wells, M.K. Schwarz, A.E. Proudfoot, and C. Rommel. 2004. Chemokine inhibition--why, when, where, which and how? *Biochemical Society transactions*. 32:366-377.
Jowhar, D., and C. Janetopoulos. 2013. The Chemotactic Compass. *In* Dictyostelids. Springer-Verlag Berlin Heidelberg
Jowhar, D., G. Wright, P.C. Samson, J.P. Wikswo, and C. Janetopoulos. 2010. Open access microfluidic device for the study of cell migration during chemotaxis. *Integrative biology : quantitative biosciences from nano to macro*. 2:648-658.
Kae, H., C.J. Lim, G.B. Spiegelman, and G. Weeks. 2004. Chemoattractant-induced Ras activation during Dictyostelium aggregation. *EMBO reports*. 5:602-606.
Kamimura, Y., Y. Xiong, P.A. Iglesias, O. Hoeller, P. Bolourani, and P.N. Devreotes. 2008. PIP3-independent activation of TorC2 and PKB at the cell's leading edge mediates chemotaxis. *Current biology : CB*. 18:1034-1043.
Kaupp, U.B., N.D. Kashikar, and I. Weyand. 2008. Mechanisms of sperm chemotaxis. *Annual review of physiology*. 70:93-117.
Kay, R.R. 2002. Chemotaxis and cell differentiation in Dictyostelium. *Current opinion in microbiology*. 5:575-579.
Keenan, T.M., and A. Folch. 2008. Biomolecular gradients in cell culture systems. *Lab on a chip*. 8:34-57.
Keizer-Gunnink, I., A. Kortholt, and P. Van Haastert. 2007. Chemoattractants and chemorepellents act by inducing opposite polarity in phospholipase C and PI3-kinase signaling. *Journal of Cell Biology*. 177:579-585.
Kessin, R.H. 1988. Genetics of early Dictyostelium discoideum development. *Microbiological reviews*. 52:29-49.
Kim, J.Y., P.V. Haastert, and P.N. Devreotes. 1996. Social senses: G-protein-coupled receptor signaling pathways in Dictyostelium discoideum. *Chemistry & biology*. 3:239-243.
Kimmel, A.R., and R.A. Firtel. 2004. Breaking symmetries: regulation of Dictyostelium development through chemoattractant and morphogen signal-response. *Current opinion in genetics & development*. 14:540-549.
Kimmel, A.R., C.A. Parent, and N.R. Gough. 2004. Teaching resources. Spatial and temporal dynamics of signaling components involved in the control of chemotaxis in Dictyostelium discoideum. *Science's STKE : signal transduction knowledge environment*. 2004:tr3.
King, J.S., and R.H. Insall. 2009. Chemotaxis: finding the way forward with Dictyostelium. *Trends in cell biology*. 19:523-530.

Klein, P.S., T.J. Sun, C.L. Saxe, 3rd, A.R. Kimmel, R.L. Johnson, and P.N. Devreotes. 1988. A chemoattractant receptor controls development in Dictyostelium discoideum. *Science*. 241:1467-1472.

Klopfenstein, D.R., M. Tomishige, N. Stuurman, and R.D. Vale. 2002. Role of phosphatidylinositol(4,5)bisphosphate organization in membrane transport by the Unc104 kinesin motor. *Cell*. 109:347-358.

Knecht, D., and K.M. Pang. 1995. Electroporation of Dictyostelium discoideum. *Methods in molecular biology (Clifton, N.J.)*. 47:321-330.

Knight, B., C. Laukaitis, N. Akhtar, N.A. Hotchin, M. Edlund, and A.R. Horwitz. 2000. Visualizing muscle cell migration in situ. *Current biology : CB*. 10:576-585.

Kolaczkowska, E., and P. Kubes. 2013. Neutrophil recruitment and function in health and inflammation. *Nature reviews. Immunology*. 13:159-175.

Korohoda, W., Z. Madeja, and J. Sroka. 2002. Diverse chemotactic responses of Dictyostelium discoideum amoebae in the developing (temporal) and stationary (spatial) concentration gradients of folic acid, cAMP, Ca(2+) and Mg(2+). *Cell motility and the cytoskeleton*. 53:1-25.

Kortholt, A., R. Kataria, I. Keizer-Gunnink, W.N. Van Egmond, A. Khanna, and P.J. Van Haastert. 2011. Dictyostelium chemotaxis: essential Ras activation and accessory signalling pathways for amplification. *EMBO reports*. 12:1273-1279.

Kortholt, A., J.S. King, I. Keizer-Gunnink, A.J. Harwood, and P.J. Van Haastert. 2007. Phospholipase C regulation of phosphatidylinositol 3,4,5-trisphosphate-mediated chemotaxis. *Molecular biology of the cell*. 18:4772-4779.

Kortholt, A., and P.J. van Haastert. 2008. Highlighting the role of Ras and Rap during Dictyostelium chemotaxis. *Cellular signalling*. 20:1415-1422.

Kriebel, P.W., V.A. Barr, and C.A. Parent. 2003. Adenylyl cyclase localization regulates streaming during chemotaxis. *Cell*. 112:549-560.

Kumagai, A., J.A. Hadwiger, M. Pupillo, and R.A. Firtel. 1991. Molecular genetic analysis of two G alpha protein subunits in Dictyostelium. *The Journal of biological chemistry*. 266:1220-1228.

Kuwayama, H., S. Ishida, and P.J. Van Haastert. 1993. Non-chemotactic Dictyostelium discoideum mutants with altered cGMP signal transduction. *The Journal of cell biology*. 123:1453-1462.

Laevsky, G., and D.A. Knecht. 2001. Under-agarose folate chemotaxis of Dictyostelium discoideum amoebae in permissive and mechanically inhibited conditions. *BioTechniques*. 31:1140-1142, 1144, 1146-1149.

Landree, M.A., and P.N. Devreotes. 2004. Analyzing chemotaxis using Dictyostelium discoideum as a model system. *Methods in molecular biology (Clifton, N.J.)*. 239:91-104.

Lazennec, G., and A. Richmond. 2010. Chemokines and chemokine receptors: new insights into cancer-related inflammation. *Trends in molecular medicine*. 16:133-144.

Le, Y., Y. Zhou, P. Iribarren, and J. Wang. 2004. Chemokines and chemokine receptors: their manifold roles in homeostasis and disease. *Cellular & molecular immunology*. 1:95-104.

Lee, S., F.I. Comer, A. Sasaki, I.X. McLeod, Y. Duong, K. Okumura, J.R. Yates, 3rd, C.A. Parent, and R.A. Firtel. 2005. TOR complex 2 integrates cell movement during chemotaxis and signal relay in Dictyostelium. *Molecular biology of the cell*. 16:4572-4583.

Levchenko, A., and P.A. Iglesias. 2002. Models of eukaryotic gradient sensing: application to chemotaxis of amoebae and neutrophils. *Biophysical journal*. 82:50-63.

Levine, H., D.A. Kessler, and W.J. Rappel. 2006. Directional sensing in eukaryotic chemotaxis: a balanced inactivation model. *Proceedings of the National Academy of Sciences of the United States of America*. 103:9761-9766.

Li, G., H. Alexander, N. Schneider, and S. Alexander. 2000. Molecular basis for resistance to the anticancer drug cisplatin in Dictyostelium. *Microbiology (Reading, England)*. 146 (Pt 9):2219-2227.

Liao, X.H., J. Buggey, and A.R. Kimmel. 2010. Chemotactic activation of Dictyostelium AGC-family kinases AKT and PKBR1 requires separate but coordinated functions of PDK1 and TORC2. *Journal of cell science*. 123:983-992.

Lin, F., W. Saadi, S.W. Rhee, S.J. Wang, S. Mittal, and N.L. Jeon. 2004. Generation of dynamic temporal and spatial concentration gradients using microfluidic devices. *Lab on a chip*. 4:164-167.

Liu, M., J. Zhao, K. Chen, X. Bian, C. Wang, Y. Shi, and J.M. Wang. 2012. G protein-coupled receptor FPR1 as a pharmacologic target in inflammation and human glioblastoma. *International immunopharmacology*. 14:283-288.

Loovers, H.M., M. Postma, I. Keizer-Gunnink, Y.E. Huang, P.N. Devreotes, and P.J. van Haastert. 2006. Distinct roles of PI(3,4,5)P3 during chemoattractant signaling in Dictyostelium: a quantitative in vivo analysis by inhibition of PI3-kinase. *Molecular biology of the cell*. 17:1503-1513.

Louis, J.M., G.T. Ginsburg, and A.R. Kimmel. 1994. The cAMP receptor CAR4 regulates axial patterning and cellular differentiation during late development of Dictyostelium. *Genes & Development*. 8:2086-2096.

Luster, A.D. 1998. Chemokines--chemotactic cytokines that mediate inflammation. *The New England journal of medicine*. 338:436-445.

Lux, R., and W. Shi. 2004. Chemotaxis-Guided Movements in Bacteria. *Critical Reviews in Oral Biology & Medicine*. 15:207-220.

Ma, L., C. Janetopoulos, L. Yang, P.N. Devreotes, and P.A. Iglesias. 2004. Two complementary, local excitation, global inhibition mechanisms acting in parallel can explain the chemoattractant-induced regulation of PI(3,4,5)P3 response in dictyostelium cells. *Biophysical journal*. 87:3764-3774.

Malchow, D., R. Bohme, and H.J. Rahmsdorf. 1981. Regulation of phosphorylation of myosin heavy chain during the chemotactic response of Dictyostelium cells. *European journal of biochemistry / FEBS*. 117:213-218.

Mao, Y.S., and H.L. Yin. 2007. Regulation of the actin cytoskeleton by phosphatidylinositol 4-phosphate 5 kinases. *Pflugers Archiv : European journal of physiology*. 455:5-18.

Maxwell, P.J., J. Coulter, S.M. Walker, M. McKechnie, J. Neisen, N. McCabe, R.D. Kennedy, M. Salto-Tellez, C. Albanese, and D.J. Waugh. 2012. Potentiation of Inflammatory CXCL8 Signalling Sustains Cell Survival in PTEN-deficient Prostate Carcinoma. *European urology*.

Meier, B., A. Zielinski, C. Weber, D. Arcizet, S. Youssef, T. Franosch, J.O. Radler, and D. Heinrich. 2011. Chemotactic cell trapping in controlled alternating gradient fields. *Proceedings of the National Academy of Sciences of the United States of America*. 108:11417-11422.

Meinhardt, H. 1999. Orientation of chemotactic cells and growth cones: models and mechanisms. *Journal of cell science*. 112 (Pt 17):2867-2874.

Merlot, S., and R.A. Firtel. 2003. Leading the way: Directional sensing through phosphatidylinositol 3-kinase and other signaling pathways. *Journal of cell science*. 116:3471-3478.

Mueller, S.G., W.P. Schraw, and A. Richmond. 1994. Melanoma growth stimulatory activity enhances the phosphorylation of the class II interleukin-8 receptor in non-hematopoietic cells. *The Journal of biological chemistry*. 269:1973-1980.

Muller, A., B. Homey, H. Soto, N. Ge, D. Catron, M.E. Buchanan, T. McClanahan, E. Murphy, W. Yuan, S.N. Wagner, J.L. Barrera, A. Mohar, E. Verastegui, and A. Zlotnik. 2001. Involvement of chemokine receptors in breast cancer metastasis. *Nature*. 410:50-56.

Muthuswamy, S.K., and B. Xue. 2012. Cell polarity as a regulator of cancer cell behavior plasticity. *Annual review of cell and developmental biology*. 28:599-625.

Niggli, V., and H. Keller. 1997. The phosphatidylinositol 3-kinase inhibitor wortmannin markedly reduces chemotactic peptide-induced locomotion and increases in cytoskeletal actin in human neutrophils. *European journal of pharmacology*. 335:43-52.

O'Boyle, G., I. Swidenbank, H. Marshall, C.E. Barker, J. Armstrong, S.A. White, S.P. Fricker, R. Plummer, M. Wright, and P.E. Lovat. 2013. Inhibition of CXCR4-CXCL12 chemotaxis in melanoma by AMD11070. *British journal of cancer*. 108:1634-1640.

Octtaviani, E., J.C. Effler, and D.N. Robinson. 2006. Enlazin, a natural fusion of two classes of canonical cytoskeletal proteins, contributes to cytokinesis dynamics. *Molecular biology of the cell*. 17:5275-5286.

Panbianco, C., and M. Gotta. 2011. Coordinating cell polarity with cell division in space and time. *Trends in cell biology*. 21:672-680.

Parent, C.A. 2004. Making all the right moves: chemotaxis in neutrophils and Dictyostelium. *Current opinion in cell biology*. 16:4-13.

Parent, C.A., B.J. Blacklock, W.M. Froehlich, D.B. Murphy, and P.N. Devreotes. 1998. G protein signaling events are activated at the leading edge of chemotactic cells. *Cell*. 95:81-91.

Parent, C.A., and P.N. Devreotes. 1999. A cell's sense of direction. *Science*. 284:765-770.

Park, W.S., W.D. Heo, J.H. Whalen, N.A. O'Rourke, H.M. Bryan, T. Meyer, and M.N. Teruel. 2008. Comprehensive identification of PIP3-regulated PH domains from C. elegans to H. sapiens by model prediction and live imaging. *Molecular cell*. 30:381-392.

Pfeffer, W. 1884. Lokomotorische Richtungsbewegungen durchchemische Reize. *Untersuchungen aus dem Botanischen Institut Tübingen*.

Rachakonda, G., K.R. Sekhar, D. Jowhar, P.C. Samson, J.P. Wikswo, R.D. Beauchamp, P.K. Datta, and M.L. Freeman. 2010. Increased cell migration and plasticity in Nrf2-deficient cancer cell lines. *Oncogene*. 29:3703-3714.

Rahdar, M., T. Inoue, T. Meyer, J. Zhang, F. Vazquez, and P.N. Devreotes. 2009. A phosphorylation-dependent intramolecular interaction regulates the membrane association and activity of the tumor suppressor PTEN. *Proc Natl Acad Sci U S A*. 106:480-485.

Raper, K.B. 1935. Dictyostelium discoideum, a new species of slime mold from decaying forest leaves. *J. Agric. Res*. 50:135-147.

Reiland, J., L.T. Furcht, and J.B. McCarthy. 1999. CXC-chemokines stimulate invasion and chemotaxis in prostate carcinoma cells through the CXCR2 receptor. *The Prostate*. 41:78-88.

Richmond, A., J. Yang, and Y. Su. 2009. The good and the bad of chemokines/chemokine receptors in melanoma. *Pigment cell & melanoma research*. 22:175-186.

Rifkin, J.L., and R.R. Goldberg. 2006. Effects of chemoattractant pteridines upon speed of D. discoideum vegetative amoebae. *Cell motility and the cytoskeleton*. 63:1-5.

Romeralo, M., J.C. Cavender, J.C. Landolt, S.L. Stephenson, and S.L. Baldauf. 2011. An expanded phylogeny of social amoebas (Dictyostelia) shows increasing diversity and new morphological patterns. *BMC evolutionary biology*. 11:84.

Roussos, E.T., J.S. Condeelis, and A. Patsialou. 2011. Chemotaxis in cancer. *Nature reviews. Cancer*. 11:573-587.

Rubino, S., M. Fighetti, E. Unger, and P. Cappuccinelli. 1984. Location of actin, myosin, and microtubular structures during directed locomotion of Dictyostelium amebae. *The Journal of cell biology*. 98:382-390.

Rupper, A., K. Lee, D. Knecht, and J. Cardelli. 2001a. Sequential activities of phosphoinositide 3-kinase, PKB/Aakt, and Rab7 during macropinosome formation in Dictyostelium. *Molecular biology of the cell*. 12:2813-2824.

Rupper, A.C., J.M. Rodriguez-Paris, B.D. Grove, and J.A. Cardelli. 2001b. p110-related PI 3-kinases regulate phagosome-phagosome fusion and phagosomal pH through a PKB/Akt dependent pathway in Dictyostelium. *Journal of cell science*. 114:1283-1295.

Sai, J., G. Walker, J. Wikswo, and A. Richmond. 2006. The IL sequence in the LLKIL motif in CXCR2 is required for full ligand-induced activation of Erk, Akt, and chemotaxis in HL60 cells. *The Journal of biological chemistry*. 281:35931-35941.

Sameshima, M., Y. Imai, and Y. Hashimoto. 1988. The position of the microtubule-organizing center relative to the nucleus is independent of the direction of cell migration in Dictyostelium discoideum. *Cell motility and the cytoskeleton*. 9:111-116.

Sasaki, A.T., C. Chun, K. Takeda, and R.A. Firtel. 2004. Localized Ras signaling at the leading edge regulates PI3K, cell polarity, and directional cell movement. *The Journal of cell biology*. 167:505-518.

Sasaki, A.T., and R.A. Firtel. 2006. Regulation of chemotaxis by the orchestrated activation of Ras, PI3K, and TOR. *European journal of cell biology*. 85:873-895.

Sasaki, A.T., C. Janetopoulos, S. Lee, P.G. Charest, K. Takeda, L.W. Sundheimer, R. Meili, P.N. Devreotes, and R.A. Firtel. 2007. G protein-independent Ras/PI3K/F-actin circuit regulates basic cell motility. *The Journal of cell biology*. 178:185-191.

Saxe, C.L., 3rd, R. Johnson, P.N. Devreotes, and A.R. Kimmel. 1991. Multiple genes for cell surface cAMP receptors in Dictyostelium discoideum. *Developmental genetics*. 12:6-13.

Schindelin, J., I. Arganda-Carreras, E. Frise, V. Kaynig, M. Longair, T. Pietzsch, S. Preibisch, C. Rueden, S. Saalfeld, B. Schmid, J.Y. Tinevez, D.J. White, V. Hartenstein, K. Eliceiri, P. Tomancak, and A. Cardona. 2012. Fiji: an open-source platform for biological-image analysis. *Nature methods*. 9:676-682.

Schliwa, M., U. Euteneuer, R. Graf, and M. Ueda. 1999. Centrosomes, microtubules and cell migration. *Biochemical Society symposium*. 65:223-231.

Schmidt, S., M. Moser, and M. Sperandio. 2013. The molecular basis of leukocyte recruitment and its deficiencies. *Molecular immunology*. 55:49-58.

Schneider, L., M. Cammer, J. Lehman, S.K. Nielsen, C.F. Guerra, I.R. Veland, C. Stock, E.K. Hoffmann, B.K. Yoder, A. Schwab, P. Satir, and S.T. Christensen. 2010. Directional cell migration and chemotaxis in wound healing response to PDGF-AA are coordinated by the primary cilium in fibroblasts. *Cellular physiology and biochemistry : international journal of experimental cellular physiology, biochemistry, and pharmacology*. 25:279-292.

Segall, J.E. 1988. Quantification of motility and area changes of Dictyostelium discoideum amoebae in response to chemoattractants. *Journal of muscle research and cell motility*. 9:481-490.

Singer, A.J., and R.A. Clark. 1999. Cutaneous wound healing. *The New England journal of medicine*. 341:738-746.

Skandarajah, A., C. Janetopoulos, J.P. Wikswo, and P.C. Samson. 2010.

Smythies, L.E., A. Maheshwari, R. Clements, D. Eckhoff, L. Novak, H.L. Vu, L.M. Mosteller-Barnum, M. Sellers, and P.D. Smith. 2006. Mucosal IL-8 and TGF-beta recruit blood monocytes: evidence for cross-talk between the lamina propria stroma and myeloid cells. *Journal of leukocyte biology*. 80:492-499.

Sorensen, S.D., D.A. Linseman, E.L. McEwen, A.M. Heacock, and S.K. Fisher. 1998. A role for a wortmannin-sensitive phosphatidylinositol-4-kinase in the endocytosis of muscarinic cholinergic receptors. *Molecular pharmacology*. 53:827-836.

Sorensen, S.D., D.A. Linseman, E.L. McEwen, A.M. Heacock, and S.K. Fisher. 1999. Inhibition of beta(2)-adrenergic and muscarinic cholinergic receptor endocytosis after depletion of phosphatidylinositol bisphosphate. *The Journal of pharmacology and experimental therapeutics*. 290:603-610.

Srinivasan, K., G.A. Wright, N. Hames, M. Housman, A. Roberts, K.J. Aufderheide, and C. Janetopoulos. 2013a. Delineating the core regulatory elements critical for directed cell migration by examining folic acid-mediated responses. *J Cell Sci*.

Srinivasan, K., G.A. Wright, N. Hames, M. Housman, A. Roberts, K.J. Aufderheide, and C. Janetopoulos. 2013b. Delineating the core regulatory elements crucial for directed cell migration by examining folic-acid-mediated responses. *Journal of cell science*. 126:221-233.

Sroka, J., Z. Madeja, A. Galanty, M. Michalik, S. Przestalski, L. Rakoczy, and W. Korohoda. 2001. Trimethyltin inhibits the chemotaxis ofDictyostelium discoideum amoebae. *European Journal of Protistology*. 37:313-326.

Strader, C.D., T.M. Fong, M.P. Graziano, and M.R. Tota. 1995. The family of G-protein-coupled receptors. *FASEB journal : official publication of the Federation of American Societies for Experimental Biology*. 9:745-754.

Suire, S., C. Lecureuil, K.E. Anderson, G. Damoulakis, I. Niewczas, K. Davidson, H. Guillou, D. Pan, C. Jonathan, T.H. Phillip, and L. Stephens. 2012. GPCR activation of Ras and PI3Kc in neutrophils depends on PLCb2/b3 and the RasGEF RasGRP4. *The EMBO journal*. 31:3118-3129.

Sun, T.J., and P.N. Devreotes. 1991. Gene targeting of the aggregation stage cAMP receptor cAR1 in Dictyostelium. *Genes & Development*. 5:572-582.

Surmi, B.K., and A.H. Hasty. 2010. The role of chemokines in recruitment of immune cells to the artery wall and adipose tissue. *Vascular pharmacology*. 52:27-36.

Swaney, K.F., C.H. Huang, and P.N. Devreotes. 2010. Eukaryotic chemotaxis: a network of signaling pathways controls motility, directional sensing, and polarity. *Annual review of biophysics*. 39:265-289.

Takeda, K., A.T. Sasaki, H. Ha, H.A. Seung, and R.A. Firtel. 2007. Role of phosphatidylinositol 3-kinases in chemotaxis in Dictyostelium. *The Journal of biological chemistry*. 282:11874-11884.

Tang, X. 2013. Tumor-associated macrophages as potential diagnostic and prognostic biomarkers in breast cancer. *Cancer letters*. 332:3-10.

Taraboletti, G., D.D. Roberts, and L.A. Liotta. 1987. Thrombospondin-induced tumor cell migration: haptotaxis and chemotaxis are mediated by different molecular domains. *The Journal of cell biology*. 105:2409-2415.

Taylor, A.M., M. Blurton-Jones, S.W. Rhee, D.H. Cribbs, C.W. Cotman, and N.L. Jeon. 2005. A microfluidic culture platform for CNS axonal injury, regeneration and transport. *Nature methods*. 2:599-605.

Thelen, M. 2001. Dancing to the tune of chemokines. *Nature immunology*. 2:129-134.

Ueda, M., R. Graf, H.K. MacWilliams, M. Schliwa, and U. Euteneuer. 1997. Centrosome positioning and directionality of cell movements. *Proceedings of the National Academy of Sciences of the United States of America*. 94:9674-9678.

Ueda, M., Y. Sako, T. Tanaka, P. Devreotes, and T. Yanagida. 2001. Single-molecule analysis of chemotactic signaling in Dictyostelium cells. *Science*. 294:864-867.

Van Dijken, P., A.A. Lammers, S. Ozaki, B.V. Potter, C. Erneux, and P.J. Van Haastert. 1994. Phosphorylation of inositol 1,4,5-trisphosphate analogues by 3-kinase and dephosphorylation of inositol 1,3,4,5-tetrakisphosphate analogues by 5-phosphatase. *European journal of biochemistry / FEBS*. 226:561-566.

Van Haastert, P.J., and P.N. Devreotes. 2004. Chemotaxis: signalling the way forward. *Nature reviews. Molecular cell biology*. 5:626-634.

Varani, J. 1982. Chemotaxis of metastatic tumor cells. *Cancer metastasis reviews*. 1:17-28.

Vedham, V., H. Phee, and K.M. Coggeshall. 2005. Vav activation and function as a rac guanine nucleotide exchange factor in macrophage colony-stimulating factor-induced macrophage chemotaxis. *Mol Cell Biol*. 25:4211-4220.

Veltman, D.M., I. Keizer-Gunnik, and P.J. Van Haastert. 2008. Four key signaling pathways mediating chemotaxis in Dictyostelium discoideum. *The Journal of cell biology*. 180:747-753.

Vorotnikov, A.V. 2011. Chemotaxis: movement, direction, control. *Biochemistry. Biokhimiia*. 76:1528-1555.

Wahl, S.M., D.A. Hunt, L.M. Wakefield, N. McCartney-Francis, L.M. Wahl, A.B. Roberts, and M.B. Sporn. 1987. Transforming growth factor type beta induces monocyte chemotaxis and growth factor production. *Proceedings of the National Academy of Sciences of the United States of America*. 84:5788-5792.

Walker, G.M., J. Sai, A. Richmond, M. Stremler, C.Y. Chung, and J.P. Wikswo. 2005. Effects of flow and diffusion on chemotaxis studies in a microfabricated gradient generator. *Lab on a chip*. 5:611-618.

Wang, Y., J. Liu, and J.E. Segall. 1998. MAP kinase function in amoeboid chemotaxis. *Journal of cell science*. 111 (Pt 3):373-383.

Weiner, O.D. 2002. Regulation of cell polarity during eukaryotic chemotaxis: the chemotactic compass. *Current opinion in cell biology*. 14:196-202.

Wessels, D., D.F. Lusche, S. Kuhl, P. Heid, and D.R. Soll. 2007. PTEN plays a role in the suppression of lateral pseudopod formation during Dictyostelium motility and chemotaxis. *Journal of cell science*. 120:2517-2531.

Whitman, M., C.P. Downes, M. Keeler, T. Keller, and L. Cantley. 1988. Type I phosphatidylinositol kinase makes a novel inositol phospholipid, phosphatidylinositol-3-phosphate. *Nature*. 332:644-646.

Wilkinson, P.C. 1990. How do leucocytes perceive chemical gradients? *FEMS microbiology immunology*. 2:303-311.

Williams, J.G. 2010. Dictyostelium finds new roles to model. *Genetics*. 185:717-726.

Williams, R.S., M. Eames, W.J. Ryves, J. Viggars, and A.J. Harwood. 1999. Loss of a prolyl oligopeptidase confers resistance to lithium by elevation of inositol (1,4,5) trisphosphate. *The EMBO journal*. 18:2734-2745.

Wolf, K., I. Mazo, H. Leung, K. Engelke, U.H. von Andrian, E.I. Deryugina, A.Y. Strongin, E.B. Brocker, and P. Friedl. 2003. Compensation mechanism in tumor cell migration: mesenchymal-amoeboid transition after blocking of pericellular proteolysis. *The Journal of cell biology*. 160:267-277.

Wood, W., C. Faria, and A. Jacinto. 2006. Distinct mechanisms regulate hemocyte chemotaxis during development and wound healing in Drosophila melanogaster. *The Journal of cell biology*. 173:405-416.

Wright, G.A., L. Costa, A. Terekhov, D. Jowhar, W. Hofmeister, and C. Janetopoulos. 2012. On-chip open microfluidic devices for chemotaxis studies. *Microscopy and microanalysis : the official journal of Microscopy Society of America, Microbeam Analysis Society, Microscopical Society of Canada*. 18:816-828.

Wu, J., X. Wu, and F. Lin. 2013. Recent developments in microfluidics-based chemotaxis studies. *Lab on a chip*. 13:2484-2499.

Wu, L., R. Valkema, P.J. Van Haastert, and P.N. Devreotes. 1995. The G protein beta subunit is essential for multiple responses to chemoattractants in Dictyostelium. *The Journal of cell biology*. 129:1667-1675.

Wu, X., V.C. Lee, E. Chevalier, and S.T. Hwang. 2009. Chemokine receptors as targets for cancer therapy. *Current pharmaceutical design*. 15:742-757.

Wyckoff, J., W. Wang, E.Y. Lin, Y. Wang, F. Pixley, E.R. Stanley, T. Graf, J.W. Pollard, J. Segall, and J. Condeelis. 2004. A paracrine loop between tumor cells and macrophages is required for tumor cell migration in mammary tumors. *Cancer research*. 64:7022-7029.

Xiao, Z., N. Zhang, D.B. Murphy, and P.N. Devreotes. 1997. Dynamic distribution of chemoattractant receptors in living cells during chemotaxis and persistent stimulation. *The Journal of cell biology*. 139:365-374.

Xu, J., F. Wang, A. Van Keymeulen, P. Herzmark, A. Straight, K. Kelly, Y. Takuwa, N. Sugimoto, T. Mitchison, and H.R. Bourne. 2003. Divergent signals and cytoskeletal assemblies regulate self-organizing polarity in neutrophils. *Cell*. 114:201-214.

Xu, X., M. Meier-Schellersheim, J. Yan, and T. Jin. 2007. Locally controlled inhibitory mechanisms are involved in eukaryotic GPCR-mediated chemosensing. *The Journal of cell biology*. 178:141-153.

Young, E.W., and D.J. Beebe. 2010. Fundamentals of microfluidic cell culture in controlled microenvironments. *Chemical Society reviews*. 39:1036-1048.

Zhang, N., Y. Long, and P.N. Devreotes. 2001. Ggamma in dictyostelium: its role in localization of gbetagamma to the membrane is required for chemotaxis in shallow gradients. *Molecular biology of the cell*. 12:3204-3213.

Zhu, T., J.C. Chappel, F.F. Hsu, J. Turk, R. Aurora, K. Hyrc, P. De Camilli, T.J. Broekelmann, R.P. Mecham, S.L. Teitelbaum, and W. Zou. 2013. Type I phosphotidylinosotol 4-phosphate 5-kinase gamma regulates osteoclasts in a bifunctional manner. *The Journal of biological chemistry*. 288:5268-5277.

Zicha, D., G. Dunn, and G. Jones. 1997. Analyzing chemotaxis using the Dunn direct-viewing chamber. *Methods in molecular biology (Clifton, N.J.)*. 75:449-457.

Zigmond, S.H. 1977. Ability of polymorphonuclear leukocytes to orient in gradients of chemotactic factors. *The Journal of cell biology*. 75:606-616.